DYNAMIC PROPERTIES OF SOIL IN UAE FROM FIELD AND LABORATORY TESTS

By

Ahmed Mohsen Khalil

A Thesis Presented to the Faculty of the
American University of Sharjah
College of Engineering
in Partial Fulfillment
of the Requirements
for the Degree of

Master of Science in
Civil Engineering

Sharjah, United Arab Emirates

December 2020

Declaration of Authorship

I declare that this thesis is my own work and, to the best of my knowledge and belief, it does not contain material published or written by a third party, except where permission has been obtained and/or appropriately cited through full and accurate referencing.

Signature Ahmed Mohsen Khalil

Date 12/5/2020

Approval Signatures

We, the undersigned, approve the Master's Thesis of Ahmed Mohsen Khalil

Thesis Title: Dynamic Properties of Soil in UAE from Field and Laboratory Tests

Date of Defense: 26-Nov-2020

Name, Title and Affiliation	**Signature**
Dr. Zahid Khan Associate Professor, Department of Civil Engineering Thesis Advisor	
Dr. Magdi El Emam Associate Professor, Department of Civil Engineering Thesis Co-Advisor	
Dr. Mousa Attom Professor, Department of Civil Engineering Thesis Committee Member	
Dr. Mohamed G. Arab Assistant Professor, Department of Civil Engineering University of Sharjah Thesis Committee Member	
Dr. Irtishad Ahmed Head Department of Civil Engineering	
Dr. Lotfi Romdhane Associate Dean for Graduate Studies and Research College of Engineering	
Dr. Sirin Tekinay Dean College of Engineering	
Dr. Mohamed El-Tarhuni Vice Provost for Graduate Studies Office of Graduate Studies	

Acknowledgement

Writing a thesis was harder than I thought but it was defiantly made much easier due to the support of several people in the past two years. Firstly, I would love to offer my sincere appreciation and gratitude to my research advisor Dr. Zahid Khan for his patient guidance, worthy discussion and suggestions, effective supervision, inspiration, and valuable advice throughout this research. I would, also, like to extend my thanks to my co-advisor Dr. Magdi El-Emam and committee members, Dr. Mousa Attom, Dr. Mohamed G. Arab and Dr. Samir Emam for their support and valuable comments.

Furthermore, I would like to express my thanks to the professors of the Civil Engineering department who taught me great knowledge during the past two years. I extremely appreciate their continuous dignified counsel and support. I, also, want to express my gratitude toward the department of Civil Engineering for offering me a Graduate Teacher/Research Assistantship that allowed me to learn and gain valuable teaching and research work experience from a prestigious institution like the American University of Sharjah (AUS).

My final and utmost thanks are to my parents for their endless support as they inspired me along the journey. Thanks also go to my colleagues Hakem Alkhraisha and Ahmed Eltayab for being there throughout my thesis.

Dedication

This work is dedicated to each equally, my joy, my parents, my sister and my brother.

Abstract

Dynamic properties of soil are important for the design of structures under seismic loadings. The United Arab Emirates (UAE) is experiencing significant construction development; however, there is no systematic study to characterize the regional soils for dynamic properties. Therefore, designers have to rely on correlations of dynamic properties with other static parameters. These correlations are mostly developed for other regions which may not be suitable for the UAE. This research presents the findings of a laboratory testing program involving cyclic and static triaxial (CT) tests along with bender element (BE) testing on representative samples of regional soils. The bender element tests are used to evaluate the low strain shear wave velocity (*Vs*), whereas the cyclic triaxial (CT) test is used to evaluate the shear modulus (*G*) and the damping ratio (ξ) at different strain levels and confinement pressures. Correlations of *Vs* with Standard Penetration Tests N (SPT-N) values are developed. Two different sample sizes are used to evaluate the effect of sample size on dynamic properties. Static triaxial tests are also performed to develop correlations between *Vs* and friction angle (ϕ). The results of the experimental program indicate that the degradation of dynamic properties generally agrees with previous studies however the model parameters are different. The correlation of Vs with SPT-N values follows a power model whereas the correlation between Vs and friction angle presents as a linear model. A comparison of developed correlations with previous studies validates the importance of regional specific nature of soils as most of the models in literature neither agree with each other nor with the findings of this study.

Keywords: ***Dynamic properties; Laboratory tests; Triaxial test; Bender element test; United Arab Emirates; Correlation; Shear wave velocity; Shear modulus; Damping ratio.***

Table of Contents

List of Figures

List of Tables

Chapter 1. Introduction

The United Arab Emirates (UAE) has seen a great economic growth in recent years. One factor contributing to the country's economy is construction of high-rise buildings. Modern building codes require seismic design of the structure which is based on the dynamic properties of subsurface soil. In addition, the dynamic properties of soil provide the basis of the site response analysis.

1.1. Overview

The most significant dynamic properties of soil are the shear modulus (G), and the damping ratio (ξ). These parameters can be obtained from numerous laboratory and field tests such as the Cyclic Triaxial (CT), Resonant Column (RC), and Bender Element test (BE). Additionally, field seismic surveys such as Seismic Refraction and Seismic Reflection can be used. Each particular test requires specialized equipment and analytical tools to process, gather, and evaluate the data.

Projects in the UAE compel designers to use values of dynamic properties that are either conservative or unreliable for regional soils because they rely on correlations developed for other regions. This is because there is no systematic study on the evaluation of the dynamic properties of regional soils. Typically, designers use the correlations between SPT-N and shear wave velocity (Vs). These correlations are area-specific and have to be used with caution. Similarly, dynamic properties are also strain and confinement dependent. In the absence of regional soil's behavior to these parameters, the designers typically use the characterization or models developed for other regions. This study will involve a comprehensive laboratory testing program featuring Bender Element (BE) and Cyclic Triaxial (CT), on samples of different sizes representing regional soils for evaluation of their dynamic properties and analysis.

The bender element test is widely used for small strain measurements of dynamic properties. In this study, the characteristics of the bender element's installation procedure, specimen size, waveform and frequency of the transmitted signal, and travel time determination method will be investigated and analysed. The BE will be used to measure the Vs of soil at law strain and as a function of confinement. The CT will be used to measure the G and ξ of the soil both as a function of confinement and shear strain level.

1.2. Thesis Objectives

The main objectives of the proposed study are to:

1. Evaluate the dynamic properties of representative soils of UAE as a function of confinement and shear strain level.
2. Develop correlations between static and dynamic properties for typical soils of the UAE.
3. Investigate the effect of sample size on the dynamic properties.

1.3. Research Contribution

The contributions of this research work can be summarized as follows:

Propose a comprehensive study of the dynamic properties of regional soils. Identifies urgent industry needs that have a substantial effect on construction costs. Typically, correlations between the static properties and dynamic properties such as Vs-SPT-N correlations are area specific. In UAE, no systematic study was conducted to identify the regional soil to serve the seismic design. In the present study, a comprehensive laboratory testing program such as cyclic triaxial and bender element are used to determine the dynamic properties of UAE's soil. Moreover, regression analysis is used to correlate dynamic and static properties.

1.4. Thesis Organization

The manuscript is organized as follows:

Chapter 2 provides background about bender element, cyclic triaxial and direct shear testing. A review of the literature dealing with the dynamic and static properties including the effect of sample size and correlations between them are investigated in this section. Chapter 3 discussed the experimental program of the present study, including the apparatus and methods of analysis of the bender element and cyclic triaxial tests. Chapter 4 presents the results and discussion of the laboratory findings. Finally, Chapter 5 concludes the thesis and outlines the future research work based on the findings of laboratory tests presented in Chapter 4.

Chapter 2. Background and Literature Review

2.1. Bender Element Analysis

The shear wave velocity (*Vs*) of soil is an important parameter for seismic investigation and dynamic analysis. The bender element (BE) testing was implemented to measure *Vs* for laboratory specimens [1]. One of the bender elements generates multiple voltage signals through the specimen as a transmitter, while the other element, the receiver, receives the signals. The bender element's software detects the difference in time between the transmitter signal and first arrival at receiver *Δ(t)* for wave travel distance *Δ(x)* as shown in Figure 1 The equation of the shear wave velocity (*Vs*) is therefore formulated by dividing the difference in time *Δ(t)* by the travel distance *Δ(x)* as represented in (1). It is important to precisely detect the values of both the travel time and distance as they directly affect the accuracy of the shear wave velocity estimation [2].

$$V_S = \frac{\Delta(\mathrm{X})}{\Delta(T)} \tag{1}$$

In the traditional bender element test, the arrival time of the shear waves *Δ(t)* is analyzed by finding the difference between the input signal *x(t)* and the output signal *y(t)*. The travel time *Δ(t)* represents the summation of multiple time delays (t_1 , t_2 & t_3) in the bender element test as represented in Figure 1. The first delay (t_1) is measured between the input voltage and the transmitter response. The second delay (t_2) is measured through the transmitter and the receiver's reaction. The third delay (t_3) is calculated by finding the difference between the receiver's response and the output voltage. The most critical stage in the bender element test is in the estimation of those delays as they directly affect the accuracy of the result [3].

Lee and Santamarina specified in their study that the quality of travel time depends on the manufacturing of bender elements which controls the accuracy of the travel time $\Delta(t)$ [4]. Moreover, in another study, Gohl and Finn discovered that the coupling and alignment of bender elements in the soil specimen dominate the accuracy of the results [5]- [6]. In addition, the type of input excitation pulse performs a major role in determining the shear wave velocity as Lee and Santamarina noted [4].

Two methods could be used in order to achieve the highest accuracy in determining *Δ(t)*: The time-domain method and frequency domain method. The time-domain method is usually the preferred method due to its dependence on the first arrival wave after the travel time *Δ(t*), assuming that the wave reflection is nonexistent. The time-domain method requires a physical inspection because no systematic analyses are available for the detection of the first arrival. Measurement of the time difference between peaks and troughs is an identification process in the time domain method. However, the shortcoming of this method becomes evident due to the reflection effects. For example, the time-domain method assumes wave propagation without considering any wave reflection. A study conducted by Viggiani and Atkinson [7] used the time domain method that computed a cross-correlation between input and output signals [7].

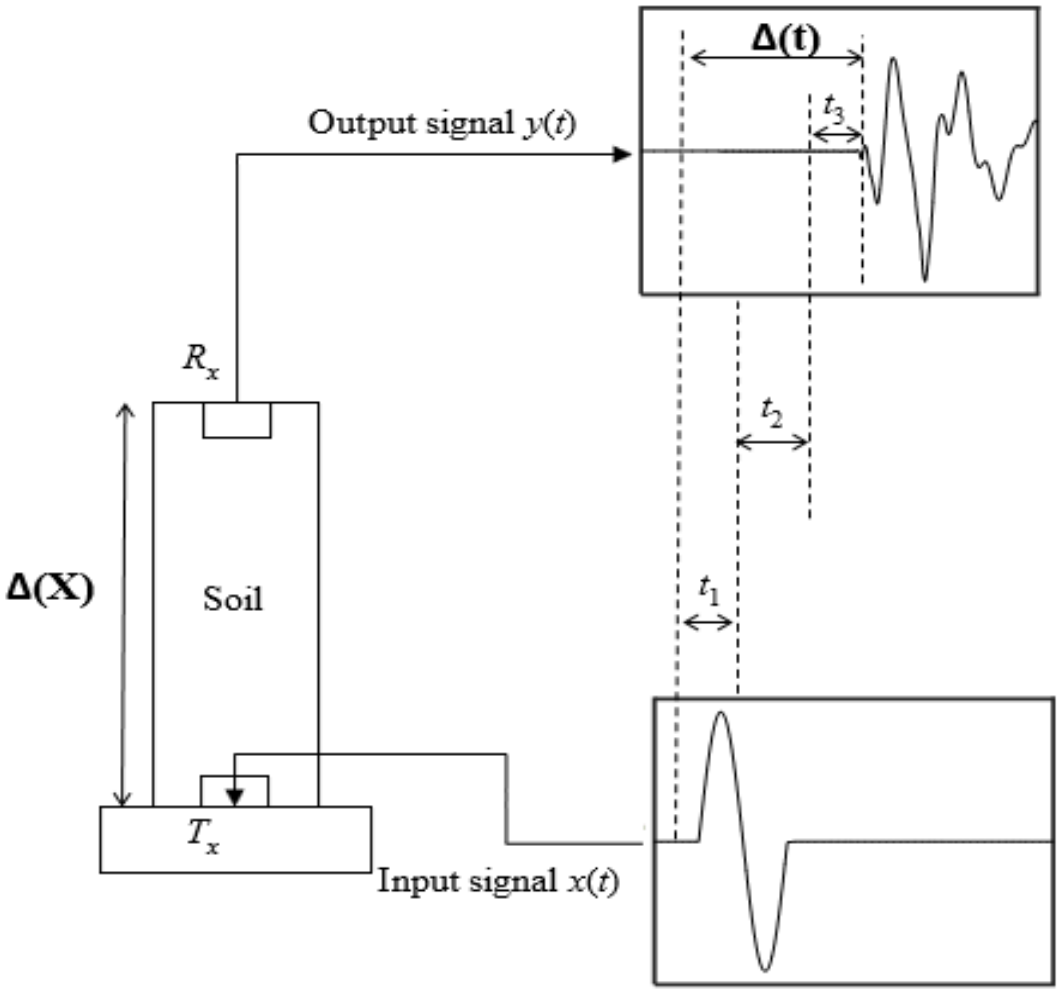

Figure 1: The time span between the major first peak of the input and output waveforms, and the wave travel distance which are using to obtain the Shear wave velocity. Also, breakdown of travel time $\Delta(t)$ into 3 major delays in conventional BE test setup [3].

Similarly, there is a limitation in the time domain method, since it assumes an identical frequency for the input and output signals. This assumption is not always true since the behavior of the signal in the soil specimen impacts the wave frequency. To solve this issue a new modification was proposed by Arulnathan et.al. [8] on the time domain method. This modification uses the second wave arrival instead of the first arrival after the travel time $\Delta(t)$. Lee and Santamarina supported Arulnathan's modification to use the second arrival of wave in order to measure the shear wave velocity [4]- [9]. They reasoned that the second arrival relied on the sample's travel distance and boundary characteristic which could optimize the error of each bender element setup. However, another limitation appeared as the second arrival becomes too weak to be reliably detected, and therefore the wave cannot be used to represent all bender element setups.

Due to these limitations of the time domain method, the frequency domain method was suggested. The frequency-domain method analyzes the signals with respect to frequency, rather than time. The frequency-domain graph represents the original signals lies within each given frequency band over a range of frequencies. In the frequency domain method, the phase angle (φ) of the sinusoid wave should be determined in order to recover the original time signal.

The accuracy of the frequency domain method relies on π-point identification. The π-point identification is a method in which a sinusoidal sweep is performed manually [10]. Sachse and Pao assumed that the input sine frequencies that result in a perfect phase were shifted between the signals and should be picked as the π-point frequencies [10]. As Eq. 2 represents, there is a relationship among input sine frequency (f), shear wave velocity (Vs), wavelength (λ), travel length of the wave (L), and phase angle (φ) to obtain the phase angle.

$$V = f\lambda = 2\pi f \frac{L}{\phi} \tag{2}$$

The linear relationship is illustrated by plotting the sine frequencies against the respective phase angles and the slope gives an estimation of $\Delta(t)$. The linear relationship is illustrated by (3).

$$\Delta(t) = \frac{1}{2\pi} = \frac{d\phi}{df} \tag{3}$$

The frequency domain is more precise than the time domain; however, it consumes more time and only a limited number of π-points can be recorded, since the identification of the π-points requires a manual sweeping. Greening and Nash achieved a setup that has a continuous sine sweep and obtained a plot relation between the unwrapped phases and frequency. Camacho-Tauta et.al. [11] performed a comparison between the estimated shear wave velocity that was achieved from the bender element using the frequency domain method [11] and the Vs that were obtained from the resonant column (RC) tests. Alvarado and Coop evaluated the performance of the bender element system by setting different voltage inputs and measuring the voltage outputs [12]. Viana da Fonseca et al. [12] implemented the concept of the frequency domain by using the moving windows algorithm for the unwrapped phase that was plotted for different frequency bandwidths [12].

The bender element (BE) testing is a well-established test that is used to determine correlations between the shear wave velocity (*Vs*) and any soil parameters i.e. the confining pressure ($\sigma 3$), void ratio (e), etc... A study involving the piezoceramic bender element was developed by Víctor Rinaldi, which conducted a correlation between the shear wave velocity and isotropic confinement pressure on dry silica sandy specimens. Figure 2 illustrates the developed correlation between shear wave velocity and confinement pressure [13]. Víctor Rinaldi used the typical power function shown in (4) to express his correlations.

$$V_S = A\sigma^B \tag{4}$$

where *A*, and *B* were the correlation coefficients that were adapted for dry silica sand by several regression models. Víctor Rinaldi [13] has implemented both methods; the time domain method and the frequency domain method, in his study for validation purposes. Theoretically, the accuracy of the correlation developed by Víctor Rinaldi [13] is fair enough since it's based on estimation of shear wave velocity from two methods (Time domain method and frequency domain method). Moreover, the test established an analysis of the damping ratio (ξ) based on the frequency domain [13].

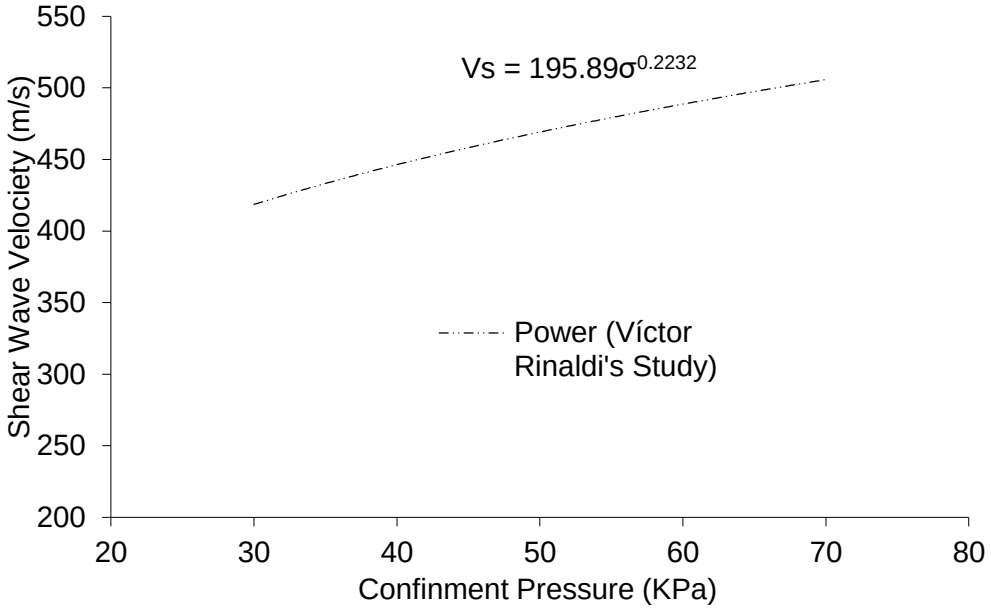

Figure 2: Variation of shear wave velocity with the confinement of dry silica sandy specimen using the time domain method [13].

2.2. Cyclic Triaxial Analysis

CT is widely used in the geotechnical laboratories to evaluate the dynamic and static properties under cyclic and static loading conditions. Moreover, the CT test simulates the conditions that may include excessive dynamic loading obtained from earthquakes, wind turbines, passing vehicles, sea waves and vibrating machines. In fact, several devices measure the dynamic properties of soil and the user should choose the device that performs the most accurate representation of the field condition.

Additionally, the CT estimates the dynamic properties of soil for stains between 0.001% to 1% and frequency level between 1 to 5 Hz. In contrast, another device like Resonant Column (RC) is used for lower strain levels compared to CT [14]. In the case of an earthquake, the strain range is between 0.001 to 1%, and the frequency is between 0.01 to 15Hz. Therefore, in order to simulate a condition like an earthquake, a combination of CT and RC testing should be performed as demonstrated in Figure 3.

Furthermore, the CT is capable to estimate the deviator stress with the axial stain under dynamic loading. During dynamic loading, the dynamic actuator and a couple of Linear Variable Differential Transformers (LVDT) are used to analyze the cyclic loading on the specimens through a specified waveform, i.e. sinusoidal waveform. Furthermore, the generated hysteretic loops show the ability of the specimen to store or

dissipate energy in a finite period of time as demonstrated in Figure 4 [14]. The elastic Young's modulus (E) is evaluated by dividing the deviator stress ($\Delta\sigma$) over the axial strain(E_a), as shown in (4). The corresponding shear modulus (G) is computed from Equation 6, based on the evaluated E and assumed Poisson's ratio (v). In addition, Eq.7 illustrates the criteria used to estimate the damping ratio (ξ); using the ratio between the total area of the loop (A_L) and the area of hatched triangle (A_T). The shaded area represents the area of the triangle (Figure 4).

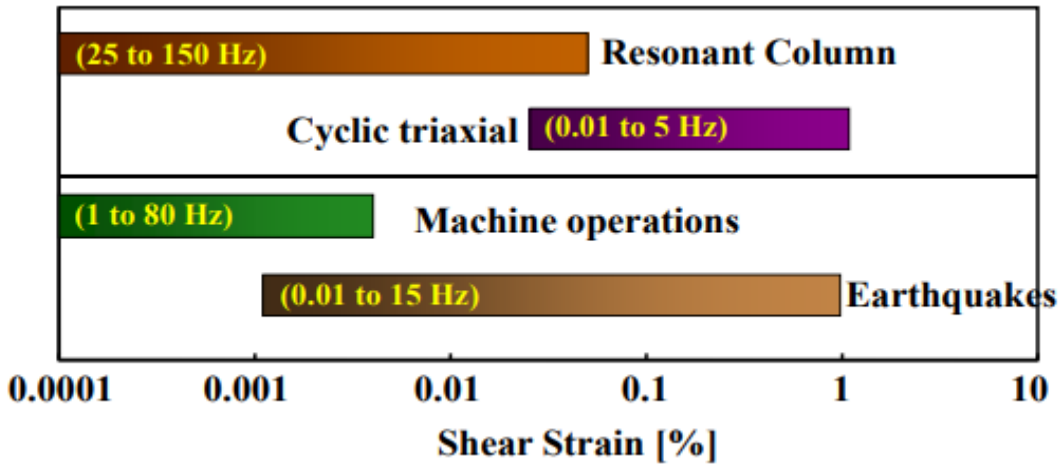

Figure 3: The shear stain and frequency level of RC, and CT devices and earthquake and machine operation.

$$E = \frac{\Delta\sigma}{E_a} \tag{5}$$

$$G = \frac{E}{2(1+v)} \tag{6}$$

$$\xi = \frac{A_L}{4\pi\ A_T} \tag{7}$$

Another study was conducted by Seed and Idriss to recapitulate the available information on the normalized shear modulus (G/Gmax) and damping ratios for the sandy specimens (Figure 5) [16]. where Gmax is density multiple to squared shear modulus (Eq.8).

$$G_{max} = \frac{\gamma}{g} * {V_S}^2 \tag{8}$$

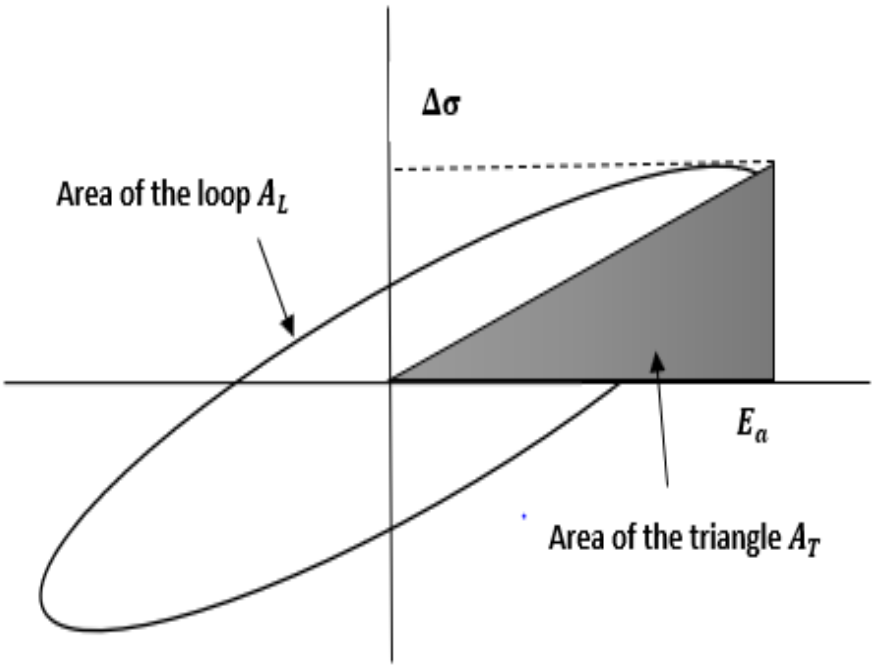

Figure 4: The typical Hysteretic loop obtained from CT test [14]

This study generated new data regarding the properties of the cohesion-less soils which provided a valuable guide in the selection of the soil characteristics. Moreover, the authors have reviewed the influence of the confining pressure on the damping ratio of dry sands from two different studies [8]- [17], as represented in Figure 6.

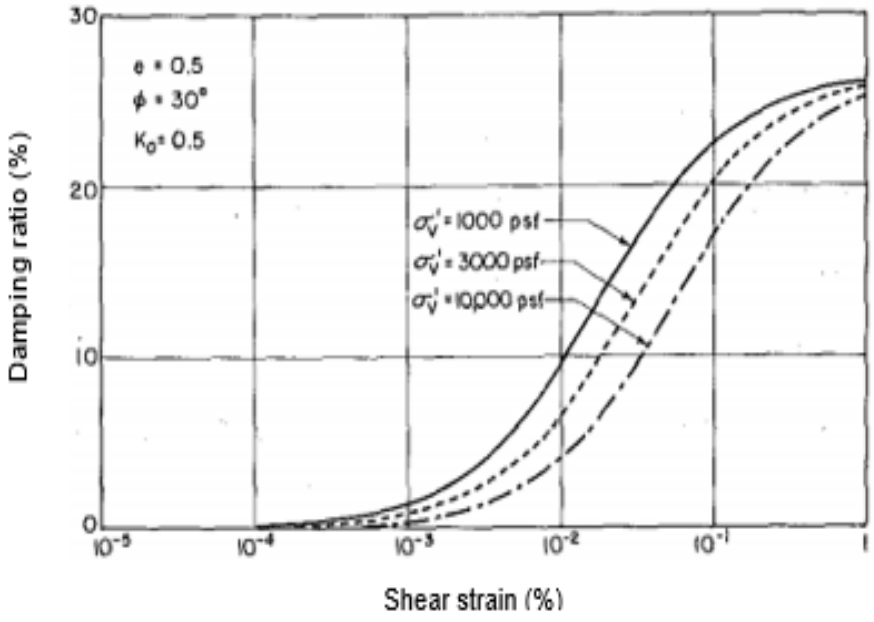

Figure 5: Influence of Confining Pressure on Damping Ratio (ξ) of Saturated Sand [15].

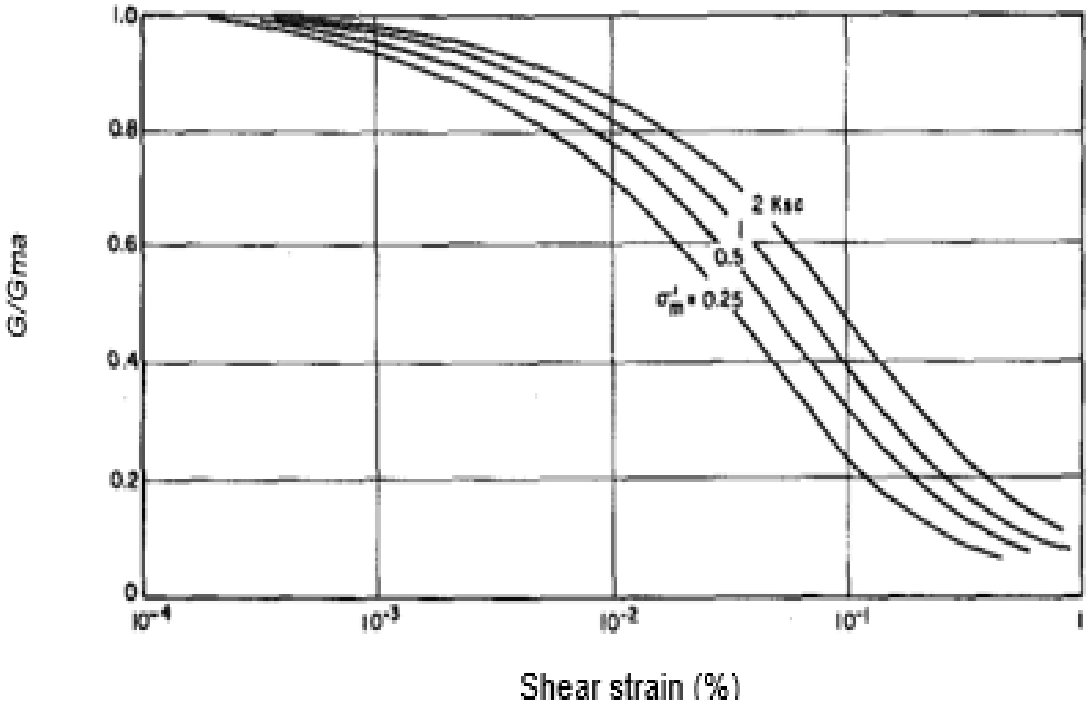

Figure 6: Variation of Shear Modulus with Shear Strain for dry sands influence [18].

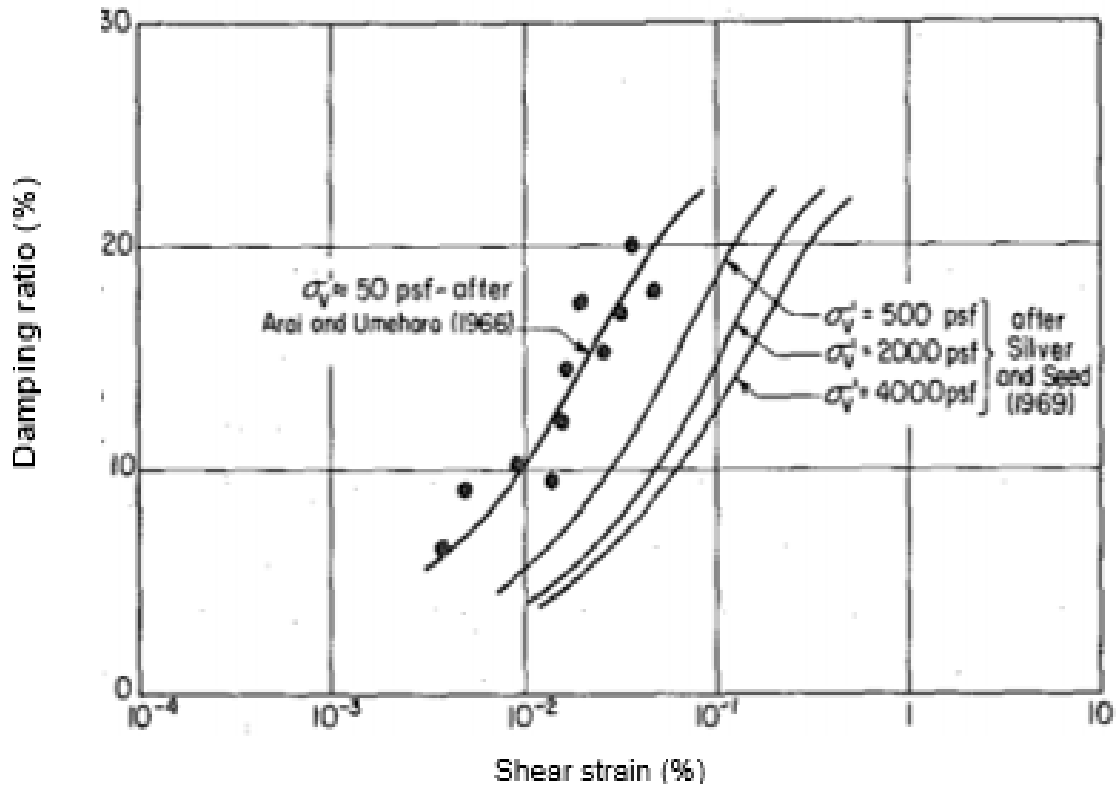

Figure 7: Influence of confining pressure on damping ratio (ζ) of dry sand [16].

2.3. Sample Size Effect

Triaxial and direct shear tests are commonly used to measure the soil strength by subjecting the soil specimens to multiple of stresses and loading conditions. In the literature, few studies observed the influence of sample size on the static soil properties [18] - [27]. Some researchers have focused on the effect of sample size on the dynamic properties [28] - [33].

2.3.1. Effect of sample size on the static parameters. Several researchers have examined different sample sizes using DS in order to investigate the influence of the sample size on the static properties of soil. The literature showed a significant effect on the friction angle as a result of different sizes specimen, especially at high confinement pressures. Table.1 summarizes the different geometries of the sandy specimens that were considered by different researchers in order to study the effect of sample size on static properties.

In his research, Scott [19] has conducted a study on two different sample diameters: 38 and 100mm to evaluate the effect of the sample size on the maximum axial strain. Moreover, he maintained an identical confining pressure and void ratio for all tested samples [19]. He noticed a significant increase in the failure rate of the axial strain when the sample diameter decreased [19].

Table 1: The variation of sample sizes tested by multiple researchers using the triaxial set.

Sample Size (mm)		**Material**	**Researchers**
Diameter	**Height**		
50.8	101.6	Ottawa and Mississppi sand	[18]
38	76	Leighton Buzzard Sand	[19]
50	100	Unimmin Sand	[20]
74	150	Monterey Sand	[21]
100	200	Sydeny sand	[22]
1000	1500	Loire river sand	[22]

In another study by Garga [23], the impact of sample geometry on the shear strength using two residual soil that derived from basalt was studied: dense basaltic and vesicular basaltic soils. He studied the influence of the shape of the specimen (square versus cylindrical specimens) on the results provided by the direct shear and the triaxial tests. The square specimens were 500 x100 mm whereas the cylindrical specimens were 36 mm in diameter. The results clearly indicated an effect of the ground fissure on the shear strength of dense basaltic soil whereas it was absent in the vesicular soil. In his study, the smaller cross-sectional area showed a reduction in the shear strength of the cohesive materials [23].

In an additional study by Wan et al. [24], it was highlighted that the sample size has a clear influence on the shear strength of the sandy soil [24]. Four sample diameters were prepared to have a diameter of 35, 75, 150, and 300 mm in a dry condition were tested under a confining pressure of 100 kPa. The study highlighted the impact of sample size on the relationship of the deviator stress versus the axial strain. A relationship between volumetric strain and the axial strain was also established, as illustrated in Figures 8-9, where the volumetric strain was defined as the unit change in the original volume. Figure 8 represents the relation that was developed by Wan et al. [24] between the stress and strain for four different diameters. All of the curves overlap within the elastic stage, however they start to diverge at the yielding stage. The elastic modulus represents the slope of the elastic data points; therefore, the sample size didn't have a significant impact on the elastic modulus. In contrast, the sample size affected the stresses that occurred during the yielding stage significantly; i.e. the smallest sample diameter demonstrated the maximum deviator stress among the rest of the diameters. However, the larger sample diameter yielded the minimum deviator stress [24].

Figure 9 presents the relationship between the volumetric strain and axial strain for the different sample geometries [24]. The maintained dilatancy rate is identical for all sample sizes at the lower strain rates, however it diverged as the sample geometry increased at high axial strain levels. Therefore, the smallest sample diameter was responsible for the greatest dilatancy rate in the volumetric strain [24]. In most cases, the larger sample diameter showed the lowest rate of change among all sizes. The possible reason behind this trend was the shear displacement of the soil particles; the larger specimens enhance a greater shear displacement than the shorter specimens that limited the movement of the particles at the same axial strain level. In other words, the

large specimens allow the reorientation of the soil particles, while the smaller samples trap the particles redistribution [24].

In their research, Cerato and Lutenegger [25] studied the effect of the shear box size on the friction angle by testing five different types of sand using the direct shear test [25]. The five types were tested in three square shear boxes of varying sizes 60 mm, 101.6mm, and 304.8mm. Each sample was prepared at three relative densities; dense, medium, and loose [25]. The results show that the shear box size has a slight influence on the obtained friction angle. For example, the 60 mm shear box caused only a 10 degrees increase in friction angle compared to the 305 mm specimen [25]. Moreover, some other researchers have validated this study by considering a wider range of shear box sizes [26]- [27].

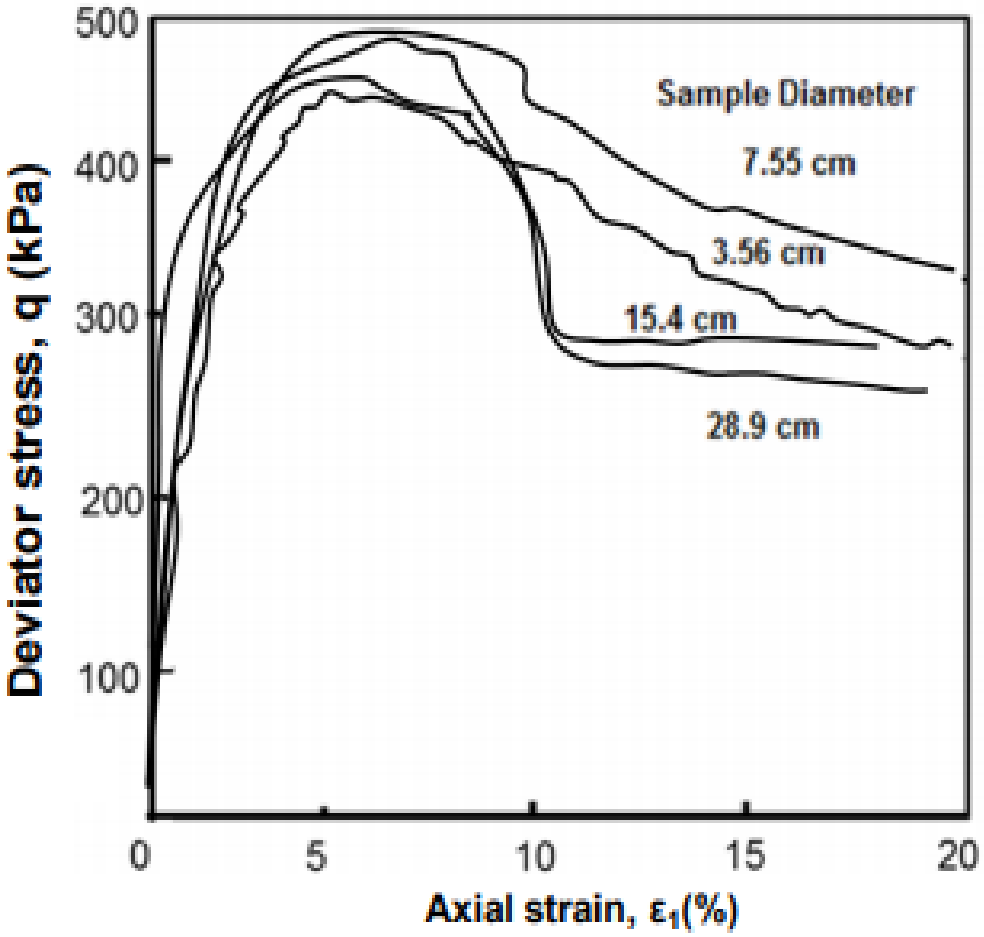

Figure 8: The relationship between the deviator stresses versus axial strain among a divergent sample sizes of Ticino 9 sand [24].

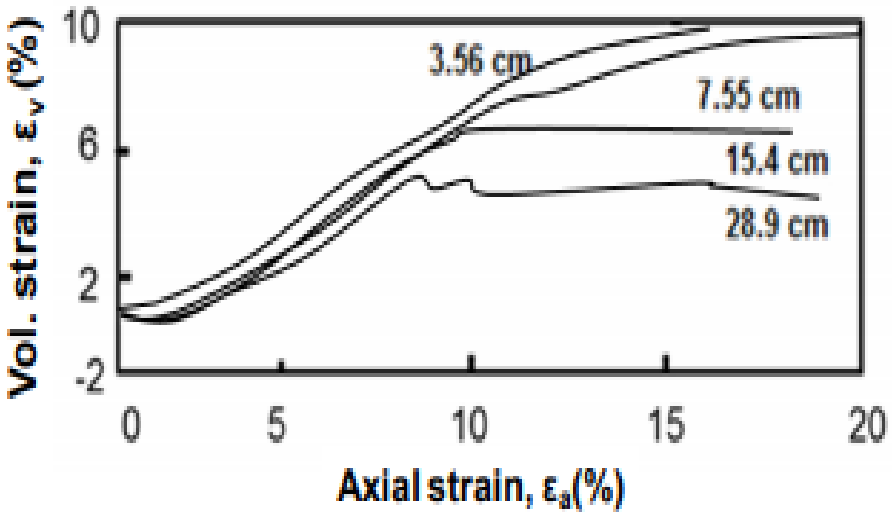

Figure 9: The relationship between volumetric strain versus axial strain among divergent sample sizes of Ticino 9 sand [24].

2.3.2. The effect of sample size on the dynamic properties. Several researchers have attempted to study the impact of sample geometry on the dynamic properties. Kovacs et al. [28] have conducted a cyclic triaxial test on dry sand using a 12in diameter specimen with specimens' lengths of 1in, 2in, and 4in. The results showed a lower damping ratio (ξ) when the sample size increased. The diameter/height (D/H) ratio was observed to influence the shear modulus at low shear strains of less than one percent. The relationship was also observed to have a slight influence at higher shear strains and at failure. Additionally, the outcomes of the tests illustrated that the hysteretic damping decreased for all results of the shear strain tested as the D/H ratio increased.

Lee has conducted a study on two different kinds of limestone [29]. The results of that study depict that both of the tested limestone showed a decrease in the tensile strength as the particle size increased [29]. Likewise, Vucetic et al conducted a similar study on the effect of height on the diameter ratio and membrane stiffness [30]. They discovered a significant influence on the resistance of the clay using a static NGI simple shear machine. Regarding the size effect, the results showed that H/D did not have a substantial impact on the strength nor the deformation properties of the examined clay [30]. In another research, Chan et al. [31] has conducted a study on three different diameters (D = 33, 40 and 50mm) of clay specimens; and by keeping constant height-to-diameter ratio (D/H) of 2. Chan et al. [31] conducted the BE testing on identical soil types and BE sensors. It was found that the specimen size does not impact the shear

wave velocity [31]. However, rock specimens showed a significant effect on the shear wave velocities [32].

A similar study was conducted by Yamashita et al. [33] on different sample geometries of Toyoura sand. The samples that were tested in the BE setup had D/H ratio that varied from 0.53 to 2.18. The results indicated that the sample size has a slight effect on the evaluated shear modulus [33].

2.4. Correlation between Vs and SPT-N value

The standard penetration test (SPT) is a field test that provides information about subsurface soil which can be used for the foundation and geotechnical designs. The standard penetration test (SPT) is an ASTM standard [34]based on the number of blows required to penetrate a soil under standard conditions and equipment. A hollow tube that has an outer diameter of 50 mm, an inner diameter of 35 mm and a length of 650 mm is used (Figure 9). The tube is hammered into the ground by a hammer that weighs 63.5kg. The hammer is guided by a tube length of 760 mm to maintain the vertical alignment of the hammer drops. Based on the number of strikes to achieve a standard penetration, the number of blows are recorded. However, the initial recording of the first 150 mm into the ground is considered. The total blows that are required to achieve a penetration of 300 mm after the initial seating of 150mm represent the penetration resistance of the soils as the N-values. Often, the blow count provides an indication of the soil type, ground density and soil penetration resistance shown in Table 2.

During the SPT, the number of blows (N-SPT) has to be corrected using several correction factors. The correction factors are machine efficiencies, borehole diameter, rod length, and sampler impact. These factors adjust the *N* values to N_{60} values. Eq. 9 illustrates the modification equation [35].

$$N_{60} = \frac{N \times \eta_H \times \eta_B \times \eta_S \times \eta_R}{60} \quad (9)$$

where, *N* is the raw number of blows, the η_H is the correction factor for the hammer efficiency, η_B is the correction coefficient for the borehole diameter, η_S is the adjustment constant for the sampler type, and η_R is the correction factor for the rod length.

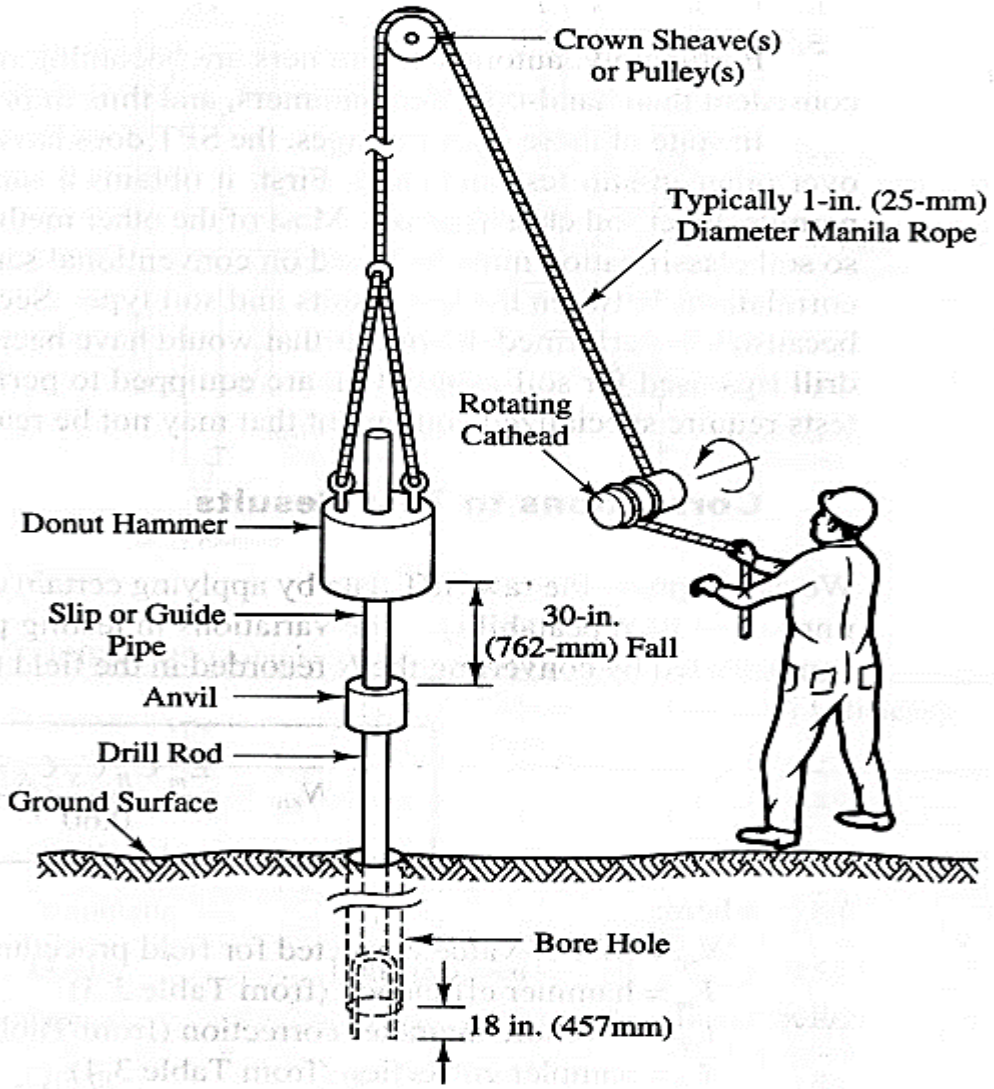

Figure 10: The equipment of SPT as per ASTM standard [35]

Table 2: Correlation of N to Relative Density, and Friction Angle [35]

SPT	Soil Packing	Relative Density	Friction Angle (°)
<4	Very Loose	<20	<30
4-10	Loose	20-40	30-35
10-30	Compact	40-60	35-40
30-50	Dense	60-80	40-45
>50	Very Dense	>80	>45

The SPT-N value is taken into consideration in several empirical geotechnical engineering problems such as foundation design. Several publications highlight the correlation between the SPT-N value and the engineering soil properties for geotechnical engineering purposes. Researchers have conducted seismic site classification based on empirical correlations between SPT- N value and the *Vs*.

Furthermore, the SPT-N value is used to develop low stain dynamic soil properties for different regions. The correlation between *Vs* and N-value has typical a power functional form as expressed in (10).

$$V_S = AN^B \tag{10}$$

where *A*, and *B* were the correlation coefficients that were adapted by several regression models introduced in the literature [36]- [37]. A and B are generally found to be inversely proportional to each other [38]- [37].

Moreover, Table 3 presents a summary of the correlations that were developed for multiple regions (*Vs* is in m/s). The previous studies introduced the consistency in the experimental correlations for the clay specimens compared to the sandy soil. The correlations of the clayey soil were identical, however; the correlations of the sandy soil were inconsistent. In contrast, the sandy soil showed higher shear velocities than the cohesive soils [39]. Therefore, the soil type becomes a critical parameter for the seismic site investigation. In another study, Ohta and Goto [40] developed the correlations based on the type of soil. They sorted the type of soil according to their average shear wave velocity. Often, the gravel had the greatest average shear wave velocity than sand and clay as represented in (11) [40].

$$V_S(Gravel) \geq V_S(sand) \geq V_S(clay) \tag{11}$$

Rollins et al. [41] reported an experimental correlation between SPT-N and shear wave velocity. This study was conducted based on the concept of including the effective stress in order to improve the shear wave velocity. Rollins rejected the samples that had the values of (SPT-N) less than 2 and more than 50 from the analysis due to fact that it has poor reliability [41].

In addition, a comprehensive study conducted by Anbazhagan proposed a correlation between the SPT-N and shear wave velocity for Indo-Gangetic Basin soil. This particular study used the multichannel analysis of surface waves (MASW) test to estimate the Vs for different types of soil [42]. Anbazhagan used MASW to ensure the reliability in the field seismic surveys, since its more suitable in measuring the dynamic properties at low strain levels. Moreover, Anbazhagan obtained a total of 215 data pairs of uncorrected SPT-N and Vs for overburden stress correction. These data points are based on 47 seismic surface wave tests using MASW in order to consider a variety of

soil types [42]. Also, the subsurface profiles of the region showed low-to medium-compressible clay and silts to poorly graded sand in wide range depths. Also, he simplified the behavior of combined soil in this region in one comprehensive correlation to account for the feasibility of the correlation in the engineering field especially, when the detailed soil investigation is missing [42]. Moreover, the relative density was measured from in-situ samples using undisturbed samples in order to estimate the low strain shear modulus G_{max} [42].

In another study, Dikmen [43] proposedan experimental correlation that is valid for all types of soil. This study developed the correlation between shear wave velocity and soil penetration resistance. This was based upon borehole logs that were constructed in Eskisehir, Turkey. Dikmen performed the SPT-N and CPT for 309 locations to obtain more continuous soil parameter profiles [43]. Also, he used the seismic test of MASW and refraction for 9 locations. Dikmen executed 700 disturbed and undisturbed soil samples for further laboratory testing and he characterized their physical properties from sieve analysis, consolidation, water content analysis, and triaxial shear tests. A total of 193 data pairs of uncorrected SPT-N and Vs (overburden stress corrected) were obtained. Finally, he performed a non-linear regression analysis based on those data pairs [43] . Table 3 represents the summary of correlations that were developed between Vs and SPT- N values.

Table 3: Summary of the correlations

Author	Correlation	Type of the soil	Country	Reference
Khan et.al (2015)	$V_S = 94.7N^{0.35}$	All	UAE	[44]
Anbazhagan (2012)	$V_S = 60.2N^{0.56}$	Sandy	India	[42]
Dikmen (2009)	$V_S = 73.0{N_{60}}^{0.33}$	All	Turkey	[43]
Hanumantharao (2008)	$V_S = 82.6N^{0.43}$	All	India	[36]
Rollins et al (1998)	$V_S = 63.0{N_{60}}^{0.43}$	Gravel	USA	[41]
Lee (1990)	$V_S = 57.0N^{0.49}$	Sand	USA	[45]
Imai et.al (1982)	$V_S = 97.0N^{0.31}$	All	Japan	[37]
Ohta et.al (1978)	$V_S = 85.3N^{0.35}$	All	Japan	[40]
Imai (1977)	$V_S = 91.0N^{0.34}$	All	Japan	[39]
Ohsaki et.al (1973)	$V_S = 82.0N^{0.39}$	All	Japan	[38]

2.5. Geophysical Field Tests

For several years, engineers used geophysical testing to evaluate different properties of subsurface soils. They were mostly implemented in foundation applications where geophysical testing was utilized to obtain the general characteristics of the soil in order to provide a suitable type of foundation. Specifically, geophysical testing determines the dynamic properties of the soil such as shear wave velocity, attenuation characteristics, and compression index. Furthermore, geophysical methods provide the stiffness and moduli of soils in the field. Since the field test are performed are based on in-situ soils, it is more representative of actual soil properties. The results are based on the actual behavior of soil strata and are not affected by sample scaling and disturbances effects. The shear wave velocity is used in many applications such as seismic analysis, site classification, soil-structure interaction, site response analysis, and hazard analysis.

In geophysical testing, waves are generated by the hammer strikes at the ground surface. Receivers are placed along a predetermined line (receiver array) to record the ground motion due to propagating waves. Digital equipment, such as seismographs record and perform the analysis of the data. A seismograph record may contain the direct waves which represent the waves that arrive at the receiver directly and reflected and the refracted wave as illustrated in Figure 11. The second node illustrates the reflection point of the waves where the wave is reflected in the receiver point. The third node shows the receiver point where all of the waves are collected and analyzed. Recently, the geophysical methods have improved significantly in hardware setup and analytical techniques.

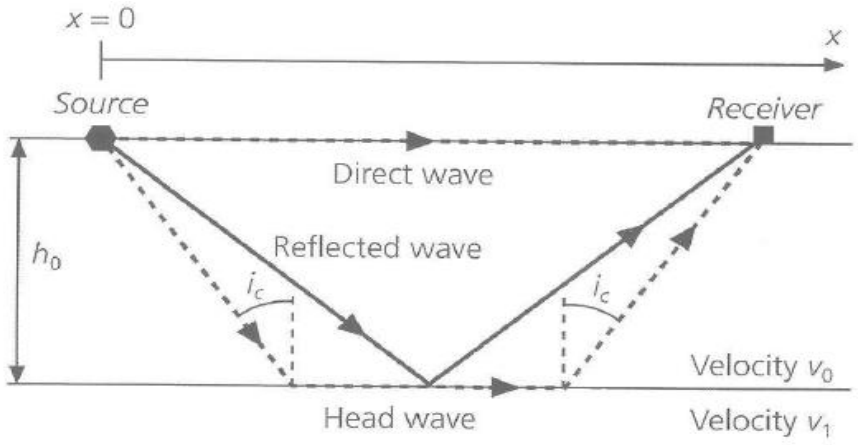

Figure 11: The shape of the generation of seismic waves [46]

2.5.1. Seismic refraction method. Typically, compression waves are generated when the seismic refraction test is performed because the compression waves are the fastest among all waves, therefore; the first arrivals at receivers always corresponds to compressional waves [46]- [47]. The shear wave velocities are estimated in the seismic refraction method by converting the compression wave velocities through assumed Poisson's ratio. Alternatively, the horizontal geophones can be utilized to detect the shear wave velocities directly [48]. The typical setup of a seismic refraction test involves a wooden plank fixed under a large weight which is struck with a hammer on its sides sequentially to simulate compression, polarized shear, vertical shear, and horizontal shear waves.

The seismic refraction method is the simplest, most common, non-invasive, less time consumption, practical, and most reliable among all geophone based methods considered for soil subsurface investigations. However, it could be inconvenient as it causes noise, which limits its use in residential areas. Therefore, some alternative methods have been suggested to obtain the results in such residential zones. According to the ASTM standard, the seismic refraction method was reported as D5777 [49]. Essential features of the seismic refraction test are accomplished for certain site conditions (e.g. when the site's purpose is to obtain an average shear wave velocity of subsurface instead of layer by layer velocity) [50].

The seismic refraction method is typically conducted to detect the depth of bedrock, water table, and define the lithology. The seismic refraction method considers mechanical properties of the site materials such as type of rock, characteristic of the material, rip-ability, degree of weathering, and other geologic information.

The traditional experimental setup of seismic refraction test involves an array of low frequency vertical and horizontal geophones [51]. The vertical geophones are frequently used to determine the measurement of the vertical motion of the particles due to their wide commercial availability and lower-price. However, the shear wave velocity is not a deterministic element in these particular tests since the particle motion during surface waves is approximate to a retrograde ellipse. Also, both vertical and horizontal motions should be optimized to the frequency of vibrations [52]

The field results that are collected from the seismic refraction test are analyzed by diverse conceptual models, such as the Generalized Reciprocal Method (GRM) [53],

Ray-tracing [54]- [55], and delay time inversion [56]. All results are plotted as the velocity against the depth of the soil, which is represented by the profile relationship. The graph displays the 1D or 2D variations of the velocities. Furthermore, seismic refraction tomography has been implemented to develop the plot of the complex 3D velocity models [57]- [58].

Both traditional and tomographic methods have advantages and limitations. For example, the is better technology in determining the depth of the bedrock layer, provides a comparatively sharp layer boundary model, and is faster to perform [59]- [60]. However, the tomography is more suitable for the sub-surfaces applications where the velocities increase at a slower rate with depth, especially when complete models of the velocity are required [60]. Furthermore, there are several assumptions in the traditional method that reduces its reliability and provides an advantage to the tomography method in terms of accuracy. Moreover, the implementation of seismic tomography performs resolvable techniques of the vertical velocity variations [60] as shown in Figure 12.

Moreover, tomography is a better choice in terms of data analysis when the condition of the site needs to be identified due to the availability of the equipment and expertise [61]. However, tomography has its limitations in terms of imaging the sharp and high contrast boundaries [61]. Some computer applications were involved in developing the data processing of seismic refraction based on both types of techniques discussed above:

1. SIPQC - Rimrock Geophysics® [62]- [63].
2. MacRay – [64]- [65].
3. Interpex IXSEG2SEGY [64].
4. Vista 7.0 (Seismic Image Software Ltd.)
5. ‘SeisOpt22D’ from Optim software® [62].
6. Seismic transmission tomographic algorithm [66].
7. Seis Imager Pick Win data analysis (OYO Corporation 2001)
8. ATOM-3D code [67].

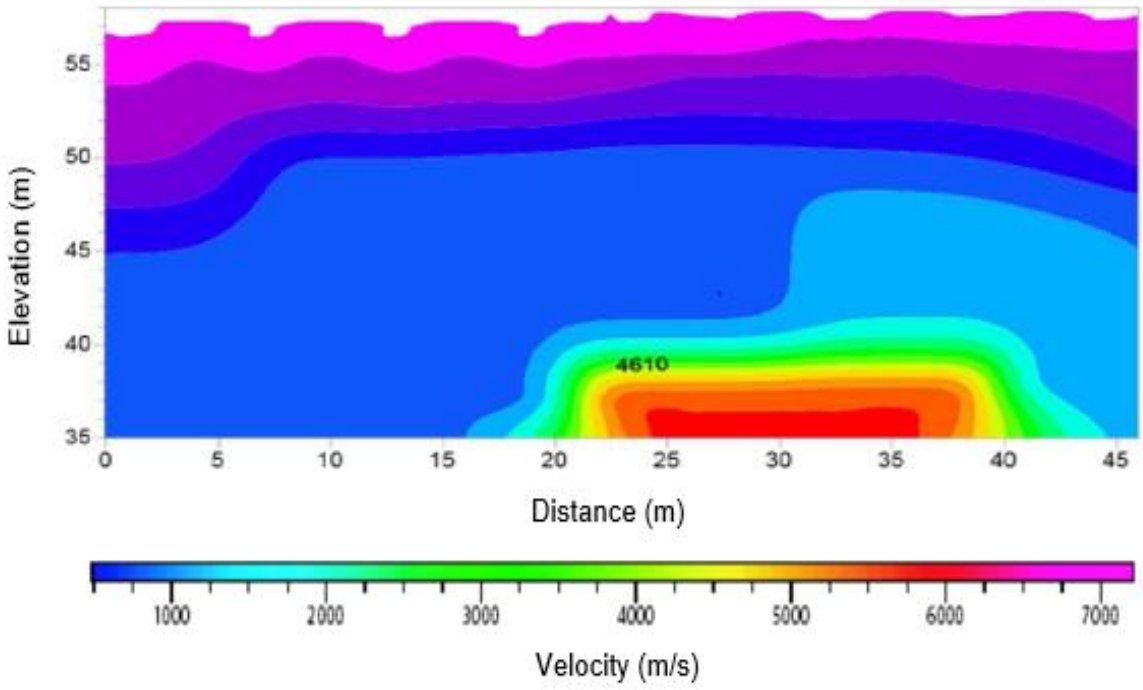

Figure 12: Seismic refraction Tomography [60].

The refraction test does not require boreholes; therefore, the cost is reduced by about four times compared to an invasive test such as a Down-hole seismic Test [67]-[68]. Furthermore, the refraction method provides reliable data in terms of determining the depth of bedrocks since the bedrocks traditionally have a high wave propagation velocity than the overburden strata [69].

The major limitation of the refraction test is its inability to detect the blind zones, i.e., a thin layer that is located between two main layers [70]. Therefore, the test is inadequate for sites that have highly non-homogeneous soil. It also provides unreliable values of the shear wave velocity at the sites that have a high water table level. False results are obtained due to the lack of detection of the bedrock depth since saturated soil has a higher velocity than unsaturated soil [71]- [72]. Moreover, the results obtained from the shallow depths using this particular test is not reliable since its restrained in detecting the variations in the soil profile such as testing the soil layer before and after the compaction [73]. However, the test performs a credible result for depths between 30 to 40 meters and a soil profile with less background noise [63], and water-table. In the seismic refraction testing array, the length is influenced by the depth of interest. Therefore, the test has a major drawback in site areas where the geophone arrays require a length of 4 to 5 times of required depth.

2.5.2. Seismic reflection method. Reflection is a geophysical method based on the principle of seismology to perform the properties of the subsurface soil using reflected seismic waves. The seismic waves as mechanical disturbances travel in the ground at a certain speed that is governed by the seismic impedance between the soil layers. While traveling through the ground layers, some energy will be reflected off because of different impedances between the layers. i.e., where a significant variation occurs in the conductivity and the density of the propagated waves and therefore some energy will be reflected. This analysis provides the velocities of the propagating waves through the soil layers and provides a full image of the subsurface conditions by analyzing the pathways of the waves.

The results obtained from the reflection method is fitted with several possible subsurface models. Also, it is sensitive to relatively small errors in the data collection, analysis, or process. As a result, great attention should be taken at the interpretation stage. One of the major limitations of the seismic reflection method is its performance through testing in a noisy geologic formation. The more complicated the layer formation is, the more complex the obtained data becomes. This method has the ability to investigate the geological formation of depths in excess of 1000-meter, which makes it useful in several applications in engineering and environmental areas and in the petroleum industry since it has the ability to explore for the oil and gas trapped in the sedimentary layers. It has the ability to resolve the soil layers that have a relatively high water table. Furthermore, the seismic reflection method is suitable for marine applications. The use of shear waves is used in the seismic reflection method to enable the transmission of shear waves through water and produce high-quality results.

From the technical perspective, the equipment used for the seismic reflection tests is similar to the equipment used for seismic refraction tests. However, the difference lies in the diversity of data collection and analysis techniques. The setup enhances the performance of the equipment in deeper construction by maximizing the reflection energy throughout the test. Since the seismic reflection method is capable of exploring large depths, it is superior to the seismic refraction method. However, the reflection data is complex to analyze since the first arrivals must be classified by overlapping shots at different geophone locations. Stacking and filtering techniques help in simplifying the complexity of the data.

The seismic reflection method is able to detect blind zones and requires a relatively shorter geophone array length than the refraction method at the same depth of investigation. The seismic reflection method is not efficient at resolving structures that are shallower than 15 meters. At shallower depths, the reflections of the wave drop due to the near field effects of the shot. Therefore, the reflections of the waves from deeper boundaries are easier to distinguish and isolate than the shallow depths.

2.5.3. Comparison of seismic refraction and reflection methods. There are numerous differences between seismic refraction and seismic reflection in terms of equipment setup, required site conditions, relative costs, target, and the vertical and horizontal resolutions. The project authorities decide based on the available information of the project specifications i.e., the required investigation depth, the site area, the soil profile conditions, the budget effectiveness analysis, and the required resolution. Table 4 has summarized important comparisons between the two techniques.

Table 4: Comparison of Seismic Refraction and Seismic Reflection methods.

	Refraction	**Reflection**
Typical Targets	Horizontal layers at depths less than 100 feet	Horizontal to slightly dipping contrast at depths greater than 50 feet
Required Site Conditions	Spatial dimensions larger than 5x the depth of the target.	None
Vertical Resolution	10 to 20 percent of the depth	5 to 10 percent of the depth
Lateral Resolution	~1/2 the geophone spacing	~1/2 the geophone spacing
Effective Practical Survey Depth	1/5 to 1/4 the maximum shot-geophone separation	>50 feet
Relative Cost	$	$x3 to $x5

Chapter 3. Experimental Program

3.1. Tested Soils

Undisturbed sandy soil samples were taken from various sites of the capital city of the United Arab Emirates, Abu Dhabi. The samples were collected from sites that cover the major developing areas. The sandy specimens obtained from the Khalifa City region (Abu Dhabi, UAE) are used for the study. In addition, the samples were collected from different depths to represent different confining stresses. The samples were numbered and noted down alongside their relevant information such as location, depth, and SPT-N values. Table 5 summarizes the material description, depth and SPT-N value for the tested samples. Additionally, standard tests and index densities were performed in the laboratory. Table 6 illustrates an example of the borehole log including the material description, depth and SPT-N value.

Table 5: Samples identification

Sample Name	The Borehole and site number	Material Description	Depth (m)	SPT-N Value
Sample A	BH1, Site number 1	Weak, light brown to light grey sandstone with inclusions of crystalline gypsum	11 to 12	50
Sample B		Dense to very dense, poorly graded sand with silt and trace fine to medium gravels	7 to 8	48
Sample C		Medium dense to very dense, poorly graded sand with silt and trace fine to medium gravels	1.5-2	21
Sample D	BH2, Site number 2	Medium dense, light grey to grey wet, non-plastic, silty sand, trace fine gravel, shell fragment, (SM)	4-5	17
Sample E	BH1, Site number 3	Medium dense to very dense, light brown to light grey wet, non-plastic, silty sand, trace fine gravel, shell fragment, (SM)	5-6	14

Table 6: Typical borehole log with SPT-N value

Depth Below Ground Level (m)	Soil description	Layer thickness	Legend	Soil classification	Sample Type	Depth	SPT N-Value
0.0 1.0 2.0 3.0 4.0 5.0 6.0 7.0 8.0 9.0 10.0 11.0 12.0.	**Fill Materials (0.01-1.5m).** **SILTY-SAND (1.5-9.6) m** **MUDSTONE (9.6-50) m**	**1.5m** **8.1m** **BELOW 9.6m**		**SP-SM** **SP-SM** **SP-SM** **SP-SM** **SP-SM**	**DISTURBED UNDISTURBED SPT** **UNDISTURBED SPT** **UNDISTURBED SPT** **UNDISTURBED SPT** **UNDISTURBED SPT** **UNDISTURBED SPT**	**1** **2** **3** **4.5** **6** **7.5** **9**	**N=20** **N=24** **N=26** **N=24** **N=45** **N=48** **N=50/27**

3.2. Test Equipment

The triaxial equipment and bender elements were supplied by VJ Tech to perform various tests on the soil specimens. The equipment consists of bender elements fitted with top caps of different sizes, Dynamic Servo Controller (DSC), triaxial cell, Bender Element Scope (BES), Confining Pressure Controller (CPC), and Back Pressure Controller (BPC), as shown in Figure 13. Table 7 presents a description of each component in the triaxial equipment.

3.2.1. Bender element (BE) test. In the bender element test, a small shearing movement was produced over one end of the cylindrical soil specimen as the voltage signal was applied by recording the arrival of waves at the other end. Bender elements can test different sample dimensions such as, 7cm × 14cm, and 10cm × 20cm. For

each dimension, the corresponding cap and base was used. The effect of sample size was evaluated by testing the same soil under similar conditions, but using different sample dimensions.

In the bender setting, the pulse frequency was about 5kHz and a time window of 2mSec. Amplitude of 10 volts was used to obtain the highest amplitude of the wave to better detect the arrival signals. To enhance the signal-to-noise ratio of the waves, the stacking of at least 10 signals was adapted. Furthermore, to increase the reliability of the first shear wave arrival, the inverted signals was also recorded. The confining pressures of 20, 40, 60, 70, 80, 100 and 120kPa were used. All the captured signals were analyzed using Excel to calculate the shear wave velocity.

Polarity inversion in received signal was used to avoid an erroneous identification of the arrival time. The BE outputs is an electrical signal which depends on the wiring of the BE receiver. The BE data was conducted twice; once when a positive signal was applied to the BE transmitter producing a negative signal on the BE receiver, and once when the inversion was applied to impose a change in polarity. Both signals were stored and named consistently. Both singles were plotted in one chart to identify the arrival time of the shear wave (S-Wave), as presents in Figure 14.

Table 7: The role of each element in the triaxial equipment.

Element	**Role**
Dynamic Servo Controller (DSC)	The DSC is used to communicate between the software and machine components.
Triaxial cell	The cell uses water to produce confining pressure.
Bender Element Scope (BES)	The BES controls the bender elements in receiving and evaluating the preoperational waves throughout the soil sample.
Confining Pressure Controller (CPC)	The CPC used to apply to confine pressure during the test.
Back Pressure Controller (BPC)	The BPC controls the amount of pore water pressure during the test.
Actuator	Applies axial load to the specimen in static and dynamic modes.
LVDT	Measure the displacement (strain) of the specimen.

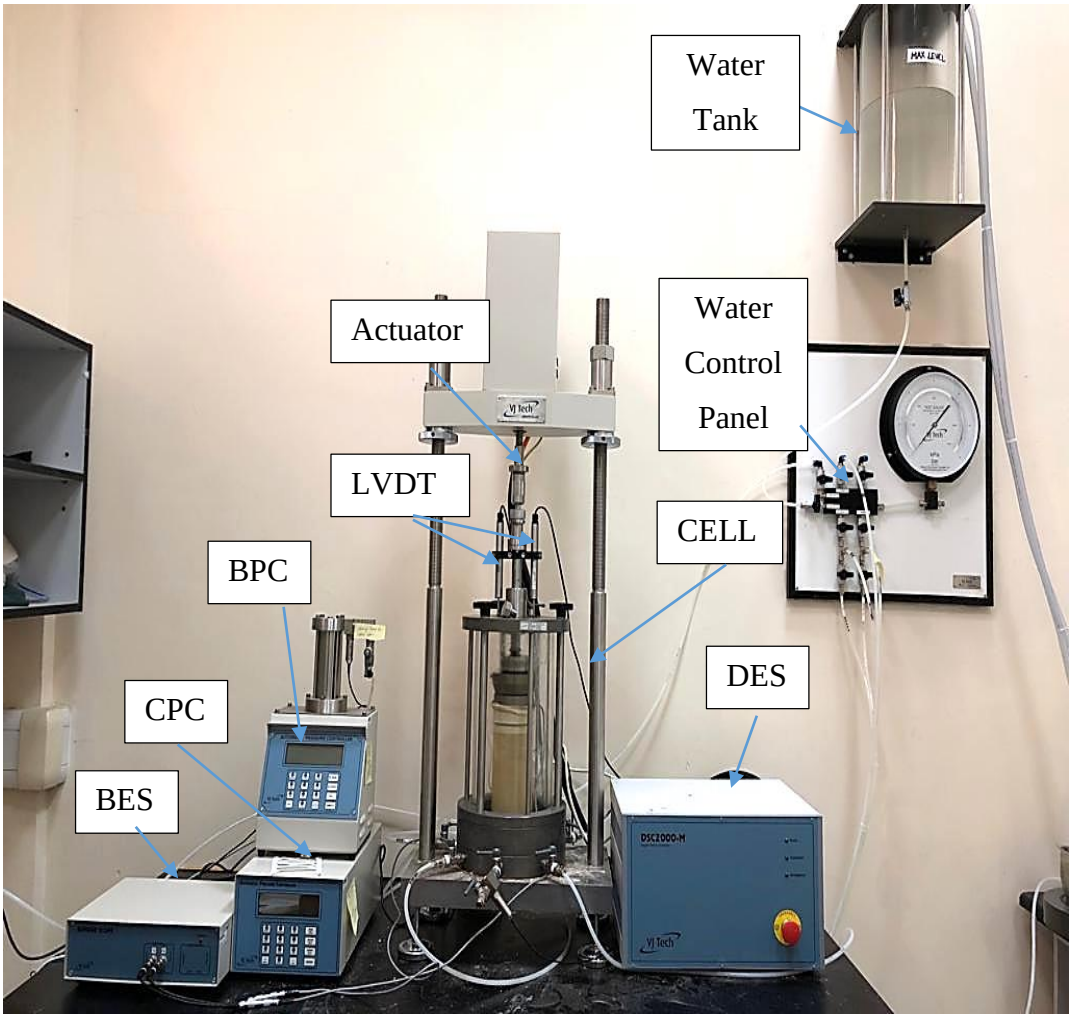

Figure 13: Triaxial Machine produced by VJ-Tech

As noted in the previous section, the shear wave velocity is equal to the difference in arrival times Δ(t) divided by the travel distance Δ(x). Therefore, the time difference between the transmitter and received signals (ΔT) should be divided by the length of the specimen, according to the equation (1).

The estimated shear wave velocities were plotted against different confinements, considering the effect of the sample size. These data were then fitted with a typical power functional form as shown in Equation 4, where *A* and *B* are the regression coefficients. The bender element testing program is presented in Table 7 for evaluation of shear wave velocity (Vs).

The shear wave velocities were obtained at conditions similar to the field. Hence, the data was obtained at multiple confining pressures to simulate the ground condition

at depths between 5 and 12 m using the CT set. In the present study, the number of blows (SPT-N value) was correlated with the shear wave velocity obtained from the corresponding confining pressure. The five samples (A, B, C, D and E) were tested in two sample sizes (Table 8). Hence two correlations were developed to show the influence of sample size. The developed relations were shaped in a typical power function form shown in (9). The coefficients A and B were obtained using a typical regression analysis. Based on the bender element testing program that is presented in Table 9, the correlation between shear wave velocity and the SPT-N value were developed for the two tested sample sizes.

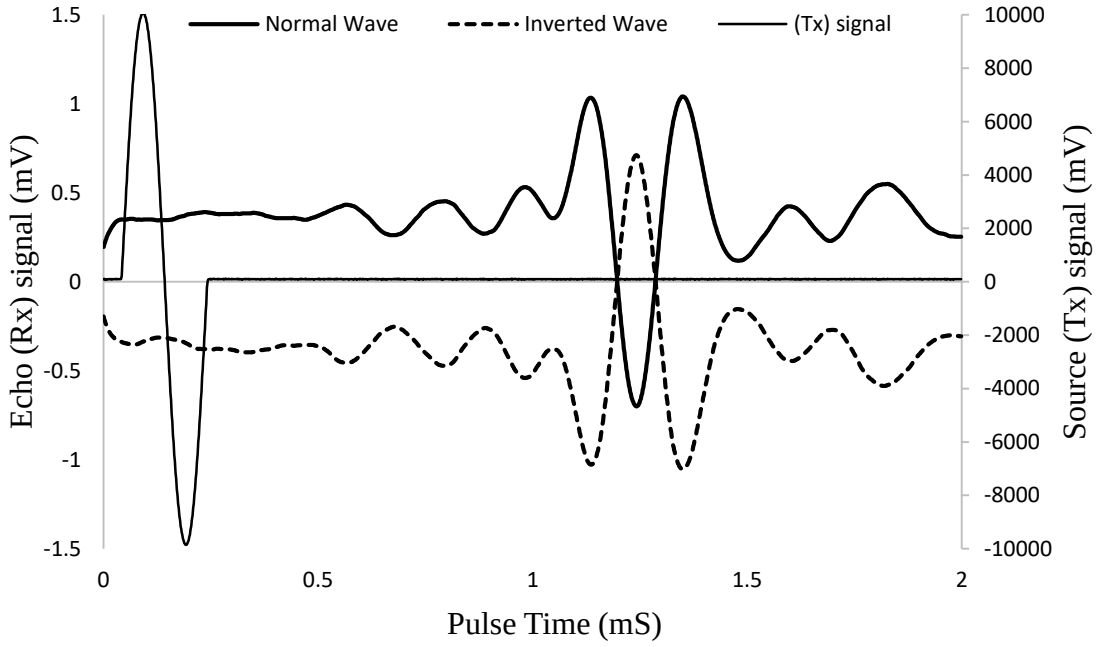

Figure 14: The identification of the first arrival time of the shear wave (S-wave) based on polarity.

3.2.2. Cyclic triaxial (CT) test. The sample for CT testing was prepared in the chamber of CT using a split mold, O-range, membranes, and silicon grease. All specimens were prepared by pluviation techniques and vacuum. The grease was applied to the bottom and top cap to ensure a better seal. The bottom porous stone was placed above the bottom cap along with the membrane and secured with O-rings. The mold was installed, and the membrane was fixed inside the mold using suction in order to remove the air between the mold and the membrane. The soil was poured into the membrane after fitting it into the mold Finally, the top porous stone and the top cap

were placed over the last layer of soil and sealed using O-rings. The chamber was placed and the Linear Variable Differential Transformer (LVDT) were installed. The valve of the cell pressure was opened in order to allow the de-aired water to flow into the cell. Figure 15 illustrates the typical CT sample.

Table 8: The required data to obtain the (Vs-N) correlation.

(N-values) of the tested Samples (From the soil investigation reports)	**The evaluated shear wave velocity (Vs) from Bender Element (BE) for the two tested sample sizes**	
Sample A	Vs (7cm Sample Diameter)	Vs (10cm Sample Diameter)
Sample B	Vs (7cm Sample Diameter)	Vs (10cm Sample Diameter)
Sample C	Vs (7cm Sample Diameter)	Vs (10cm Sample Diameter)
Sample D	Vs (7cm Sample Diameter)	Vs (10cm Sample Diameter)
Sample E	Vs (7cm Sample Diameter)	Vs (10cm Sample Diameter)

Table 9: Proposed bender element tests (The values in bracket are the diameters of the sample in cm)

σ (KPa)	**Sample**				
	A	**B**	**C**	**D**	**E**
20	Vs (7, 10)	Vs (7, 10)	Vs (7, 10)	Vs (7, 10)	Vs (7, 10)
40	Vs (7, 10)	Vs (7, 10)	Vs (7, 10)	Vs (7, 10)	Vs (7, 10)
60	Vs (7, 10)	Vs (7, 10)	Vs (7, 10)	Vs (7, 10)	Vs (7, 10)
80	Vs (7, 10)	Vs (7, 10)	Vs (7, 10)	Vs (7, 10)	Vs (7, 10)
100	Vs (7, 10)	Vs (7, 10)	Vs (7, 10)	Vs (7, 10)	Vs (7, 10)
120	Vs (7, 10)	Vs (7, 10)	Vs (7, 10)	Vs (7, 10)	Vs (7, 10)

Figure 15: The typical CT sample.

The CT testing was performed at 40, 100 and 140kPa. The CT test can either be performed as load control or displacement control. Displacement control was used in this study. The displacement was increased slowly to measure the dynamic properties at different strain levels. The typical test involves settings for samples per cycle, cycle counts, frequency, and the amplitude of cyclic load. Finally, after performing the cyclic test, the data was saved and named according to a predefined numbering system.

Excel was used to calculate shear modulus (G), damping ratio (ξ), and the shear strain (γ). In order to estimate the shear modulus (G), Young's modulus (E) is first calculated. As noted in equation (7), (8) and (9), the Poisson's ratio (υ) was assumed to be 0.25 as per the recommendations by [74]- [75]. The dynamic properties were estimated from the tests conducted at a displacement range between 0.01-0.06 mm with an increment of 0.01 mm for 5 cm samples. However, for 10 cm samples the displacement rates were adjusted to higher intervals; 0.02-0.12 mm with an increment of 0.02mm to maintain the similar influence of the dynamic loading. Both sample sizes were tested at 1 Hz loading frequency and the specimens were tested at different confining stresses of 40, 100, and 140 kPa. Tables 10-11 summarize the testing program for sample dimensions of 5 cm and 10 cm respectively.

In both sample geometries, 10 hysteresis loops were obtained. In addition, the mathematical approach illustrated in equations (7), (8) and (9) was used to evaluate the dynamic properties of soil by considering the average of three hysteresis loops obtained from different loading cycles. The literature suggests the use of varying loading cycles

to evaluate the dynamic properties of soil (e.g. 1st cycle [75] - [76], 5th cycle [16], 10th cycle [74]). For the present study, the 1st, 5th and 10th cycles of loading and the corresponding hysteresis loops were averaged and used for the evaluation of dynamic properties. In contrast, it is commonly observed that the hysteresis loops become progressively asymmetric when the displacement increase beyond 0.08mm. Poor data may lead to underestimation or overestimate of the conventionally evaluated dynamic properties. Therefore, a date adjustment methodology proposed by Shiv et. al. [77] was essential for evaluating reliable dynamic properties based on the Actual Symmetrical Hysteresis Loop (ASHL). Figure 16 illustrates the influence of the data adjustment method on the loop area that consequently impacts the dynamic properties. Hence, the adjustment method was applied for the chosen cycles and then averaged to evaluate the dynamic properties.

Table 10: The cyclic triaxial tests for 5 cm sample diameter.

σ (kPa)	**Displacement level (mm)**					
	0.01	0.02	0.03	0.04	0.05	0.06
40	*G*, *ξ*	*G*, *ξ*	*G*, *ξ*	*G*, *ξ*	*G*, *ξ*	*G*, *ξ*
100	*G*, *ξ*	*G*, *ξ*	*G*, *ξ*	*G*, *ξ*	*G*, *ξ*	*G*, *ξ*
140	*G*, *ξ*	*G*, *ξ*	*G*, *ξ*	*G*, *ξ*	*G*, *ξ*	*G*, *ξ*

Table 11: The cyclic triaxial tests for 10 cm sample diameter**.**

σ (kPa)	**Displacement level (mm)**					
	0.02	0.04	0.06	0.08	0.10	0.12
40	*G*, *ξ*	*G*, *ξ*	*G*, *ξ*	*G*, *ξ*	*G*, *ξ*	*G*, *ξ*
100	*G*, *ξ*	*G*, *ξ*	*G*, *ξ*	*G*, *ξ*	*G*, *ξ*	*G*, *ξ*
140	*G*, *ξ*	*G*, *ξ*	*G*, *ξ*	*G*, *ξ*	*G*, *ξ*	*G*, *ξ*

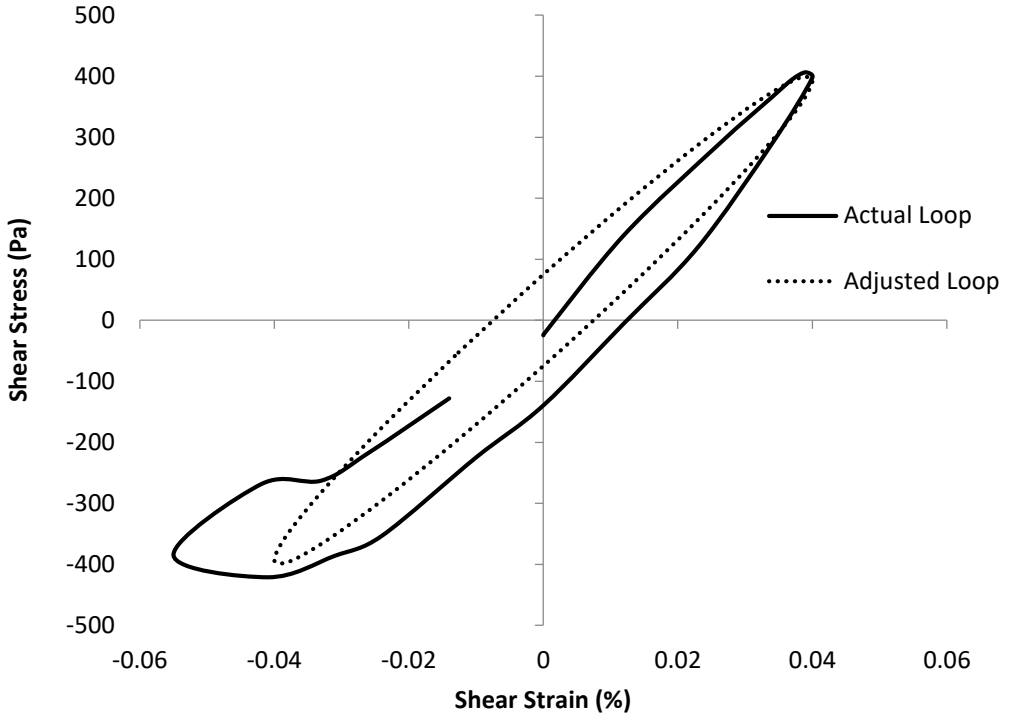

Figure 16: The influence of the adjustment method on the typical hysteresis loop (shear stress-shear strain plot) [77].

Additionally, Hardin et.al [15] recommended the hyperbolic models to describe the nonlinear soil behavior under cyclic loading. The hyperbolic is often used for the $G/G_{max} - log\ \gamma$ relationship due to its simplicity. In contrast, the hyperbolic model developed by Harden et. al. [15] result in a poor fit to the test data because it only involves one curve-fitting variable. Hence, a modified hyperbolic model suggested by Stokoe et. al. [78] provided a reasonable fit for the data points. Stokoe et. al. [78] involved two curve fitting variables. The modified hyperbolic model was used in this study. The following equations describing the modified hyperbolic equations for normalized shear modulus G/G_{max}.

$$\frac{G}{G_{max}} = \frac{1}{1 + \gamma_h} \tag{12}$$

where:

$$\gamma_h = \frac{\gamma}{\gamma_r}\left(1 + a\ exp\left(-b\frac{\gamma}{\gamma_h}\right)\right) \tag{13}$$

where γ_r is γ at G/G_{max} equal to 0.5, and "*a*" and "*b*" are the curvature coefficients (or the soil constants). The values of (*a*) and (γ_r) that provide the best fits of the hyperbolic model to the test data were determined by multiple regression.

Hardin et.al [15] proposed the relationship between the damping ratio (ξ) and the shear strain ($D - log\ \gamma$) curve according to the following equation:

$$D = D_{max} \frac{{}^{\gamma}/_{\gamma_r}}{1 + {}^{\gamma}/_{\gamma_r}} \tag{14}$$

where D_{max} was the maximum material damping ratio (ξ) and γ_r was the reference strain. The G/G_{max} is the normalized shear modulus obtained in (12).

3.2.3. Quick shear (QS) test. The quick shear test in CT equipment was performed to obtain shear strength properties of regional soils. All the soils were tested to obtain the static parameters of the soil; such as cohesion (*c*) and friction angle (ϕ). The tests were carried out under constant confinement pressures of σ_3 = 50, 100, 150 and 300 kPa, therefore; four samples were prepared to form each soil material with same density. Each sample was subjected to an axial strain rate of 1mm/min. Samples of ratios H/D = 2 (height H = 10 cm, diameter D = 5 cm, height H = 14 cm, diameter D = 7 cm and height H = 20 cm, diameter D = 10 cm) were used for experiments. Shearing data were collected and named for each sample size. Moreover, the shearing data of each cell pressure ($\sigma 3$) was analyzed using Mohr circles based on the Mohr-Coulomb approach. The slope of the tangent line through circles represents the shear strength property of friction angle (ϕ). The apparent cohesion (*c*) is taken as y-intercept (*b*) of the tangent line. Figure 17 presents a schematic of typical Mohr circles developed at multiple confinement pressure.

3.2.4. Sample size effect. The effects of the sample size were evaluated by analyzing the results of testing on three sample sizes. The effect of sample size on Vs versus confinement, Vs versus shear strain level, and ξ versus shear strain level presented and discussed.

3.3. Shear Strength of Soil

The dynamic triaxial equipment was used to perform the Quick Shear Test (QST) in order to evaluate the static properties of the region soils. Additionally, the static properties of the soil such as angle of friction (φ) and cohesion (c), and N-values for the soils were obtained from the borehole logs. Both parameters were compared and investigated. Table 12 presents the summary of the static testing program for different sample dimensions; 5cm, 7cm and 10cm. The results are analyzed to develop correlations between static and dynamic properties such as Vs with N-values.

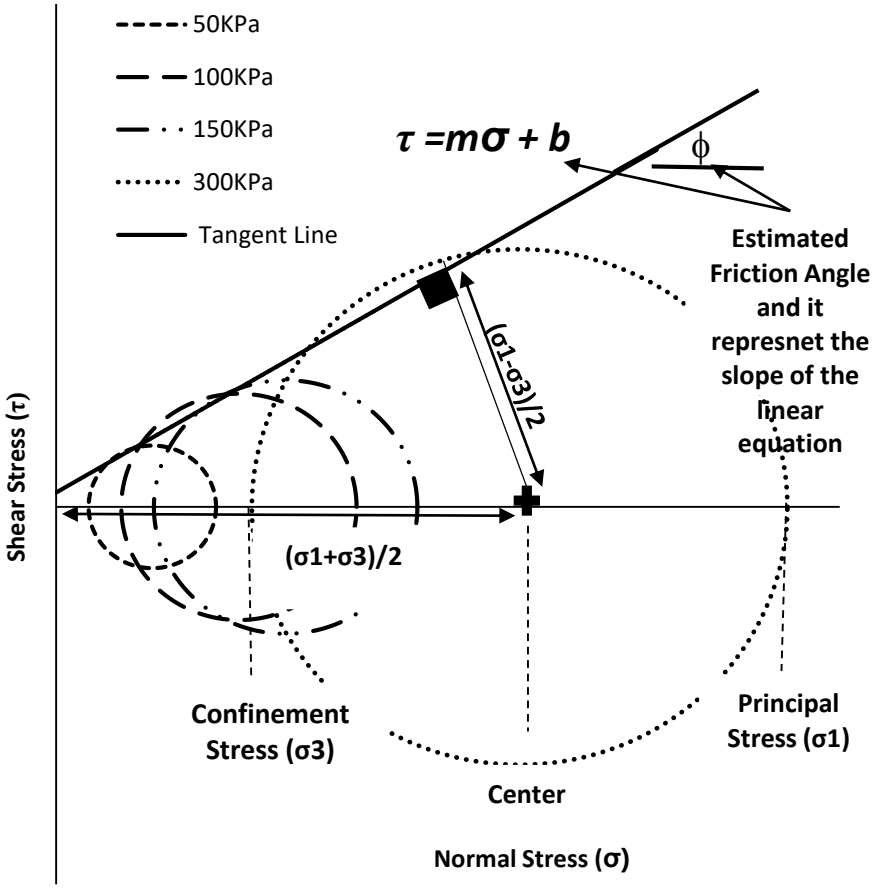

Figure 17: Typical analysis of the Mohr circle based on different cell pressure

Table 12: The static test program

Test Type	Sample (A)	Sample (B)	Sample (C)	Sample (D)	Sample (E)
QST	ϕ, C	ϕ, C	ϕ, C	ϕ, C	ϕ, C
Soil report validation	ϕ, C	ϕ, C	ϕ, C	ϕ, C	ϕ, C
Standard Penetration Test (SPT)	N	N	N	N	N

Chapter 4. Results and Discussion

The cyclic triaxial equipment and bender element were used to evaluate the dynamic properties of the representative soils of the UAE as a function of confinement and shear strain level. Correlations between static and dynamic properties for typical soils of the UAE were developed. Additionally, the effect of sample size on the dynamic properties was investigated. The main results of the study are presented in this section.

4.1. Results of Bender Element (BE)Test

4.1.1. Shear Wave Velocity (Vs) - Confinement Pressure (σ) correlations.

The results and the regression analysis of the BE data sets are presented in this section. The testing was performed on 7cm and 10cm sample diameters. During the BE testing, the samples were tested under 20, 40, 60, 70, 80, 100 and 120kPa confinement pressure. The computed shear wave velocities (*Vs*) of the two sample geometries are shown in Table 13.

Table 13: Results of BE tests

Confinement (kPa)	Vs (m/s)		
	Sample B	Sample D	Sample E
Sample Diameter of 7cm			
30	177.34	170.31	169.03
40	192.74	183.66	153.38
50	207.25	194.74	162.80
70	231.67	212.71	178.12
80	240.57	220.29	188.24
100	257.70	233.57	205.77
120	273.21	245.02	226.91
Sample Diameter of 10cm			
30	255.82	204.86	215.09
40	258.78	226.67	230.86
50	269.91	245.18	247.08
70	307.06	275.97	257.33
80	325.90	289.24	269.14
100	362.48	312.85	283.61
120	367.91	333.57	313.07

The effect of sample size was evaluated by testing the same soil under similar conditions, but using different sample dimensions. As shown in Table 13, the shear wave velocities were not the same for different dimensions indicating the size effect. The higher velocities were observed in the bigger sample geometry. The shear velocity increases as the sample diameter increases.

Correlations between shear wave velocity (*Vs*) and the confinement pressure (σ) were developed. Figures 18-19 presents the variation of the shear wave velocity (*Vs*) with the confining pressure (σ) for the tested sandy specimens. The samples were extracted from various depths in the Abu Dhabi region. According to Table 5, the tested samples were labeled with respect to the material type, depth and SPT-N value. Figure 18 presents the average of the developed *Vs*- σ correlations for samples B, D, and E (7cm sample's diameter). Figure 18 shows the average correlations of the tested samples with bigger sample geometry (10cm sample's diameter). Based on the developed correlations of the two sample sizes, the larger correlation parameters were obviously exhibited at the bigger sample size.

Table 14 summarizes the developed *Vs*-σ correlations for the silty sand specimens. The shear wave velocity obtained by the BE tests were compared with a typical power functional form that is shown in (4), where A and B are the regression coefficients obtained by curve fitting. As shown in Figures 17- 18, the results obtained in the present study were compared with Víctor Rinaldi's correlations [13] since both studies were based on sandy soil specimens but different regions.

From another perspective, a study presented a relationship between shear modulus (*G*) and confinement (σ) [79]. This relationship was directly proportional to Vs-σ correlation since the shear modulus (*G*) was directly related to the shear wave velocity (*Vs*) by a Passion's ratio (v). The results showed that, the regression parameter "A" fluctuates between 7.0–14.1 and parameter "*B*" varies between 0.4–0.5 when *G* and σ are expressed in MPa and kPA, respectively [79].

Based on the last perspective, a relationship was developed between shear modulus (*G*) and confinement (σ) on a gypsum-based soil (Sample A) in the present study. Sample A was a gypsum sandy specimen obtained from a shallow depth and tested using BE. The shear modulus was based on a passion's ratio of 0.25. The BE

results showed a slightly small variation of shear modulus (G) as the confinement pressure increase from 30-120 kPa. Sample A exhibited a variation between 15 MPa and 67 MPa in the shear modulus (G) when the two sample geometries were tested. Figure 20 shows the developed G-σ correlations for the gypsum sandy specimens (Sample A). Table 15 presents the developed G-σ correlations in the present study.

The effect of sample size was evaluated by testing the same soil under similar conditions, but using different sample dimensions. As noted in Figure 18, the silty sand specimens (Samples B, D and E) had asymmetrical variations of shear wave velocity with isotropic confinement pressures between 30 kPa and 120 kPa. Larger samples showed a variation between 210m/s and 360m/s of Vs, however; smaller samples, 7cm sample diameter, exhibited a smaller shear velocity. The variation significantly decreased between 150 m/s and 270 m/s for the 7cm sample diameter. As shown in Figures 18-19, the developed correlations were comparable to Victor Rinaldi's relation [13].

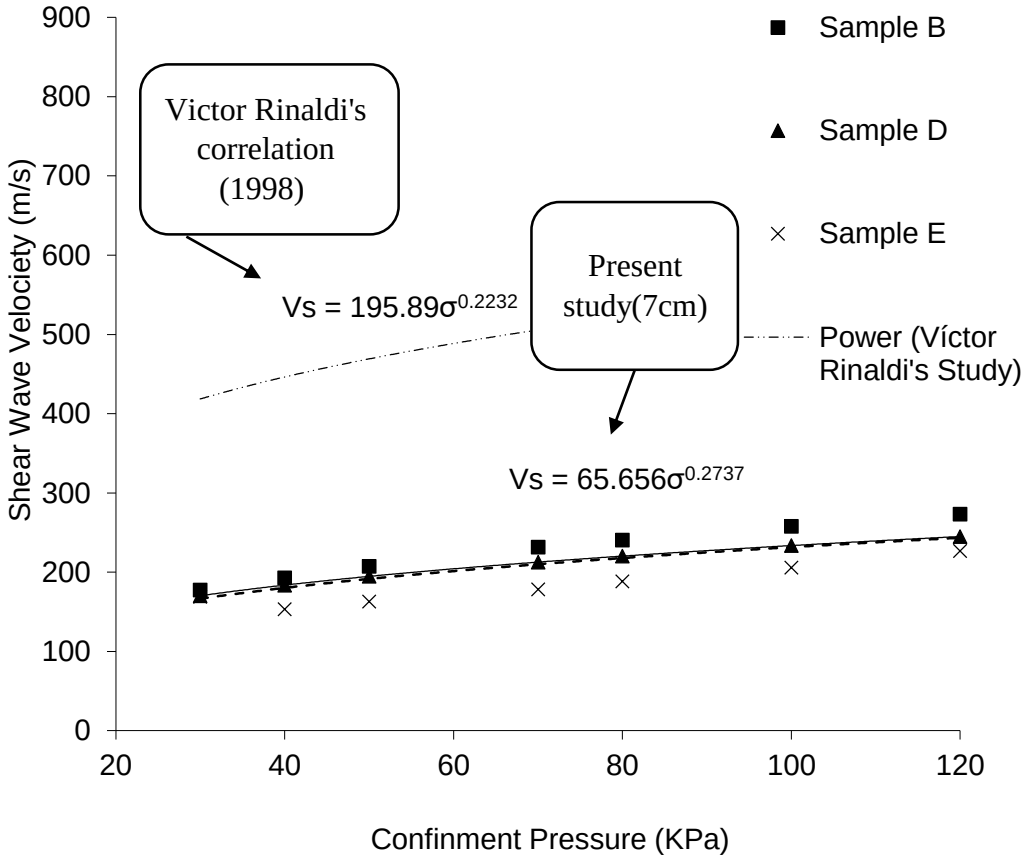

Figure 18: The variation of the shear wave velocity (Vs) with the confining pressure (σ) for 7cm sample's diameter

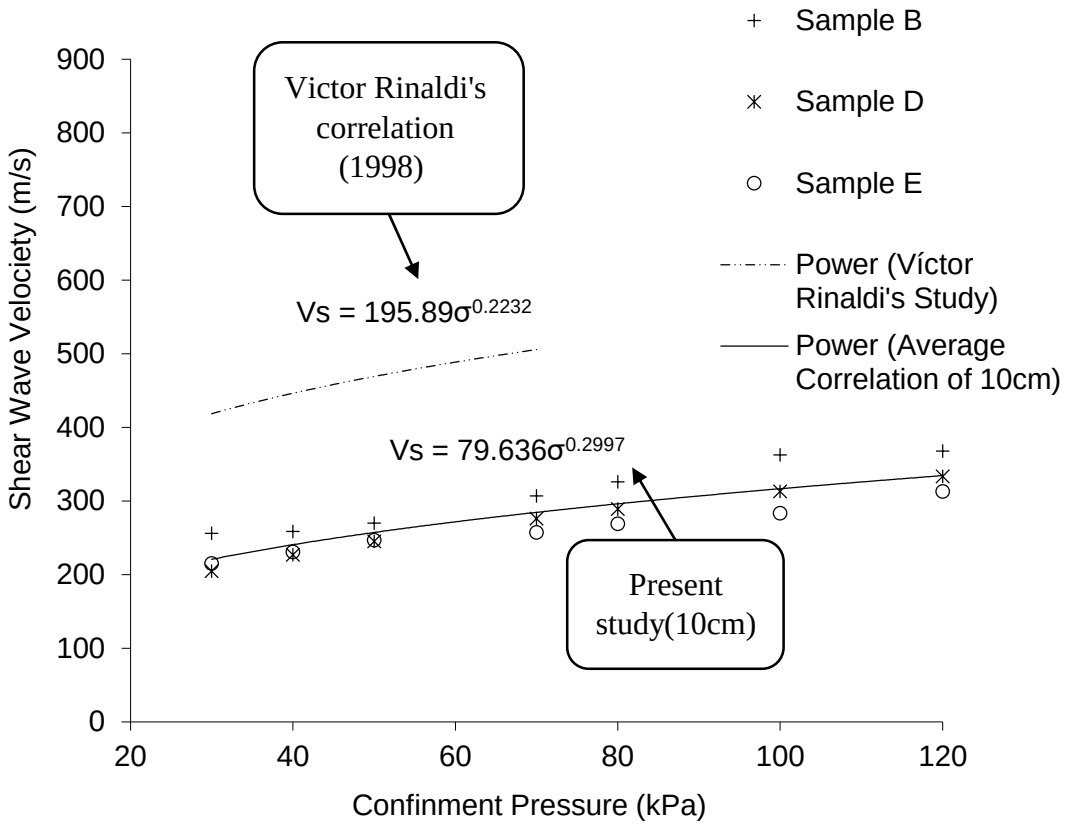

Figure 19: The variation of the shear wave velocity (Vs) with the confining pressure (σ) for 10cm sample's diameter

Table 14: The developed *Vs*- σ correlations for the silty sand specimens

Sample	7cm Sample Diameter	10cm Sample Diameter
Sample B	$Vs = 60.81\sigma^{0.31}$	$Vs = 87.91\sigma^{0.3}$
Sample D	$Vs = 69.78\sigma^{0.26}$	$Vs = 61.95\sigma^{0.35}$
Sample E	$Vs = 67.03\sigma^{0.24}$	$Vs = 92.17\sigma^{0.25}$
Average Correlations of the Present study	$\mathbf{Vs = 65.66\sigma^{0.27}}$	$\mathbf{Vs = 79.64\sigma^{0.3}}$

Table 15: The conducted *G*-σ correlations for the silty sand specimens

Sample	7cm Sample Diameter	10cm Sample Diameter
Sample A (Correlation of the present study)	$\mathbf{G = 60.81\sigma^{0.31}}$	$\mathbf{G = 87.91\sigma^{0.3}}$

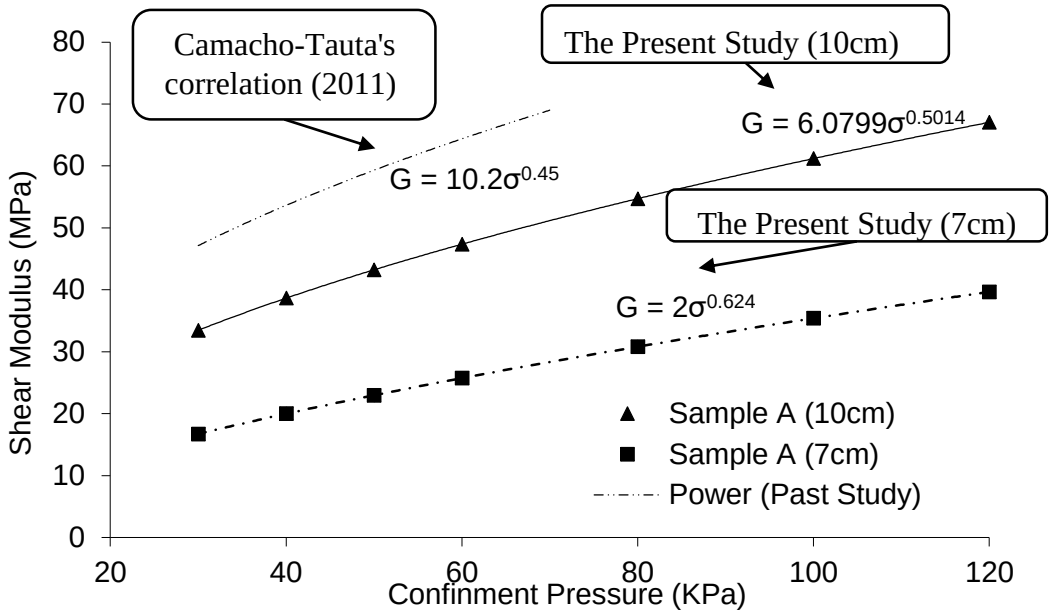

Figure 20: The variation of the shear modulus (G) with the confining pressure (σ) for the gypsum sandy specimen (Sample A).

4.2. Results of Cyclic Triaxial (CT) Test

The results and the regression analysis of the CT data sets are presented in this section. The samples were prepared as described in the previous section. The CT test was performed for four specimens; samples A, C, D, and E. According to Table 5, each sample had been labeled according to the material type, depth and SPT-N value. Where sample A represented a gypsum sandy specimen, and sample B was a mixture between sand, silt and gravel. In addition, two silty specimens labeled as sample D and E were tested. Subsequently, the CT testing was performed for two specimen diameters; 5cm and 10cm at three different confinement pressures of 40, 100 and 140kPa. The computed results of the CT tests including the variations of the sample geometries is shown in Tables 16-17.

To obtain the previous dynamic results, the dynamic actuator applied the cyclic load to the soil specimens at 1 Hz loading frequency. The loading frequency depended on the type of application and the soil type. To simulate the application of an earthquake, a frequency of 1Hz is considered suitable. Subsequently, the CT software analyzed the applied cyclic loading as a typical sinusoidal waveform where 10 sinusoidal cycles were developed. In addition, 10 hysteresis loops were developed where each hysteresis loop represented a single sinusoidal signal. For the present study, the 1st, 5th and 10th cycles of loading and the corresponding hysteresis loops were averaged and used for the evaluation of dynamic properties.

There are several factors that affect the shear modulus and damping ratio (ξ), such as shear strain, confining pressure, number of cycles, and the void ratio. The shear strain (γ) and confining pressure were found to be the greatest influencing parameters among the conventional parameters that affect the dynamic parameters. Hence, the relationships between shear strain and dynamic properties such as shear modulus and damping ratio (ξ) show the influence of confining pressure. The influence of sample size on the developed relationships was investigated.

4.3. Effect of Confining Pressure

4.3.1. Effect of shear strain and confining pressure on shear modulus. The shear modulus (G) was found to decrease with an increase of the shear strain (γ). In the present study, the relation between G and γ was developed from CT tests that were performed on different diameter samples. The trend was similar regardless of sample size, confining pressure, and relative density. The results of both sample sizes (5 and 10cm sample's diameter) are shown in Figures 21-28. The variation in the normalized shear modulus (G/G_{max}) with the shear strain (γ) were plotted into several plots for clarity (Figures 21-28). The variation of G/G_{max} with γ at each cell pressure was evaluated. It is noticed that variation of the highest confining pressure (140 KPa) showed the lowest G/G_{max} -γ variation and it increases as the cell pressure increases (Figures 21-28).

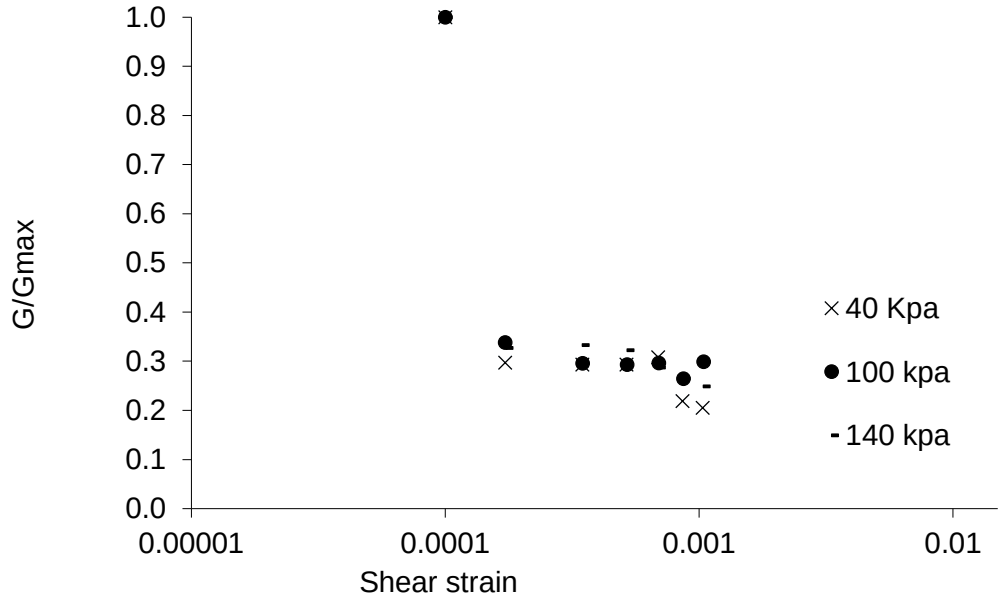

Figure 21: Variation of *G/Gmax* with shear strain for sample A (5cm Diameter)

Table 16: The results of the CT test for Sample A and Sample C

σ (kPa)	Displacement level (mm)	Shear Modulus G (MPa), Shear Strain γ (%), and Damping Ratio ξ (%)					
		Sample A			Sample C		
Sample Diameter of 5cm							
40		**G (MPa)**	**γ (%)**	**ξ (%)**	**G (MPa)**	**γ (%)**	**ξ (%)**
	0.01	44.528	1.72E-04	7.759	42.461	1.66E-04	6.346
	0.02	43.985	3.47E-04	7.899	39.261	3.28E-04	8.010
	0.03	43.937	5.17E-04	9.307	37.928	4.94E-04	9.301
	0.04	46.233	6.89E-04	9.307	32.163	6.56E-04	9.299
	0.05	32.808	8.61E-04	9.767	27.151	8.25E-04	9.364
	0.06	30.761	1.03E-03	8.075	23.653	9.85E-04	9.679
100		**G (MPa)**	**γ (%)**	**ξ (%)**	**G (MPa)**	**γ (%)**	**ξ (%)**
	0.01	50.756	1.72E-04	5.758	122.923	1.65E-04	9.307
	0.02	44.427	3.47E-04	7.790	107.175	3.30E-04	9.407
	0.03	43.985	5.20E-04	7.899	41.405	4.92E-04	9.304
	0.04	44.505	6.94E-04	6.213	91.326	6.53E-04	6.233
	0.05	39.776	8.68E-04	6.213	80.651	8.17E-04	9.321
	0.06	44.950	1.04E-03	6.213	73.310	9.85E-04	9.662
140		**G (MPa)**	**γ (%)**	**ξ (%)**	**G (MPa)**	**γ (%)**	**ξ (%)**
	0.01	49.224	1.74E-04	5.880	138.232	1.64E-04	12.427
	0.02	50.081	3.46E-04	7.934	128.541	3.30E-04	12.673
	0.03	48.546	5.21E-04	9.348	119.167	4.93E-04	12.450
	0.04	43.264	6.93E-04	6.301	105.398	6.57E-04	16.590
	0.05	39.878	8.66E-04	9.306	102.077	8.21E-04	12.434
	0.06	37.451	1.04E-03	9.298	85.733	9.88E-04	16.359
Sample Diameter of 10cm							
40		**G (MPa)**	**γ (%)**	**ξ (%)**	**G (MPa)**	**γ (%)**	**ξ (%)**
	0.02	10.135	8.39E-05	15.595	14.833	8.45E-05	5.568
	0.04	8.957	1.68E-04	12.426	14.085	1.69E-04	7.836
	0.06	8.531	2.52E-04	12.426	13.985	2.51E-04	6.244
	0.08	7.436	3.38E-04	12.628	12.956	3.34E-04	7.790
	0.1	6.954	4.22E-04	15.722	11.860	4.20E-04	7.759
	0.12	6.717	5.07E-04	12.476	10.855	5.04E-04	13.000
100		**G (MPa)**	**γ (%)**	**ξ (%)**	**G (MPa)**	**γ (%)**	**ξ (%)**
	0.02	12.211	8.44E-05	9.307	16.666	8.42E-05	4.733
	0.04	10.075	1.69E-04	12.476	16.816	1.69E-04	4.649
	0.06	9.553	2.54E-04	9.382	16.014	2.54E-04	4.640
	0.08	8.218	3.36E-04	10.862	15.553	3.38E-04	6.244
	0.1	6.742	4.23E-04	12.628	15.317	4.22E-04	7.743
	0.12	6.623	5.07E-04	9.533	15.723	5.07E-04	8.368
140		**G (MPa)**	**γ (%)**	**ξ (%)**	**G (MPa)**	**γ (%)**	**ξ (%)**
	0.02	7.316	8.44E-05	19.074	16.924	8.44E-05	3.094
	0.04	6.329	1.68E-04	20.825	16.867	1.68E-04	4.780
	0.06	6.771	2.54E-04	31.212	16.157	2.52E-04	6.415
	0.08	6.758	3.37E-04	31.687	16.380	3.36E-04	6.213
	0.1	6.150	5.05E-04	26.563	15.797	4.23E-04	4.649
	0.12	6.783	4.22E-04	30.943	15.470	5.04E-04	4.667

Table 17: The results of the CT test for Sample D and Sample E

σ (kPa)	Displacement level (mm)	Shear Modulus G (MPa), Shear Strain γ (%), and Damping Ratio ξ (%)					
		Sample D			Sample E		
Sample Diameter of 5cm							
		G (MPa)	**γ (%)**	**ξ (%)**	**G (MPa)**	**γ (%)**	**ξ (%)**
	0.01	61.282	8.68E-05	9.337	28.527	8.77E-05	4.644
	0.02	56.691	1.65E-04	9.000	25.129	1.75E-04	3.184
40	0.03	53.510	2.48E-04	7.000	24.779	2.61E-04	3.095
	0.04	42.417	3.45E-04	8.000	24.100	3.51E-04	3.097
	0.05	35.845	4.31E-04	9.301	22.194	5.22E-04	3.116
	0.06	31.524	5.21E-04	14.000	23.251	5.21E-04	3.125
		G (MPa)	**γ (%)**	**ξ (%)**	**G (MPa)**	**γ (%)**	**ξ (%)**
	0.01	132.769	8.60E-05	6.220	35.831	8.76E-05	1.545
	0.02	131.249	1.73E-04	9.670	35.794	1.75E-04	3.095
100	0.03	108.456	2.59E-04	9.700	34.673	2.63E-04	1.548
	0.04	104.443	3.47E-04	9.000	33.056	3.51E-04	1.575
	0.05	88.073	4.31E-04	9.000	32.349	4.33E-04	1.555
	0.06	86.626	5.21E-04	9.340	31.500	4.32E-04	1.432
		G (MPa)	**γ (%)**	**ξ (%)**	**G (MPa)**	**γ (%)**	**ξ (%)**
	0.01	144.022	8.61E-05	9.788	144.022	8.61E-05	1.565
	0.02	141.958	1.72E-04	6.207	141.958	1.72E-04	1.548
140	0.03	135.632	2.60E-04	7.000	135.632	2.60E-04	1.556
	0.04	129.160	3.47E-04	8.000	129.160	3.47E-04	1.545
	0.05	114.639	4.33E-04	8.000	114.639	4.33E-04	1.547
	0.06	99.262	5.17E-04	9.733	99.262	5.17E-04	1.570
Sample Diameter of 10cm							
		G (MPa)	**γ (%)**	**ξ (%)**	**G (MPa)**	**γ (%)**	**ξ (%)**
	0.02	55.981	8.29E-05	15.980	89.457	9.80E-07	10.993
	0.04	44.079	1.65E-04	20.825	87.540	3.92E-04	9.382
40	0.06	41.326	2.48E-04	22.567	56.387	3.91E-04	12.476
	0.08	45.210	3.32E-04	19.472	50.925	5.84E-04	12.426
	0.1	57.108	4.15E-04	17.706	54.406	4.86E-04	13.259
	0.12	34.674	4.98E-04	18.000	50.200	4.86E-04	12.500
		G (MPa)	**γ (%)**	**ξ (%)**	**G (MPa)**	**γ (%)**	**ξ (%)**
	0.02	167.400	8.23E-05	6.415	89.723	8.11E-05	13.259
	0.04	150.833	1.66E-04	9.382	52.065	1.63E-04	13.000
100	0.06	119.430	2.48E-04	9.298	44.392	2.45E-04	12.628
	0.08	154.192	3.29E-04	12.426	44.399	3.27E-04	21.283
	0.1	145.300	3.42E-04	7.000	40.360	4.90E-04	23.000
	0.12	140.155	4.15E-04	6.213	41.800	4.05E-04	25.000
		G (MPa)	**γ (%)**	**ξ (%)**	**G (MPa)**	**γ (%)**	**ξ (%)**
	0.02	16.924	8.44E-05	12.476	16.924	8.44E-05	13.259
	0.04	16.867	1.68E-04	15.595	16.867	1.68E-04	12.886
140	0.06	16.157	2.52E-04	16.930	16.157	2.52E-04	16.930
	0.08	16.380	3.36E-04	15.722	16.380	3.36E-04	23.944
	0.1	15.797	4.23E-04	9.767	15.797	4.23E-04	20.049
	0.12	15.470	5.04E-04	15.980	15.470	5.04E-04	22.193

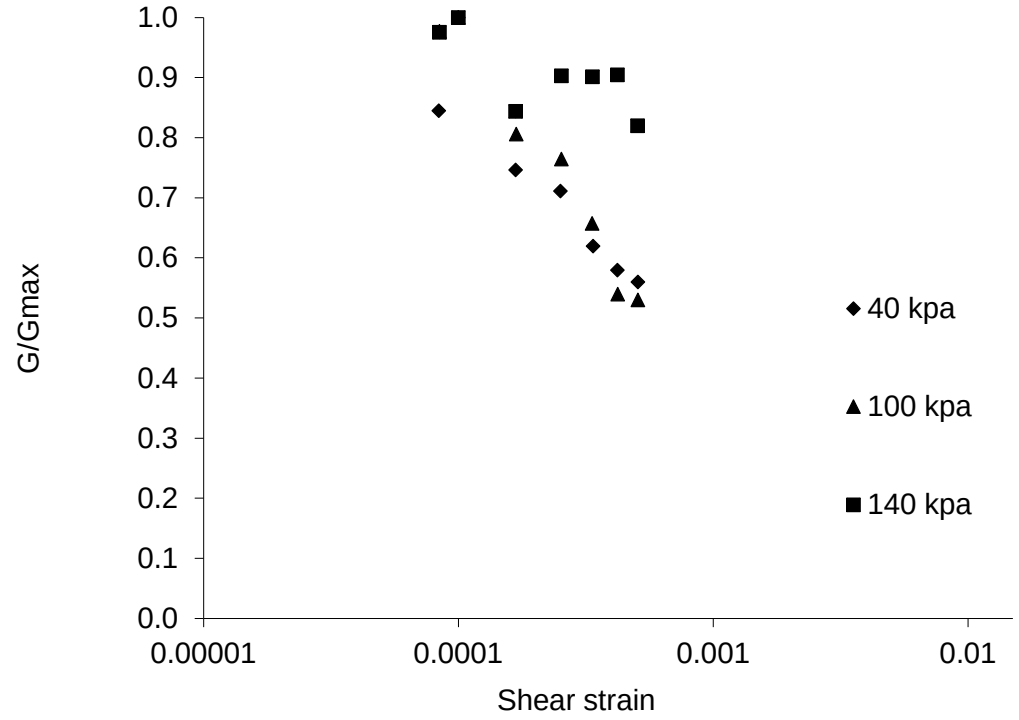

Figure 22: Variation of *G/Gmax* with shear strain for samples A (10cm Diameter)

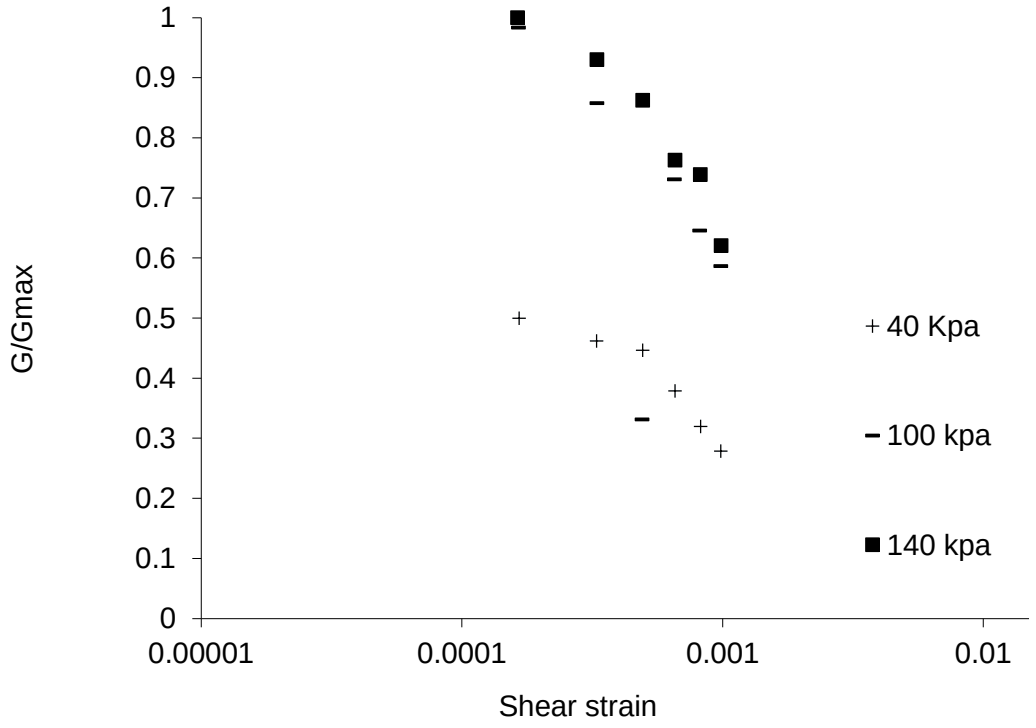

Figure 23: Variation of *G/Gmax* with shear strain for samples C (5cm Diameter)

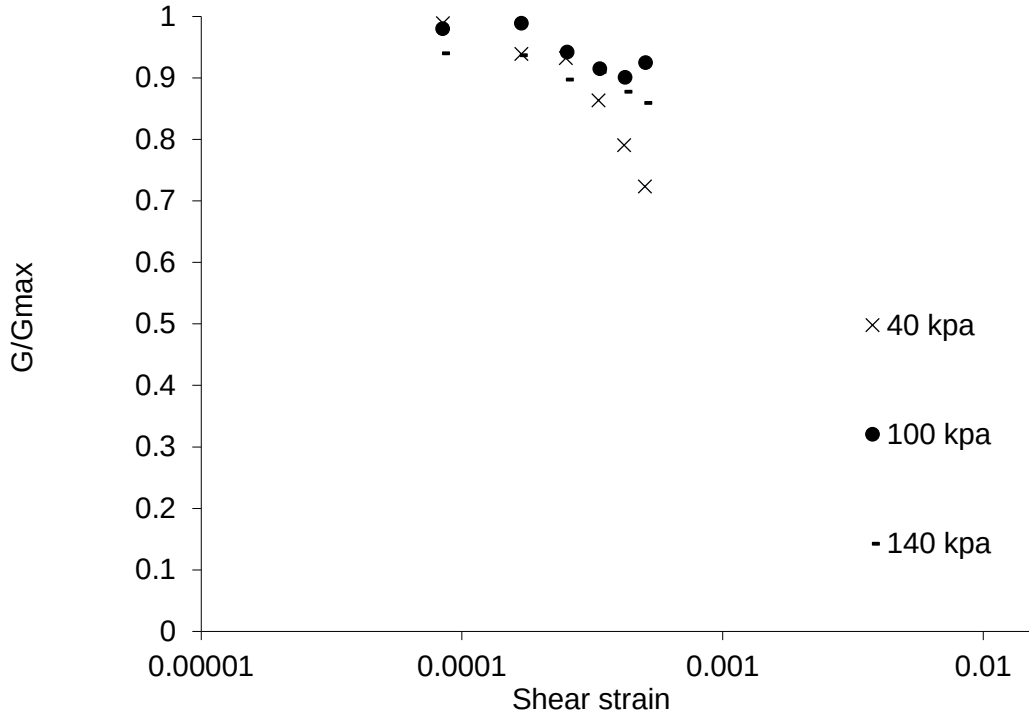

Figure 24: Variation of *G/Gmax* with shear strain for samples C (10cm Diameter)

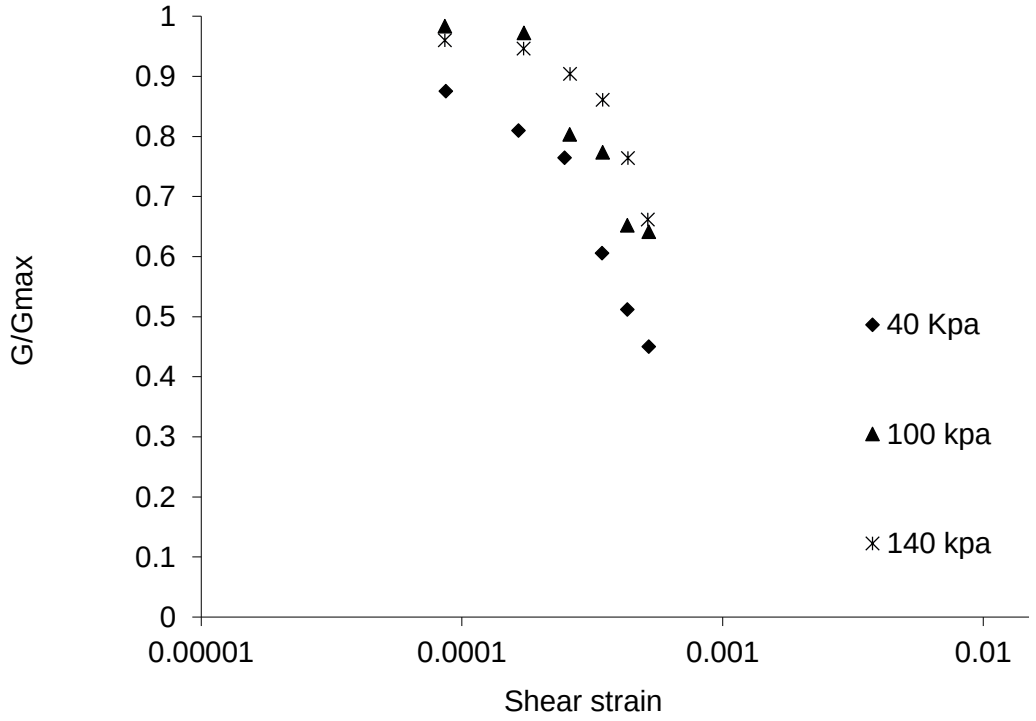

Figure 25: Variation of *G/Gmax* with shear strain for samples D (5cm Diameter)

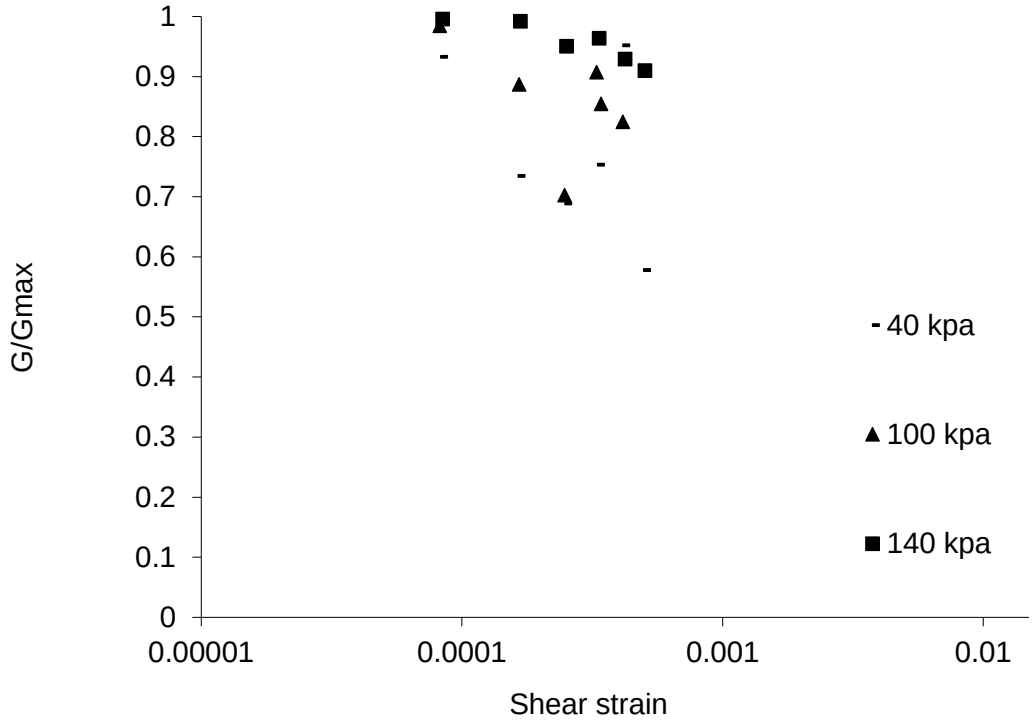

Figure 26: Variation of *G/Gmax* with shear strain for samples D (10cm Diameter)

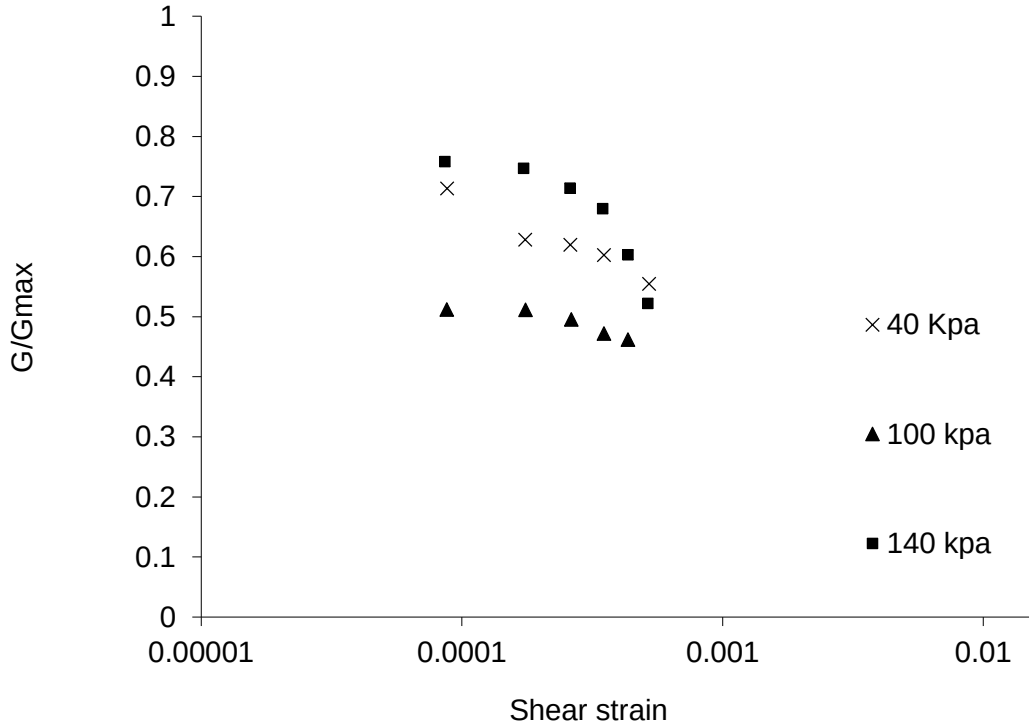

Figure 27: Variation of *G/Gmax* with shear strain for sample E (5cm Diameter)

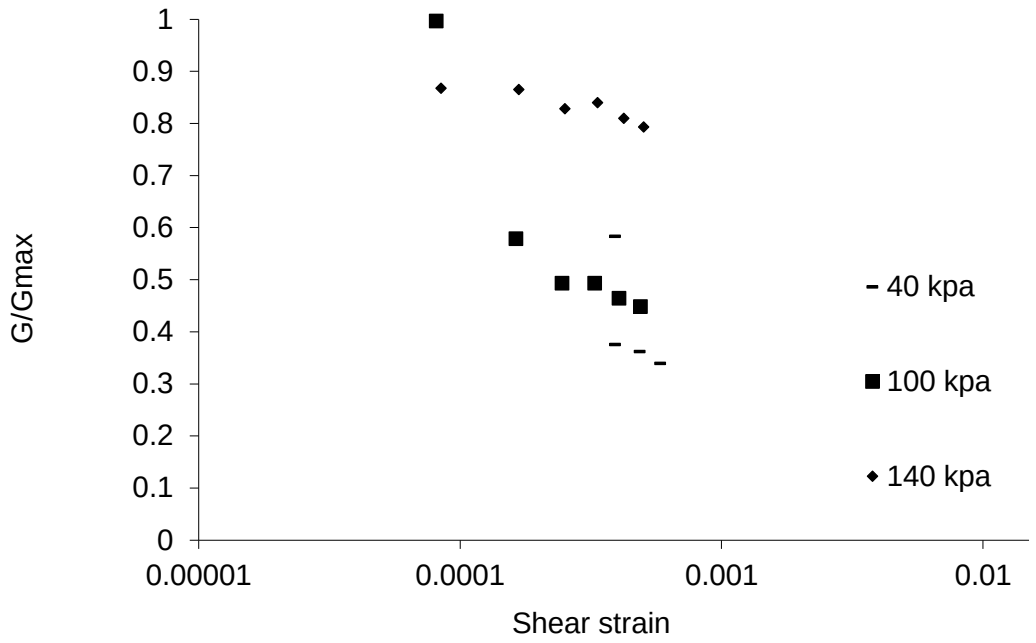

Figure 28: Variation of *G/Gmax* with shear strain for samples E (10cm Diameter)

4.3.2. Effect of shear strain and confining pressure on damping ratio (ξ).

Figures 29-36 illustrates the variation of ξ with γ as the function of cell pressure (σ). The specimens subjected to lowest confinement pressure (40kPa) presents the highest damping ratio (ξ); however, the specimens subjected to highest confining pressure (140kPa) show the lowest damping ratio (ξ) curve. This is because of increasing stiffness of the specimen with the increase in the confining pressure. It is also observed that the effect of confinement is almost negligible up to shear strain of 0.02%; however, the effect becomes significant at shear strains between 0.02 and 0.1%.

Initially, the material damping ratio (ξ) was estimated based on the conventional approach [80], and the (ξ) showed a constant trend. This result was classified as misinterpretation according to the ASTM code [80], and it was not matching the previous results that were conducted in literature [15]- [16]. Therefore, the ξ was estimated using the modified methodology that was explained in the previous section. The modified methodology showed a reasonable trend from asymmetric hysteresis loops. As demonstrated in Figure 21, the ξ increases with the increase of (γ) and decrease with increase in confinement (σ). This trend is in agreement with the findings of the literature [15]- [16].

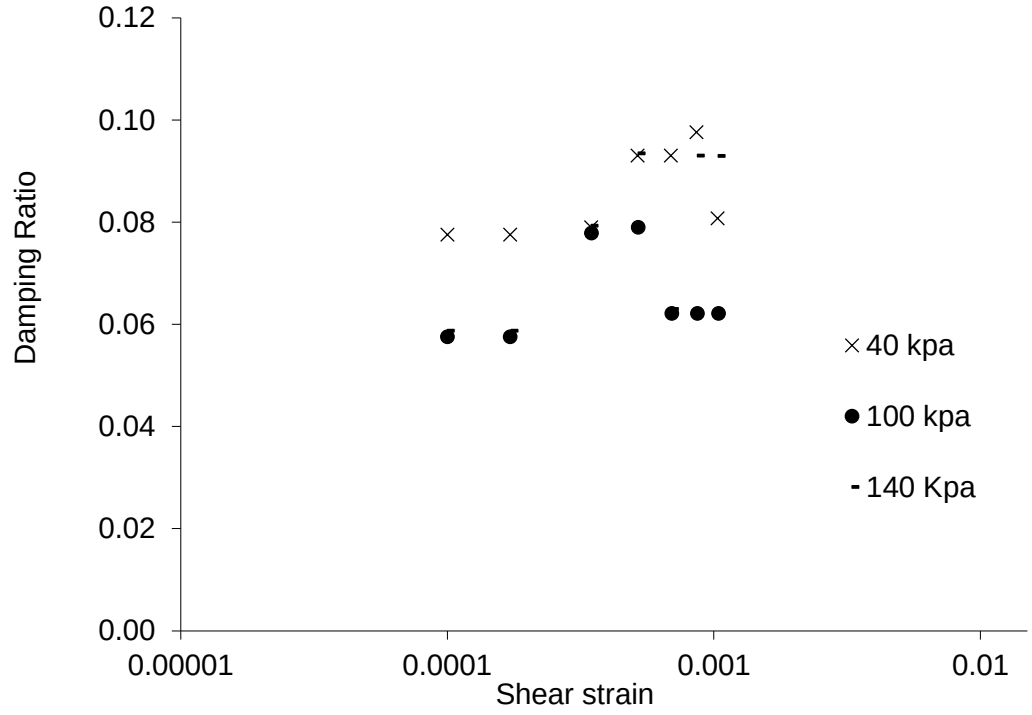

Figure 29: Variation of damping ratio with shear strain for samples A (5cm Diameter)

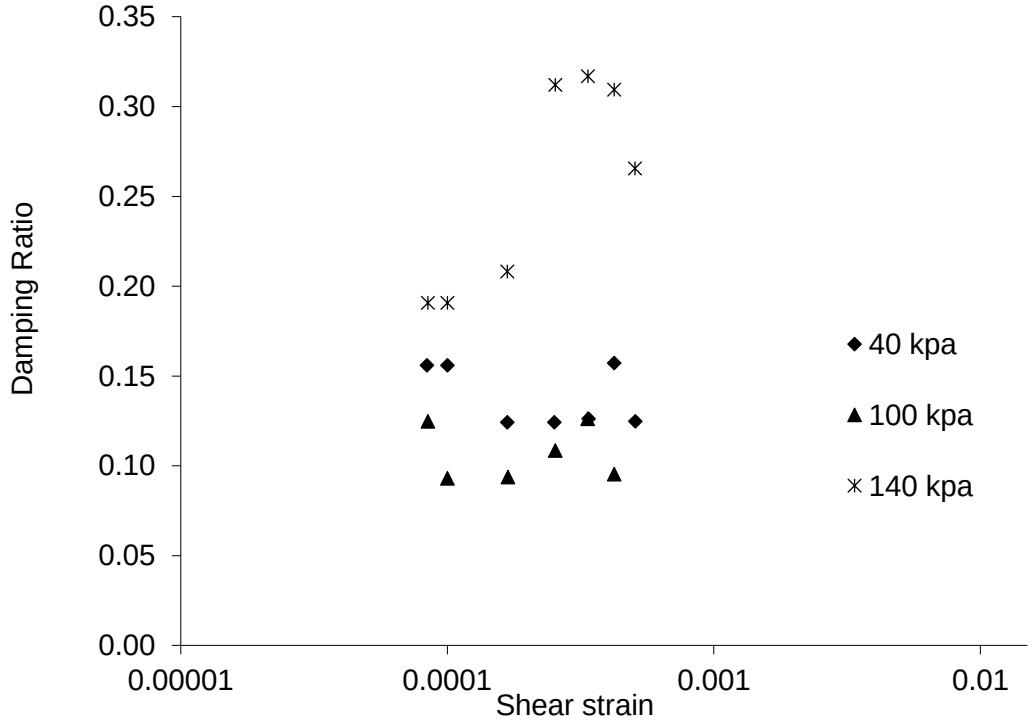

Figure 30: Variation of damping ratio with shear strain for samples A (10cm Diameter)

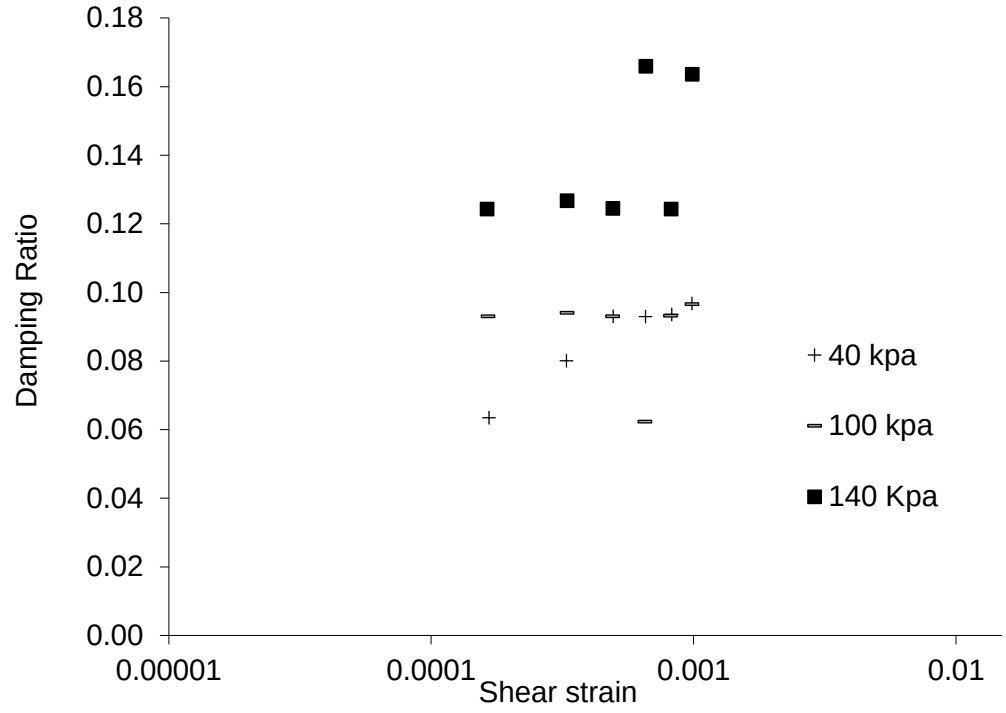

Figure 31: Variation of damping ratio with shear strain for samples C (5cm Diameter)

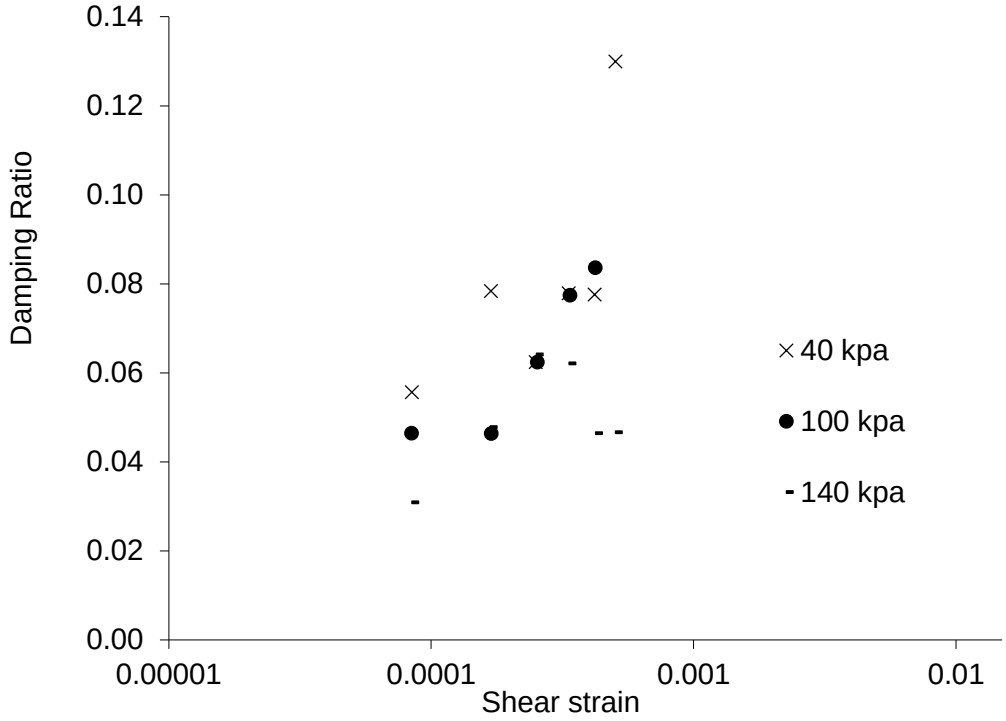

Figure 32: Variation of damping ratio with shear strain for samples C (10cm Diameter)

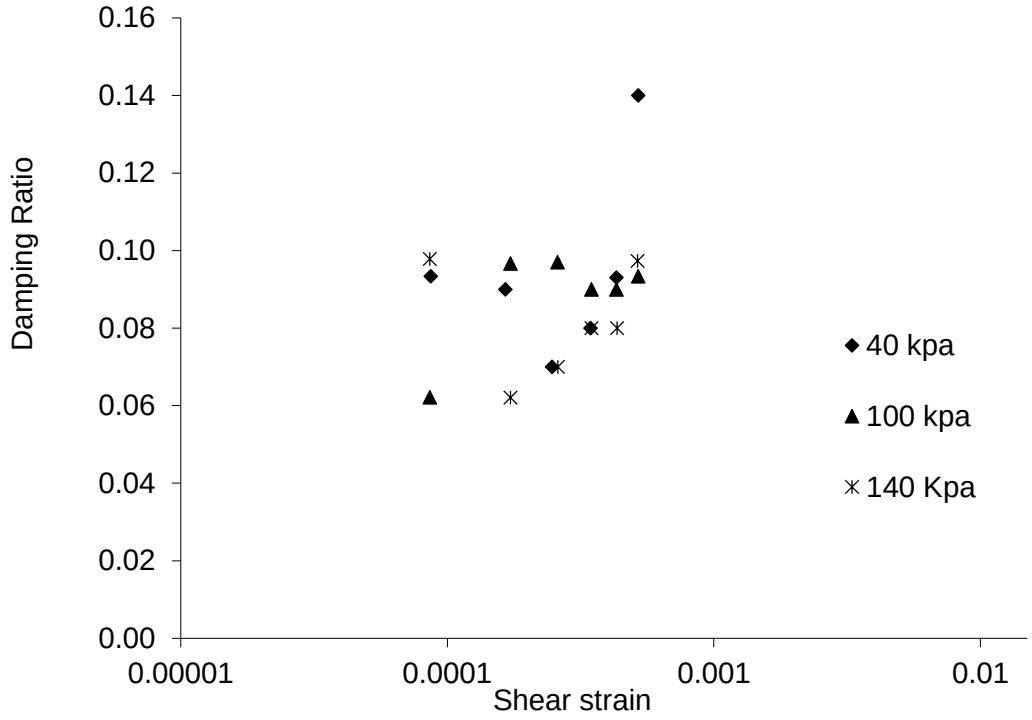

Figure 33: Variation of damping ratio with shear strain for samples D (5cm Diameter)

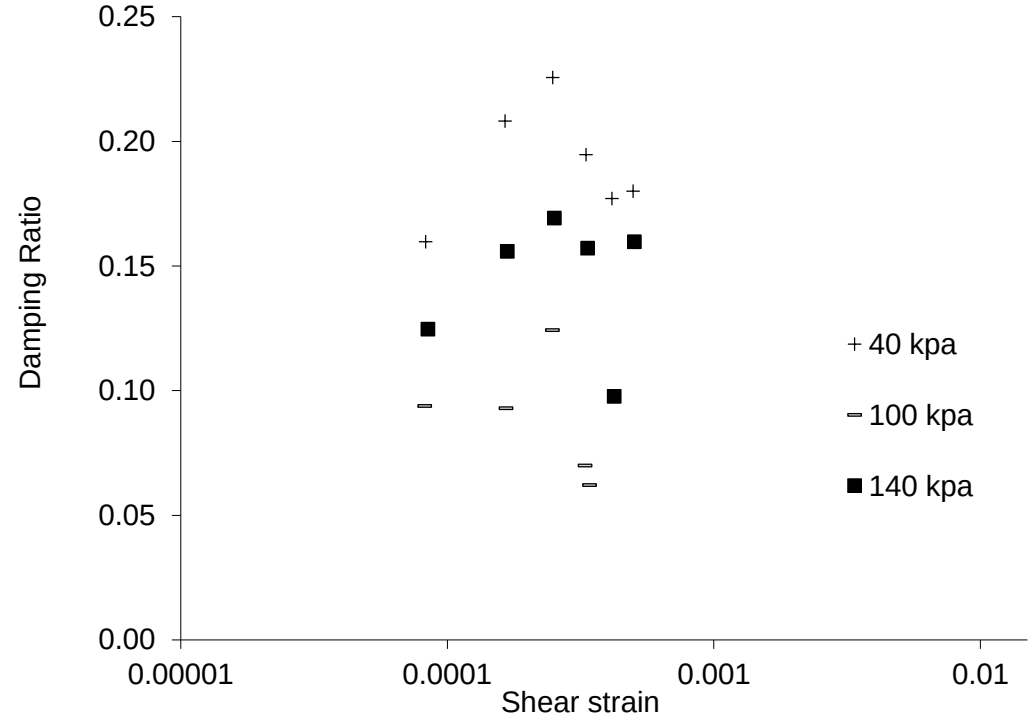

Figure 34: Variation of damping ratio with shear strain for samples D (10cm Diameter)

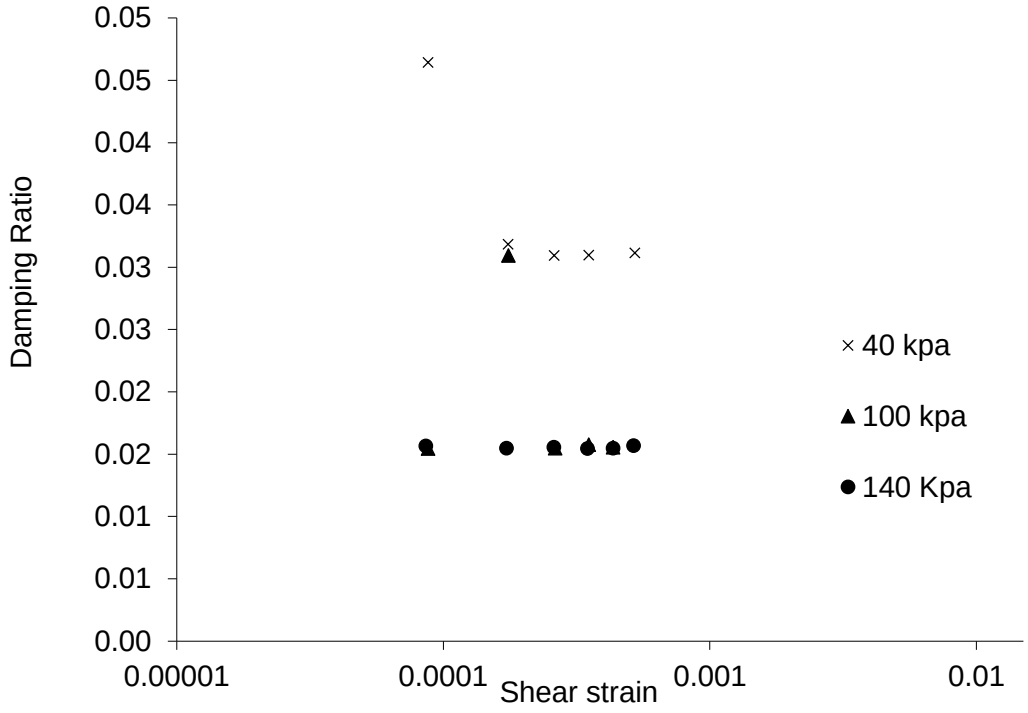

Figure 35: Variation of damping ratio with shear strain for samples E (5cm Diameter)

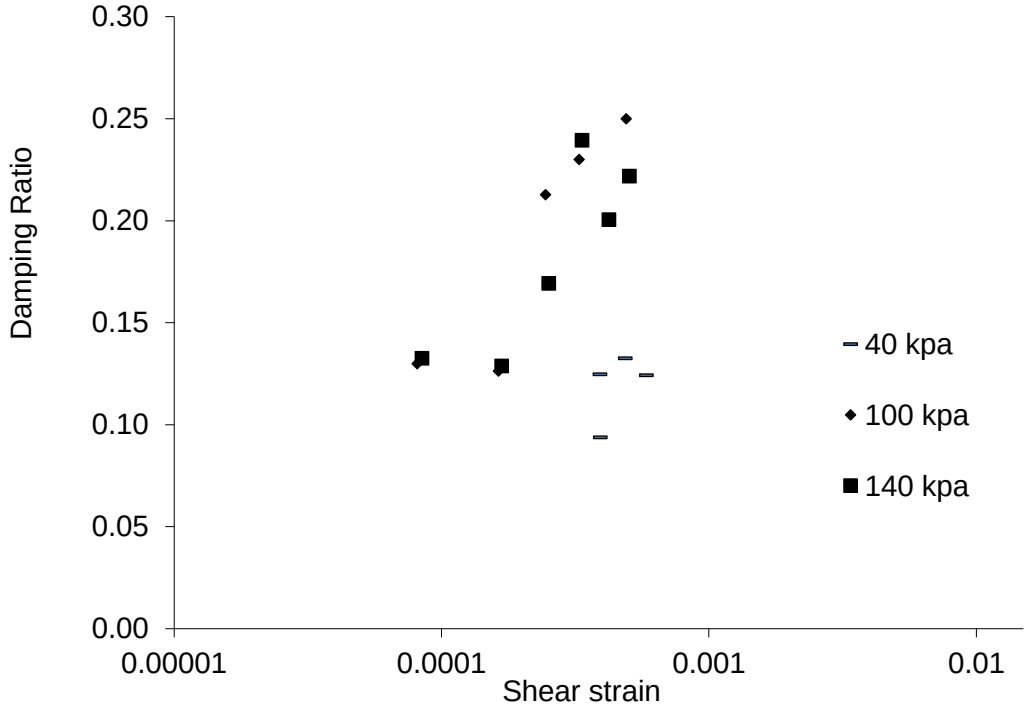

Figure 36: Variation of damping ratio with shear strain for samples E (10cm Diameter)

4.4. Hyperbolic Model

The hyperbolic model was used for curve fitting of *G/Gmax*–γ and $\xi - \gamma$ relationships of the sandy soils tested in the present study. The hyperbolic model with two curve-fitting variables was considered to fit the experimental data. The individual effect of the γ reference strain and the curvature variables "*a*" and "b" are presented in Figures 37-39. The linearity of the *G/Gmax* – Log (γ) curves increases with increasing value of the reference strain. Hence, the higher values of the reference strain show higher shear strength as shown in Figure 37. Furthermore, the overall slope of the G/Gmax – Log γ curves are controlled by the curvature coefficients "*a*" and "*b*'. Figures 38-39 demonstrate the influence of the curvature constants on the *G/Gmax* – Log γ curves. When "*a*" increases and "*b*" and γ *Reference* are kept constant, the upper slope of the G/Gmax – Log γ curves decreases, as shown in Figure 38. On the other hand, coefficient "*b*" has an opposite effect on the lower curvature of the *G/Gmax* – Log γ curves. When "*b*" increases, and "*a*" and γ *Reference* are kept constant, the lower slope of the curves increases, as presented in Figure 39.

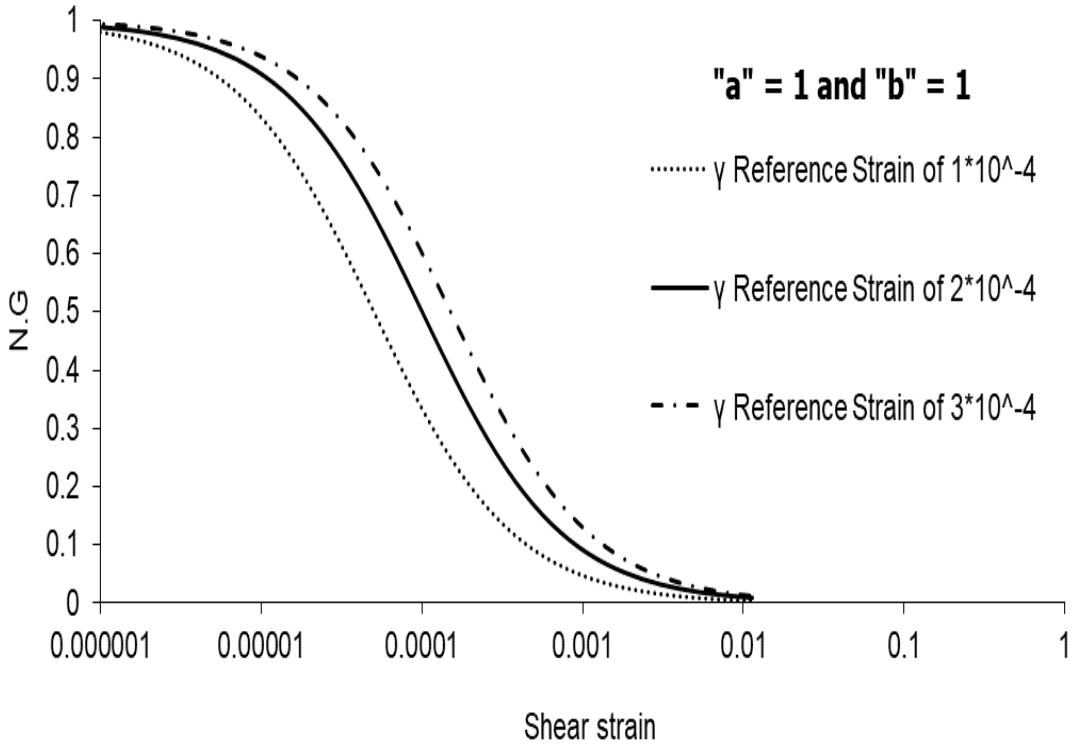

Figure 37: The effect of the reference shear strain *"γ reference"* on the normalized shear modulus (G/Gmax) versus Log γ curves.

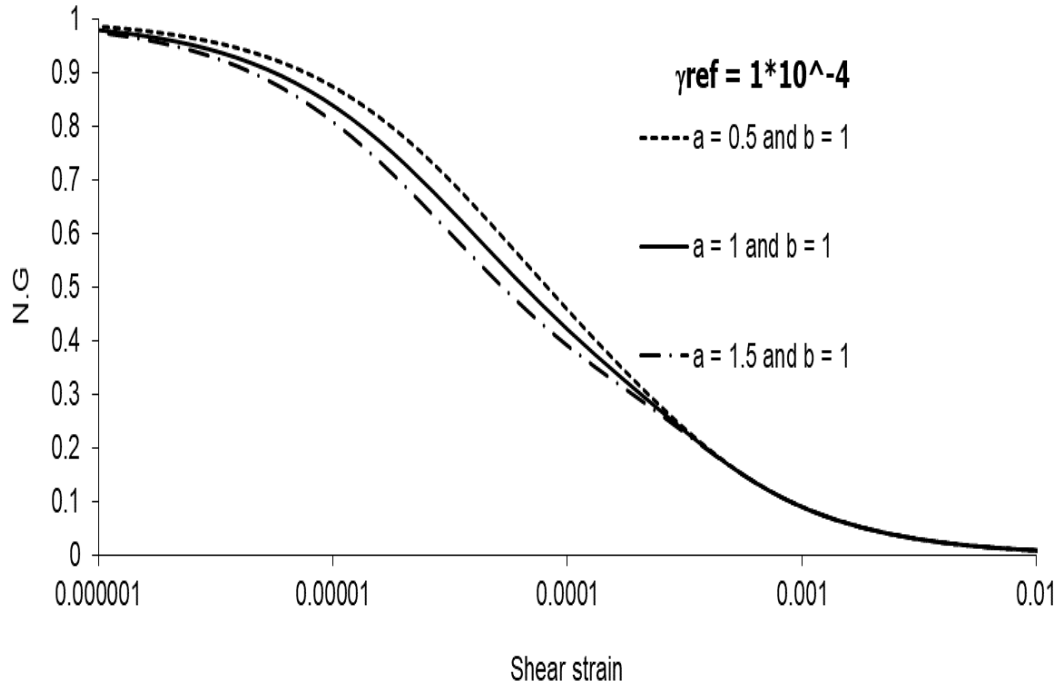

Figure 38: The effect of the curvature coefficient "a" on normalized shear modulus (G/Gmax) versus Log γ curves.

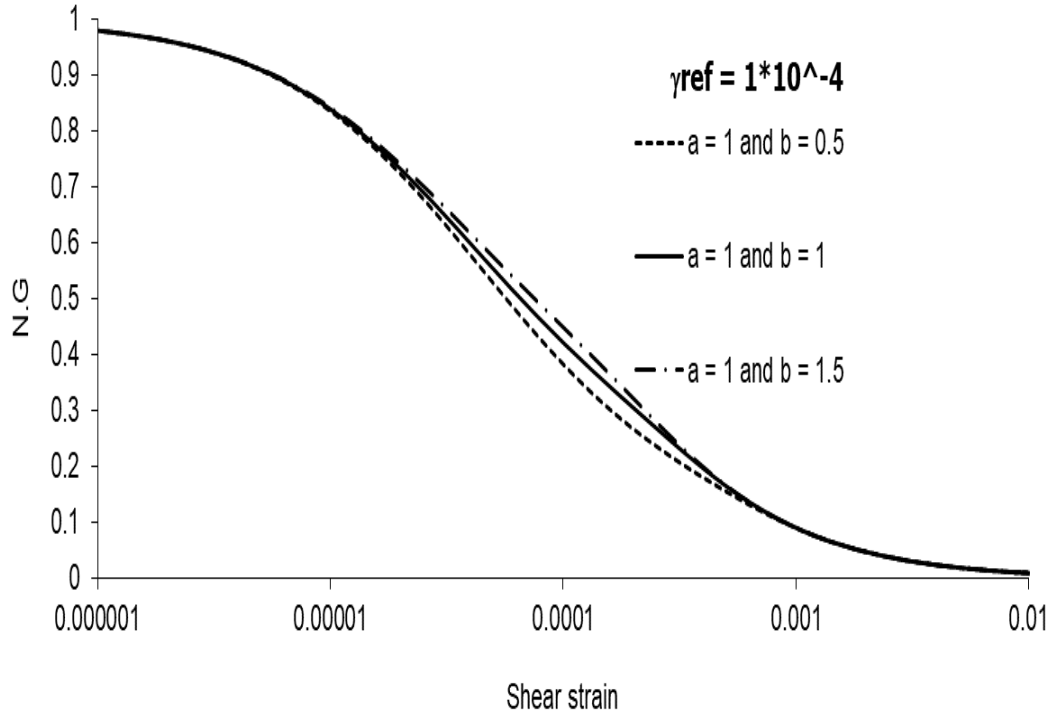

Figure 39: The effect of the curvature coefficient "b" on the normalized shear modulus (G/Gmax) versus Log γ curves.

The hyperbolic model was developed to obtain the best fit for the data evaluated from CT and BE tests. The hyperbolic models were fitted with the obtained experimental data by trying different fitting parameters including the γ reference and the curvature coefficients *"a"* and "*b*". As discussed earlier, the higher values of the γ *reference* strain show higher shear strength. Since increasing the confinement pressure increases the shear strength therefore, the γ *reference* increases as the confinement pressure increases. Moreover, the curvature coefficients *"a*" and "*b"* were almost identical for the different confinement pressures. Table 18 summaries parameters to fit the CT data. The variation of the dynamic properties with the shear strain level after in the form of hyperbolic models are shown in Figures 40-47.

4.4.1. The hyperbolic model of the normalized shear modulus (*G/Gmax*). Figures 40-47 presents the obtained hyperbolic fit for the normalized shear modulus and shear strain relationship for two sample geometries. Both samples sizes were tested at 40, 100, and 140kPa confinement pressures. Normalized shear modulus showed a slight decrease at the low strain shear levels; however, it significantly decreased when the shear strain exceeded the elastic threshold strain i.e. 0.0001. The shear modulus degradations of the two sample sizes (5cm and 10cm) for the gypsum and silty sand specimens are averaged to suits the comparison with a past study conducted by Darendel [81] (Figure 48). The curves of G/Gmax are in agreement with soil behavior identified by Darendel [81] (Figure 48). In addition, several other studies also reported similar *G/Gmax* curves e.g. Hardin and Drnevich [15], Seed et.al. [16], Iwasaki et al. [38], Kokusho [74], and Khan et.al. [82].

4.4.2. The hyperbolic model of the normalized damping ratio (ξ). Figures 49-56 presents the hyperbolic fit for damping ratio (ξ) and shear strain (γ) for two sample geometries. The hyperbolic model fitted the damping data of two sample sizes tested at 40, 100, and 140 kPa of confining pressures. The ξ curves show a constant rate at the low strain shear levels; however, it significantly increases when the shear strain exceeds the elastic threshold strain i.e. 0.0001. Furthermore, the ξ curves of the two sample sizes (5cm and 10cm) for the gypsum and silty sand specimens are averaged an compared with the Darendel's curves [81]. The general trend shown in Figure 57 is consistent with soil behavior identified by Darendel [81]. Furthermore, several other

studies proposed similar damping curves i.e., Hardin and Drnevich [15], Seed et.al [16], Iwasaki et al. [38], Kokusho [74], and Khan et.al. [82].

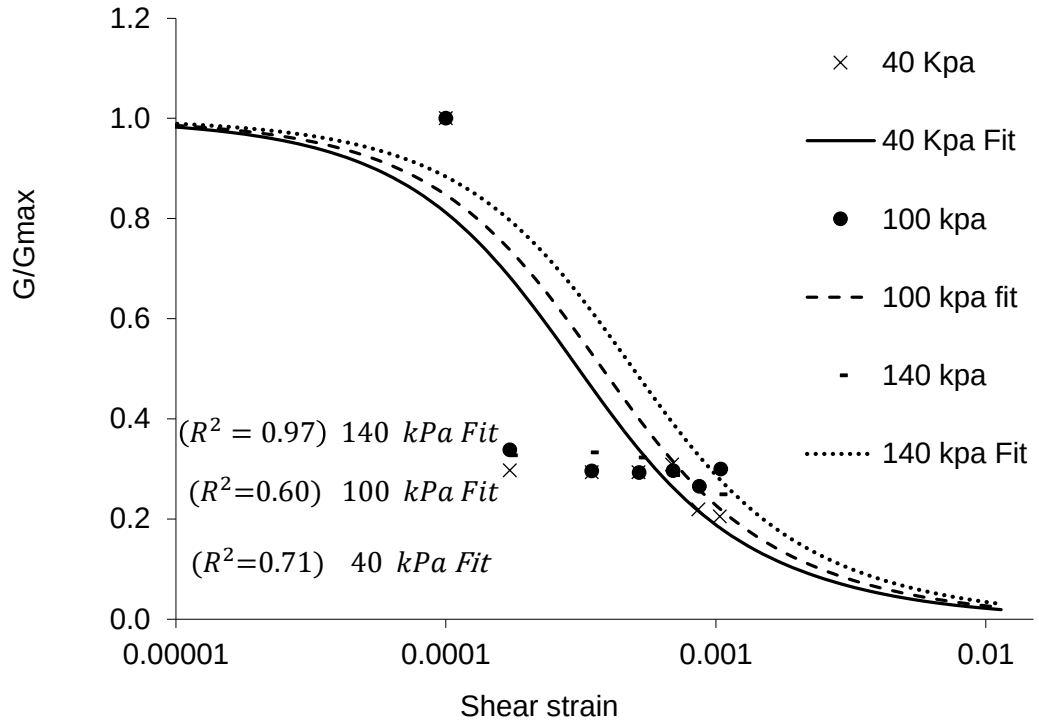

Figure 40: Curve fitting of the low-strain results from CT tests for Sample A (5cm sample diameter)

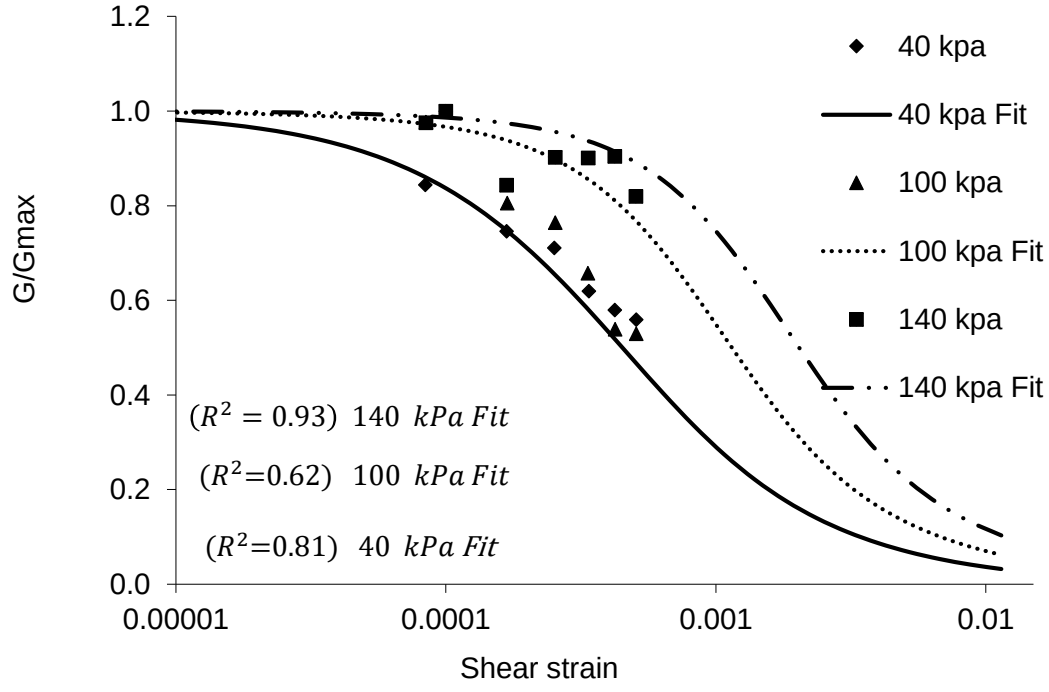

Figure 41: Curve fitting of the low-strain results from CT tests for Sample A (10cm sample diameter

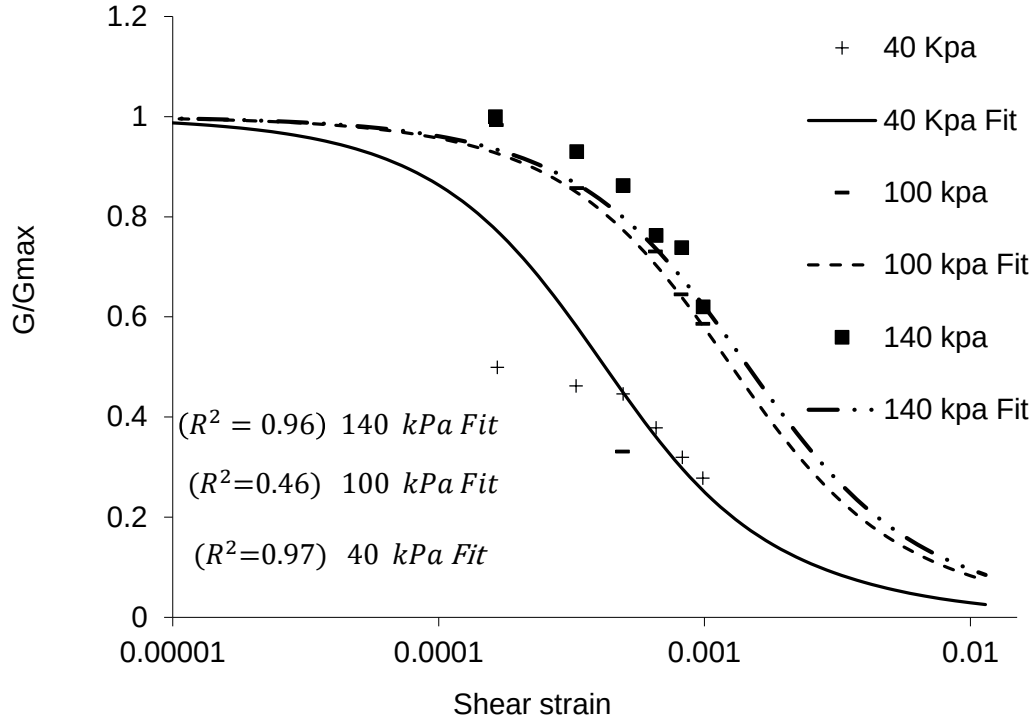

Figure 42: Curve fitting of the low-strain results from CT tests for Sample C (5cm sample diameter

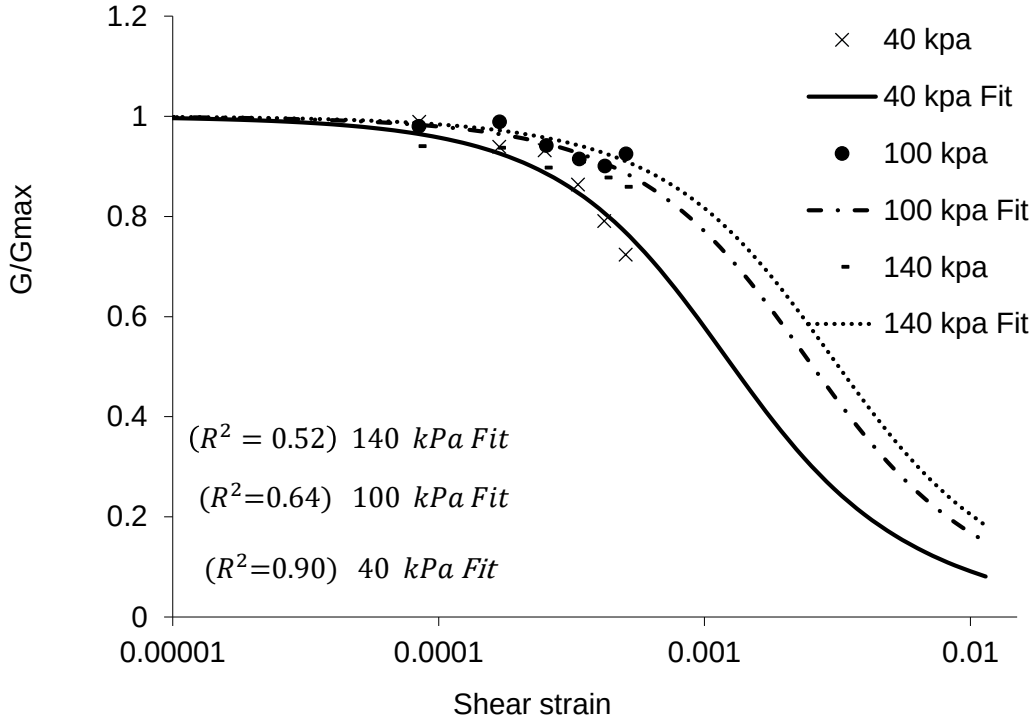

Figure 43: Curve fitting of the low-strain results from CT tests for Sample C (10cm sample diameter)

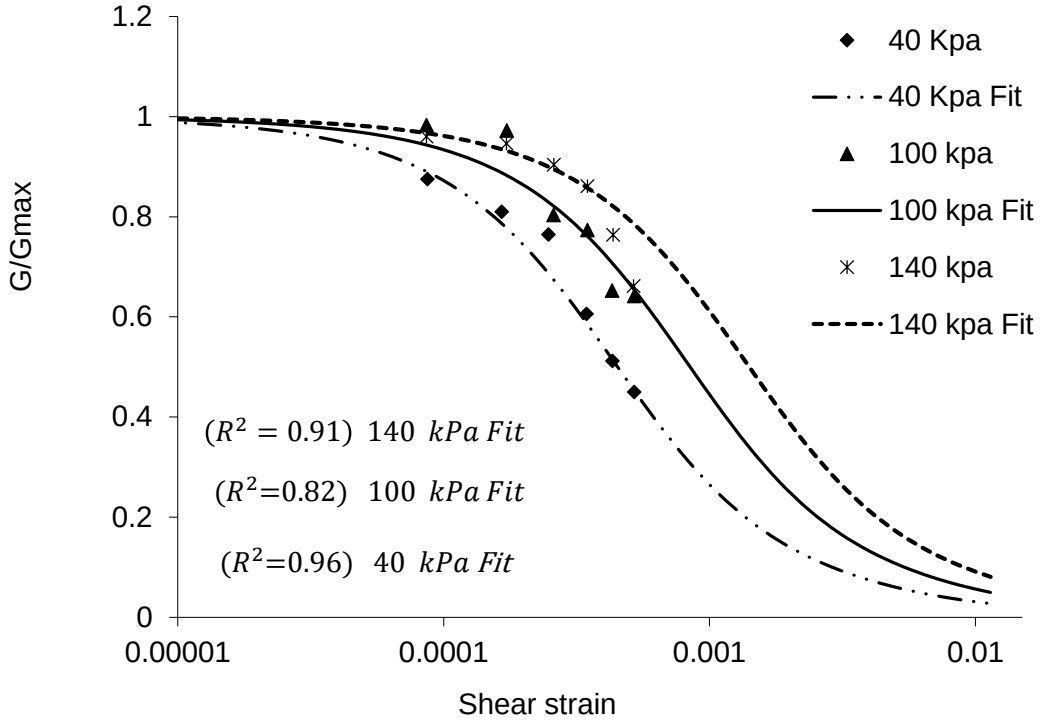

Figure 44: Curve fitting of the low-strain results from CT tests for Sample D (5cm sample diameter)

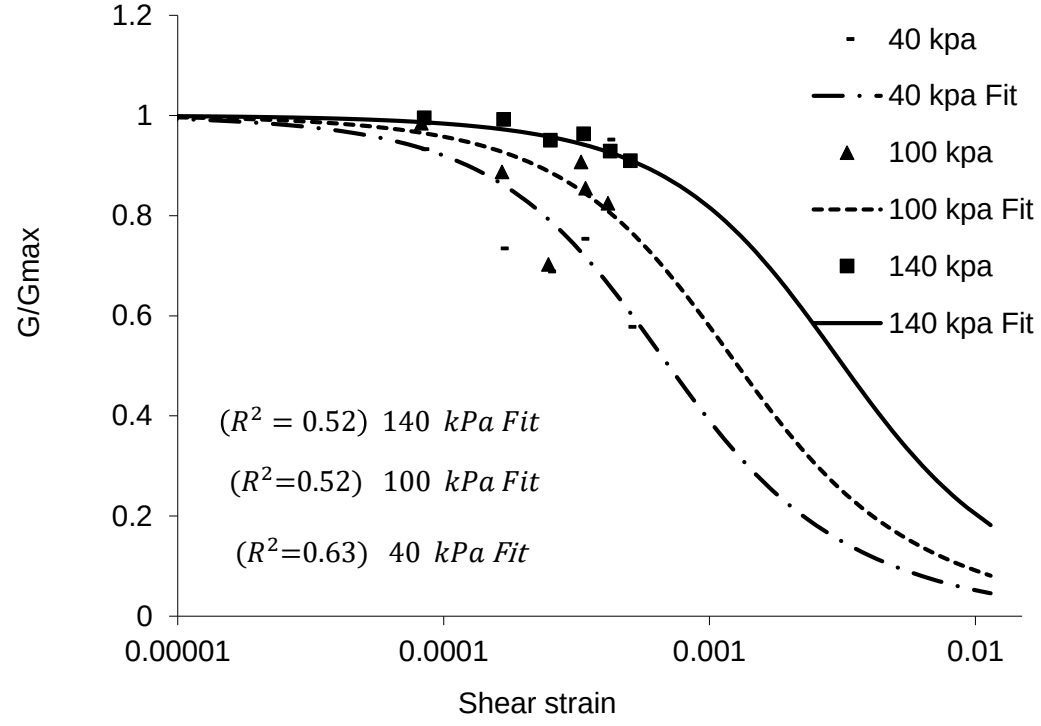

Figure 45: Curve fitting of the low-strain results from CT tests for Sample D (10cm sample diameter)

Table 18: Hyperbolic model parameters

Confinement (kPa)	The used Reference Shear strain (γ ref), and Curvature Coefficients "a" and "b"					
	Normalized G0 (G/Gmax) Fit			Damping Ratio (ξ) Fit		
	γ Ref	a	b	γ Ref	a	b
Sample A Diameter of 5cm						
40	0.00022	-0.63	0.55	0.003	-0.63	0.55
100	0.00027	-0.63	0.55	0.001	-0.63	0.55
140	0.00035	-0.63	0.55	0.01	-0.63	0.55
Sample A Diameter of 10cm						
40	0.00038	-0.3	0.55	0.005	-0.63	0.55
100	0.00075	-0.8	0.55	0.006	-0.63	0.55
140	0.0013	-0.85	0.55	0.05	-0.63	0.55
Sample C Diameter of 5cm						
40	0.0003	-0.63	0.55	0.0025	-0.63	0.55
100	0.0009	-0.63	0.55	0.003	-0.63	0.55
140	0.00105	-0.6	0.55	0.004	-0.63	0.55
Sample C Diameter of 10cm						
40	0.001	-0.6	0.8	0.002	-0.63	0.55
100	0.002	-0.6	0.8	0.007	-0.63	0.55
140	0.0025	-0.6	0.8	0.008	-0.63	0.55
Sample D Diameter of 5cm						
40	0.00032	-0.63	0.55	0.001	-0.63	0.55
100	0.0006	-0.63	0.55	0.002	-0.63	0.55
140	0.001	-0.63	0.55	0.004	-0.63	0.55
Sample D Diameter of 10cm						
40	0.00055	-0.6	0.8	0.0005	-0.8	0.55
100	0.001	-0.6	0.8	0.0007	-0.5	0.55
140	0.0025	-0.6	0.8	0.003	-1	0.55
Sample E Diameter of 5cm						
40	0.0002	-0.63	0.55	0.001	-0.63	0.55
100	0.00035	-0.63	0.55	0.0005	-0.63	0.55
140	0.00045	-0.63	0.55	0.0095	-0.63	0.55
Sample E Diameter of 10cm						
40	0.00025	-0.6	0.8	0.0009	-0.63	0.55
100	0.00038	-0.6	0.8	0.001	-0.2	0.9
140	0.0007	-0.6	0.8	0.005	-0.63	0.55

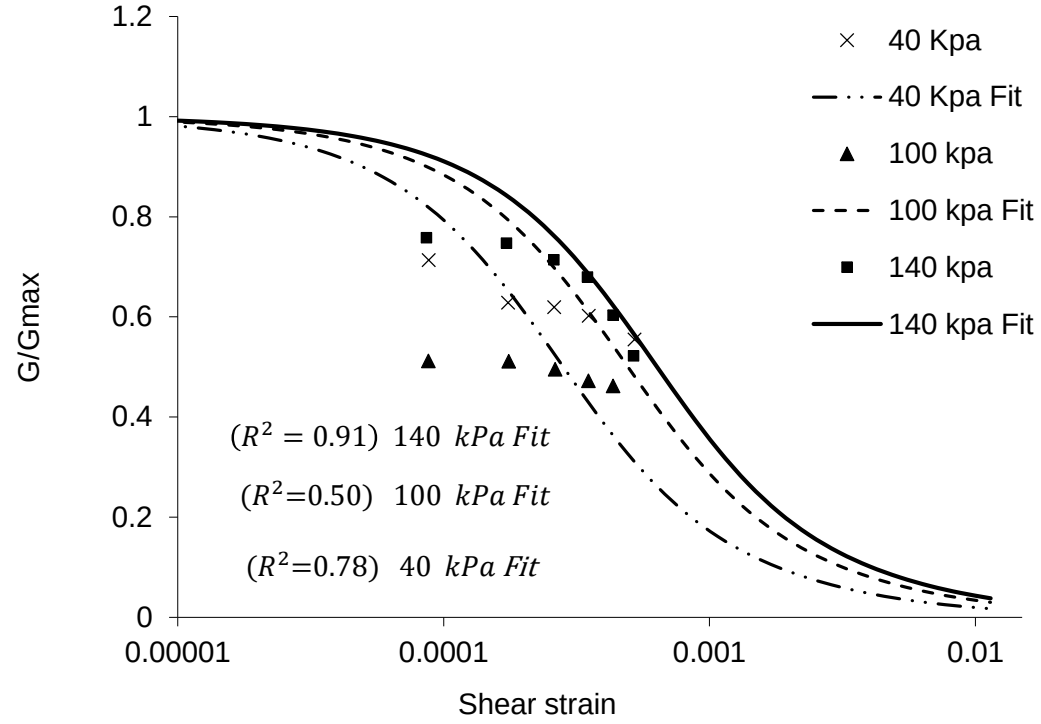

Figure 46: Curve fitting of the low-strain results from CT tests for Sample E (5cm sample diameter)

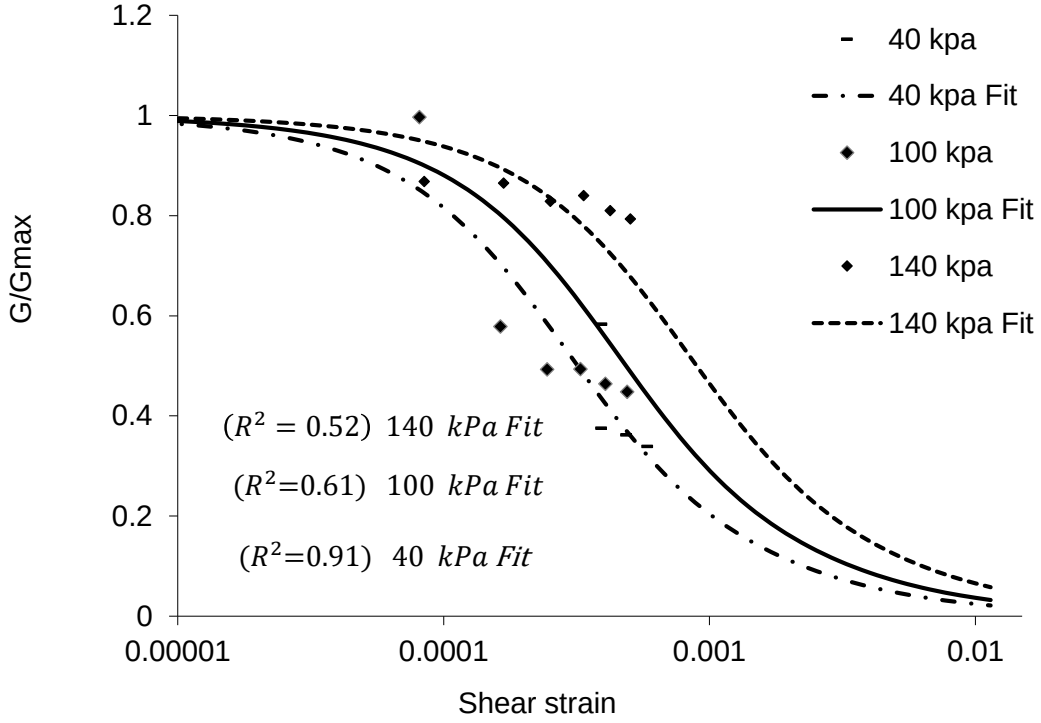

Figure 47: Curve fitting of the low-strain results from CT tests for Sample E (10cm sample diameter)

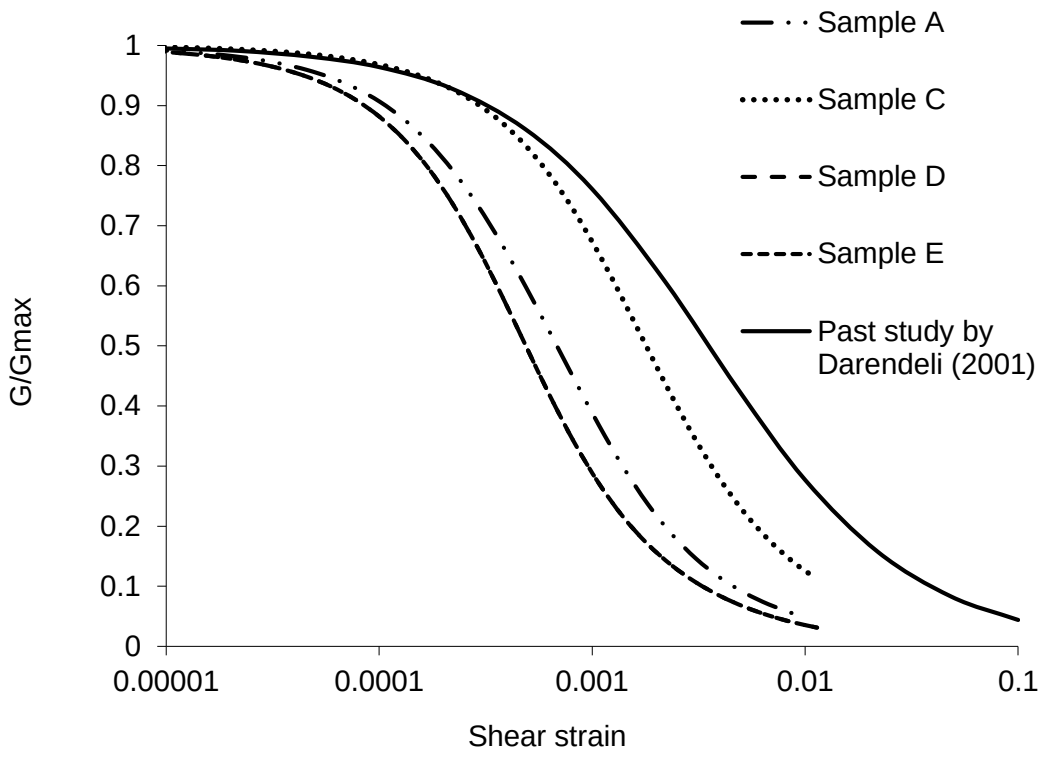

Figure 48: Compared plot of the low-strain results (shear modulus) from CT for sample A, C, D and E with the Darendeli's curve [82].

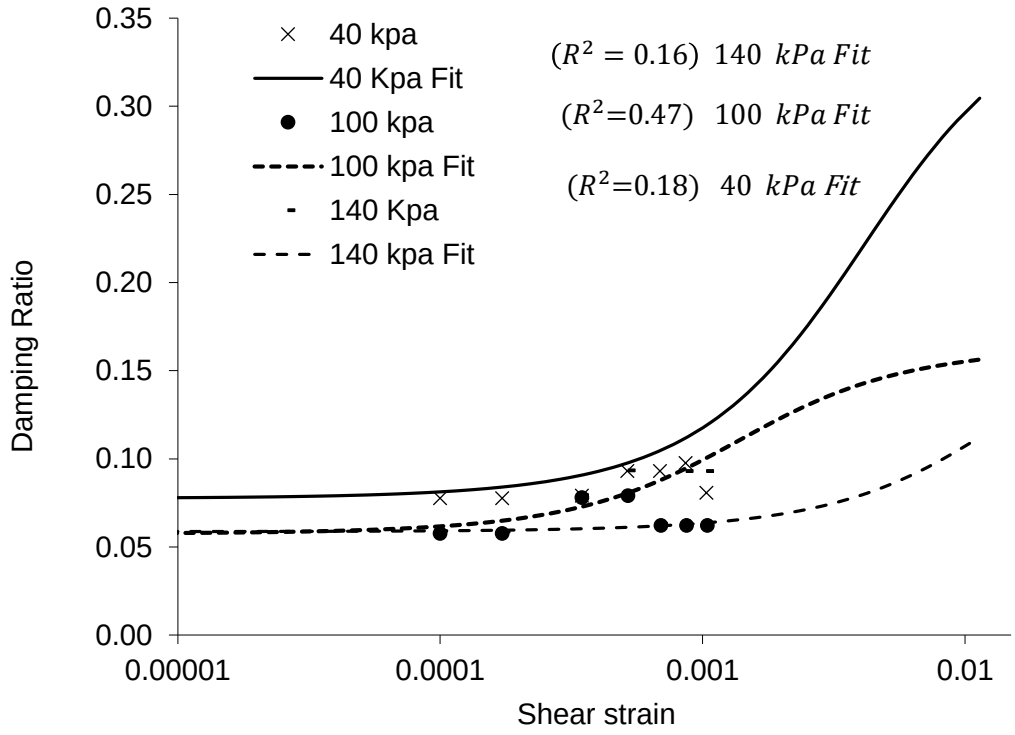

Figure 49: Curve fitting of the low-strain results from CT tests for Sample A (5cm sample diameter)

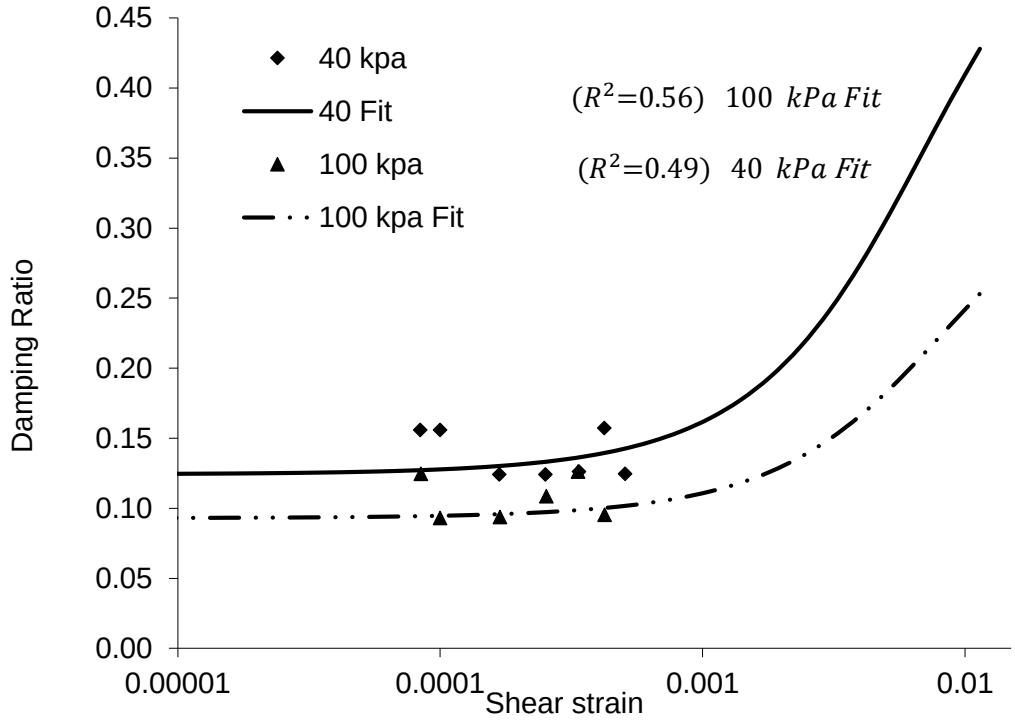

Figure 50: Curve fitting of the low-strain results from CT tests for Sample A (10cm sample diameter)

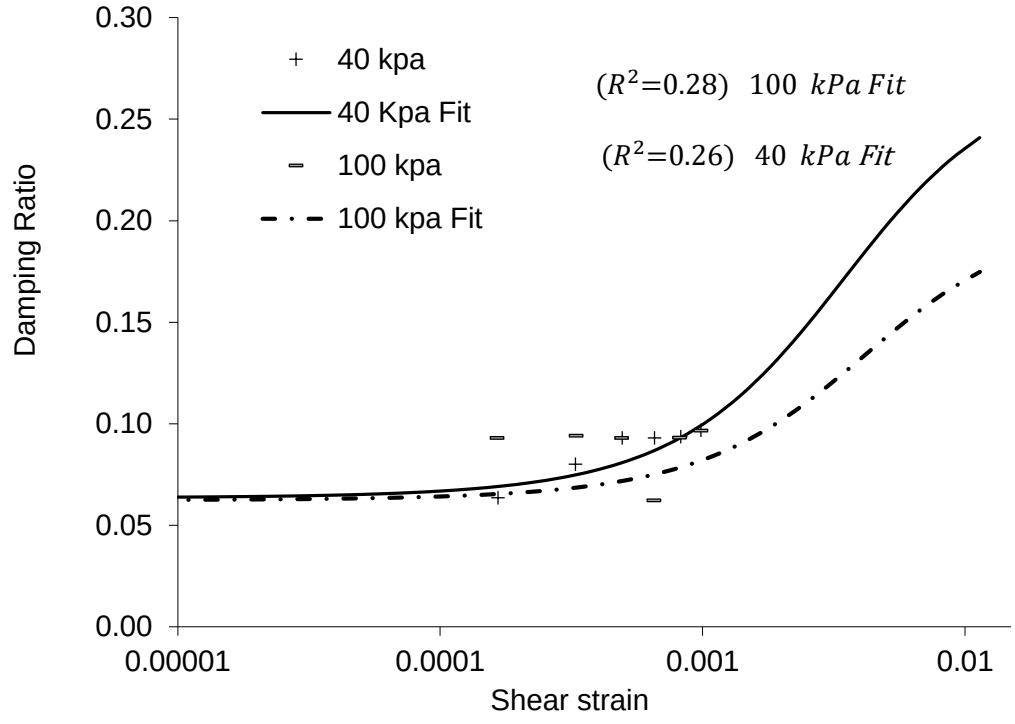

Figure 51: Curve fitting of the low-strain results from CT tests for Sample C (5cm sample diameter)

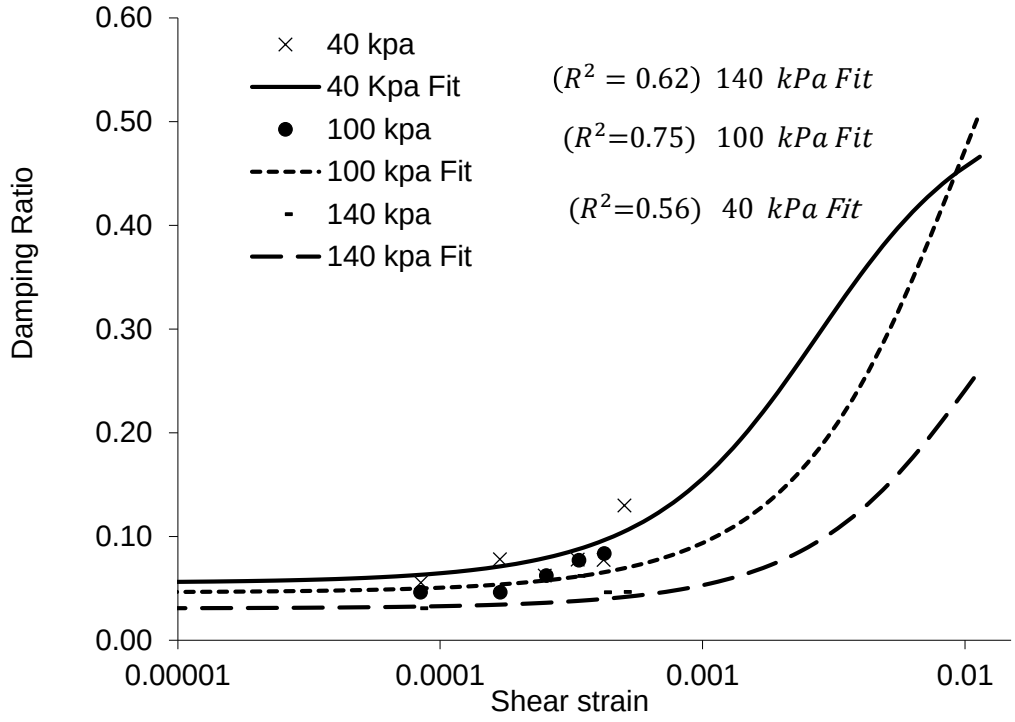

Figure 52: Curve fitting of the low-strain results from CT tests for Sample C (10cm sample diameter)

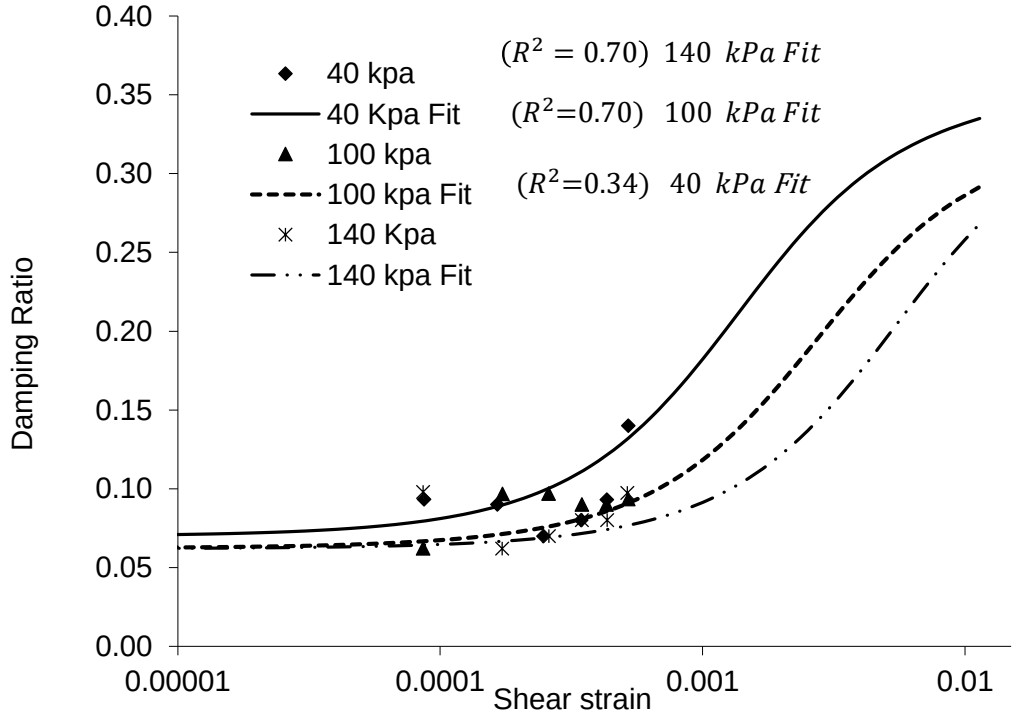

Figure 53: Curve fitting of the low-strain results from CT tests for Sample D (5cm sample diameter)

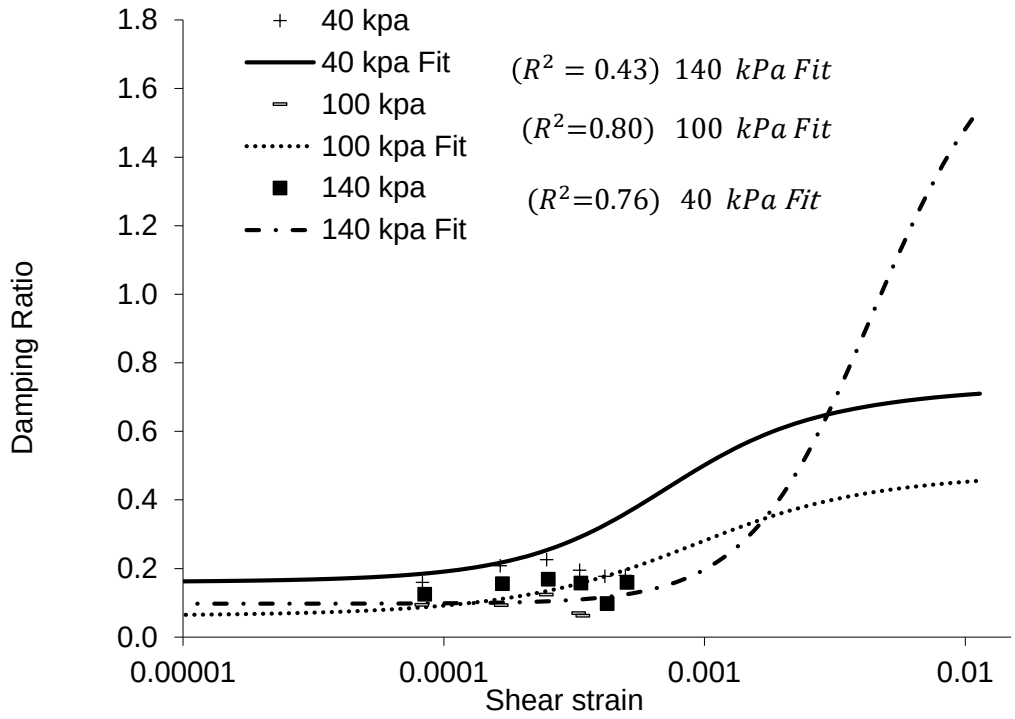

Figure 54: Curve fitting of the low-strain results from CT tests for Sample D (10cm sample diameter)

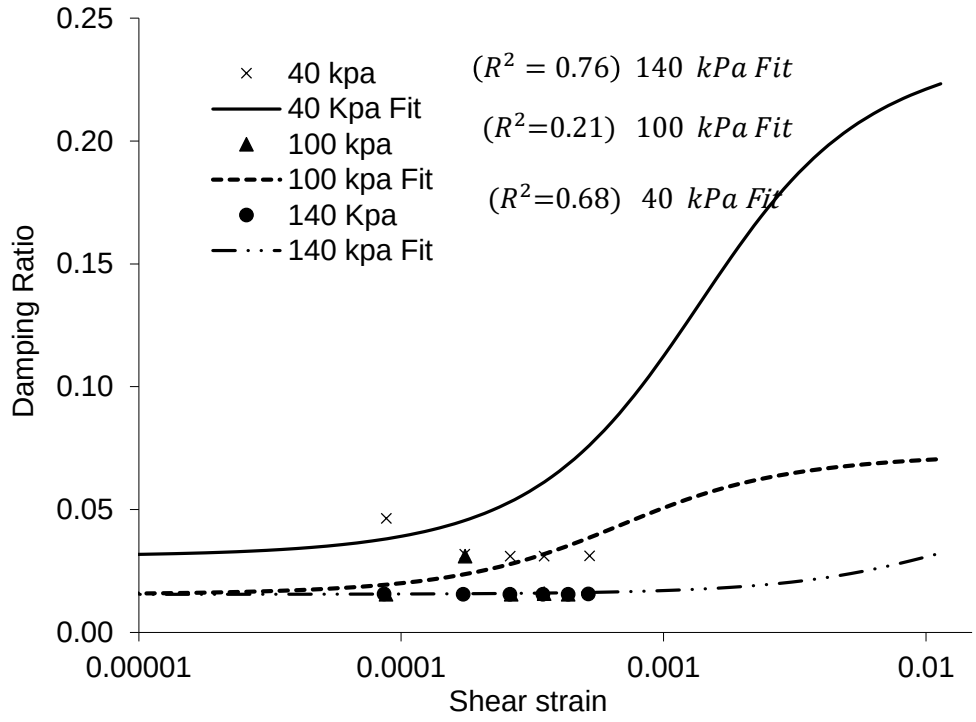

Figure 55: Curve fitting of the low-strain results from CT tests for Sample E (5cm sample diameter)

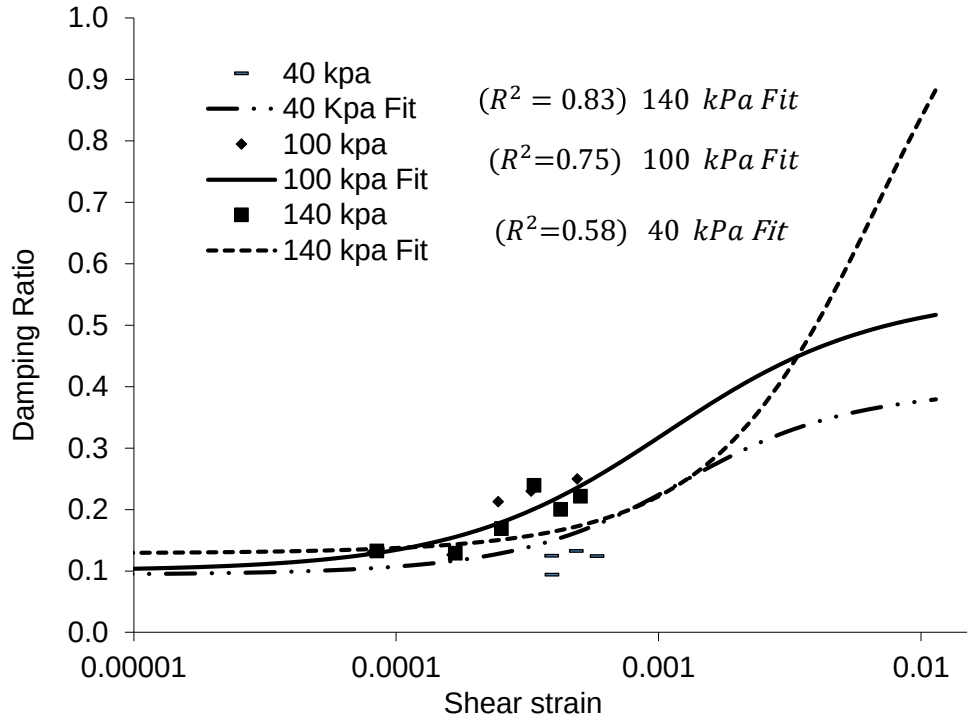

Figure 56: Curve fitting of the low-strain results from CT tests for Sample E (10cm sample diameter.

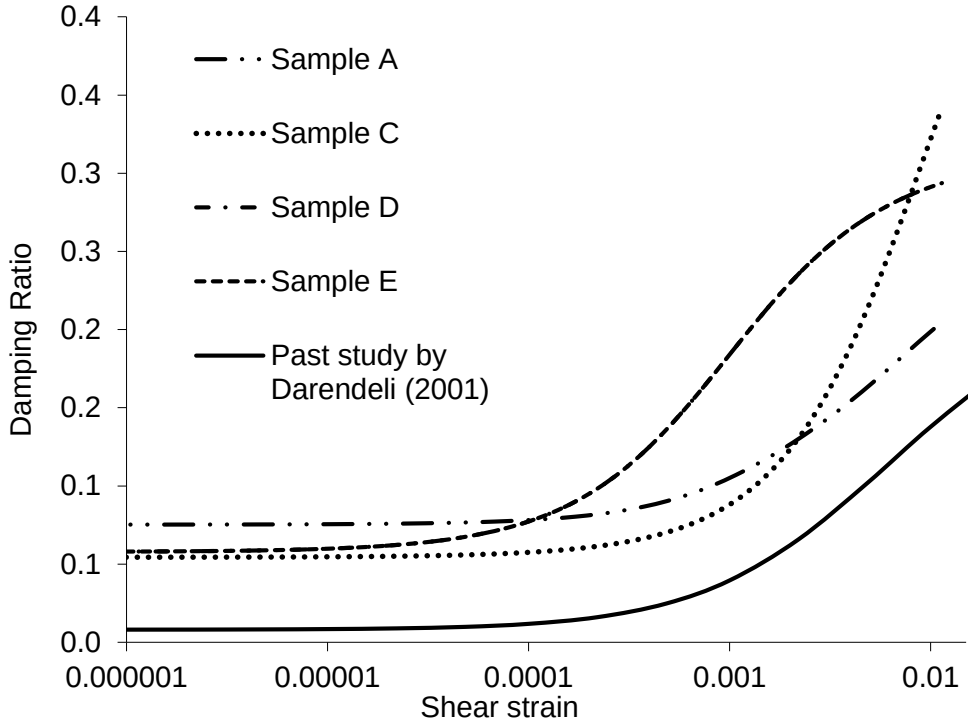

Figure 57: Compared plot of the low-strain results (damping ratio) from CT for sample A, C, D and E with the Darendeli's curve [82].

4.5. Effect of Sample Size

4.5.1. The effect of sample size on the shear modulus (*G/Gmax*). The influence of the sample size was investigated in this study, and it was observed that the shear modulus was affected by the size of the sample. As discussed in the previous section, two sample diameters and heights were tested in the present study. However, the diameter to height (D/H) ratio was kept unchanged; both sample sizes had (D/H) ratio of 2.

Figures 58-69 show the effect of varying the sample size on the normalized shear modulus G/Gmax for the four tested specimens (Sample A, C, D, and E) at different shear strain levels. The normalized shear modulus shows a slight decrease at the low shear strain levels followed by a large decrease beyond the elastic threshold strain for all tested specimens. This trend remained constant for both sample sizes. However, the difference can be observed at the location of the point of deflation where the shear strain exceeds the elastic threshold strain.

Figures 58-69 demonstrates that increasing the sample size from (5cm x 10cm) to (10cm x 20cm) results in an appreciable rise in the shear modulus for the gypsum-based sandy specimen (sample A). Similar behavior is observed in the rest of the specimens, as shown in Figures 61-69, for samples C, D and E. However, the difference in shear modulus between both sample geometries is slightly decreased in sample C in comparison to sample A. In addition, the difference decreased further in two silty specimens (sample D and sample E).

The variation of the normalized shear modulus with shear strain of both samples sizes at identical confining pressure i.e. 40, 100 and 140kPa are plotted as a single graph (Figures 58-69) to evaluate the effect of sample size on the shear modulus variation at each cell pressure. In sample A, the scatter between the two curves of G variation increases as the cell pressure increase, however; this trend is not consistent for the remaining of samples (Figures 58-60). For example, Sample C shows same influence of sample size affect as the confining pressure increases (Figures 61-63). The effect of sample size and the confining pressure is not directly proportional as the variation of the shear modulus with the shear strain.

4.5.2. The effect of sample size on the damping ratio (ξ). The ξ is influenced by several parameters. The most important parameter was found to be the shear strain

and confining pressure. It was found that the confining pressure and the shear strain were not the only important parameters affecting the ξ. The sample geometry was found to have a significant effect on the ξ. In this study, these factors were investigated along with the influence of the changing of the sample size.

Figures 70-80 show the effect of varying the sample diameter on the ξ for four different samples; samples A, C, D and E, respectively. In all plots, the damping ratio (ξ) of the 10cm samples was higher than the damping ratio (ξ) of the 5cm samples. According to the damping ratio and shear strain relationship (ξ- γ), the material damping ratio (ξ) increases with the increase of shear strain and decrease with an increase in confinement . Hence, the degradation of the damping ratio decreases with an increase in the confining pressure. The damping ratio (ξ) curve of the lower confinement shows the highest damping ratio (ξ) curve in the plot. In the present study, three confinement pressures of 40, 100 and 140kPa were applied to both sample sizes (5cm and 10cm). Therefore, damping ratio (ξ) curves decrease with an increase in confinements of 40, 100, and 140 kPa. The results show a unique trend that all of the damping ratio (ξ) curves of 10cm samples are above the damping ratio (ξ) curves of the 5cm samples in all tested specimens, as shown in Figures 70-80.

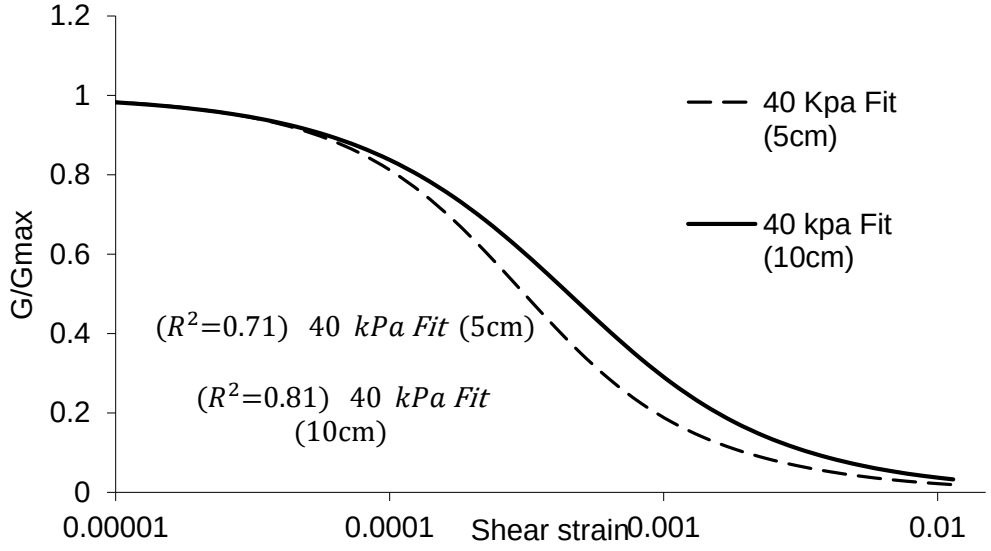

Figure 58: The effect of sample size on shear modulus variation with shear strain (Sample A, 40kPa)

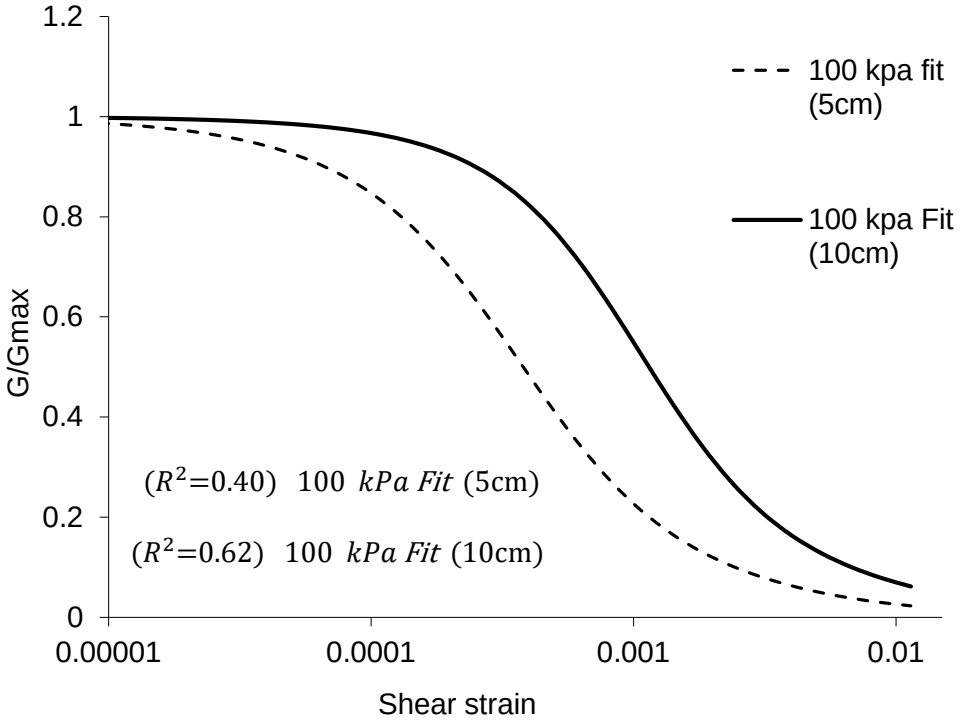

Figure 59: The effect of sample size on shear modulus variation with shear strain (Sample A, 100kPa)

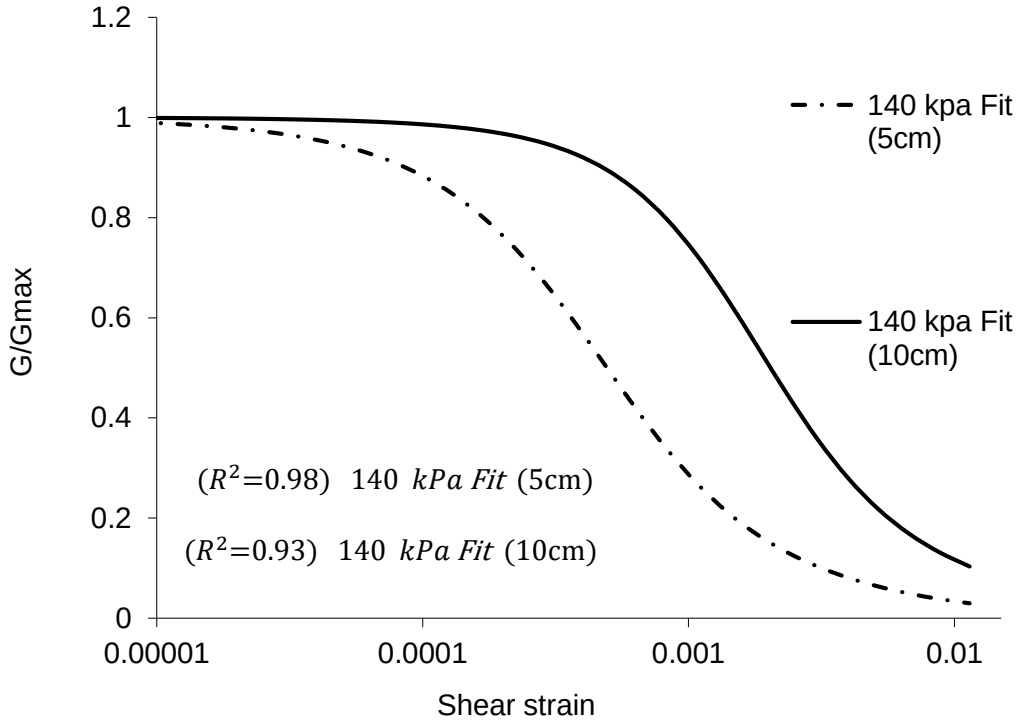

Figure 60: The effect of sample size on shear modulus variation with shear strain (Sample A, 140kPa)

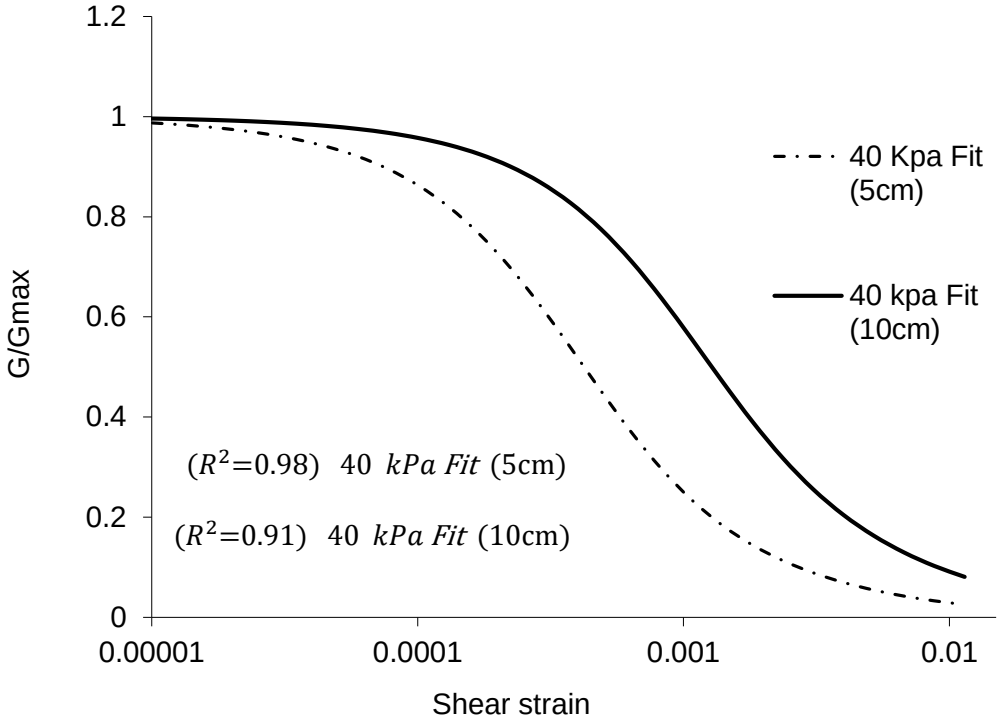

Figure 61: The effect of sample size on shear modulus variation with shear strain (Sample C, 40kPa)

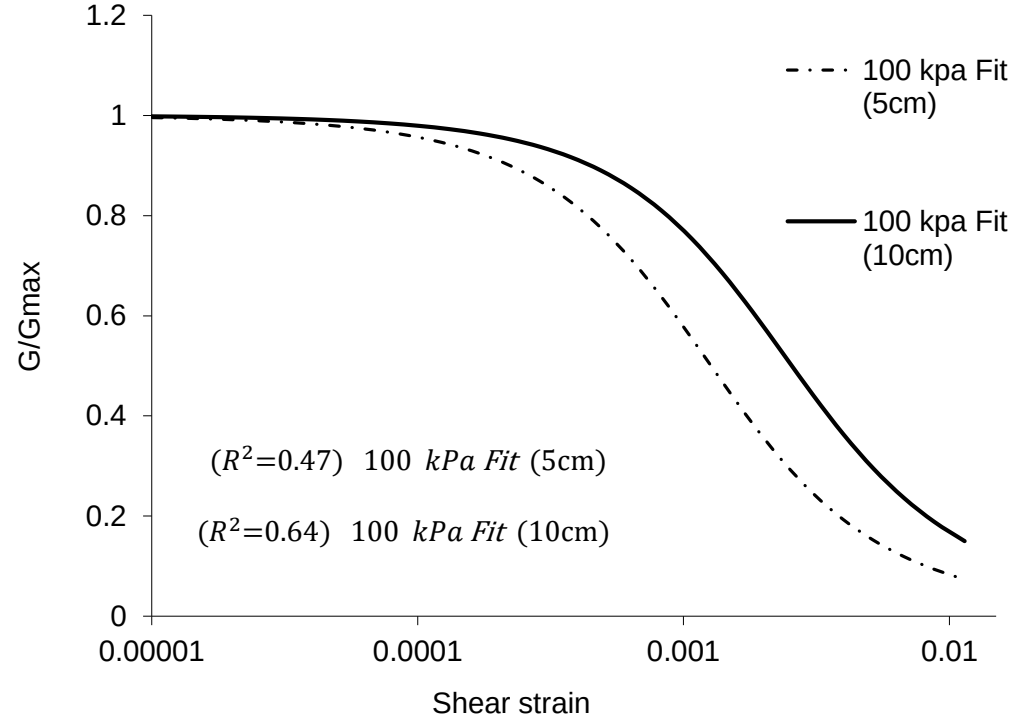

Figure 62: The effect of sample size on shear modulus variation with shear strain (Sample C, 100kPa)

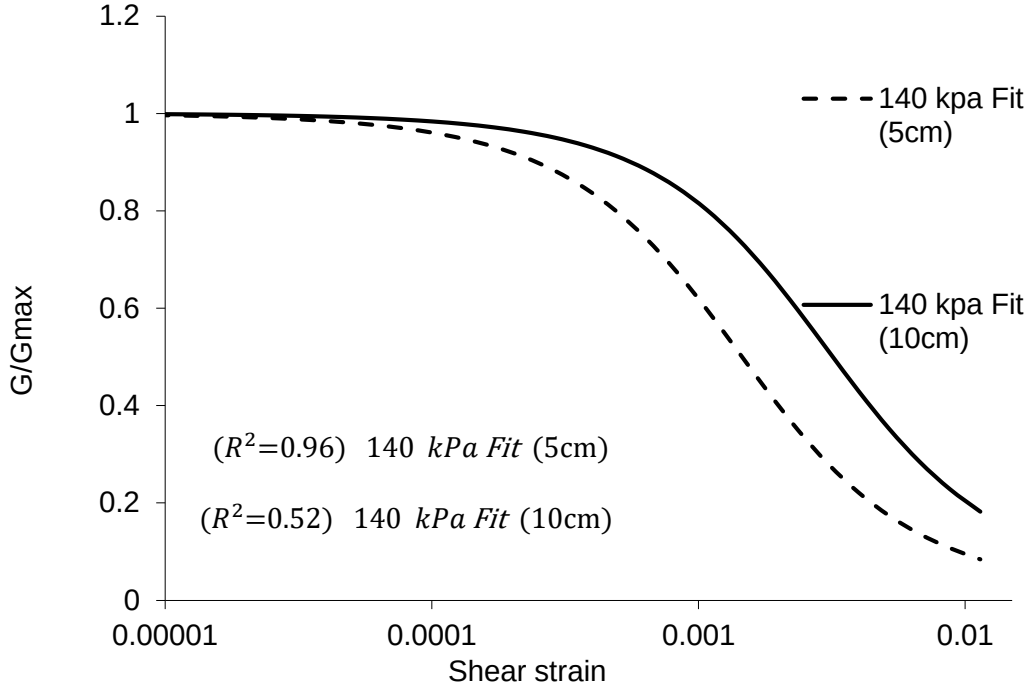

Figure 63: The effect of sample size on shear modulus variation with shear strain (Sample C, 140kPa)

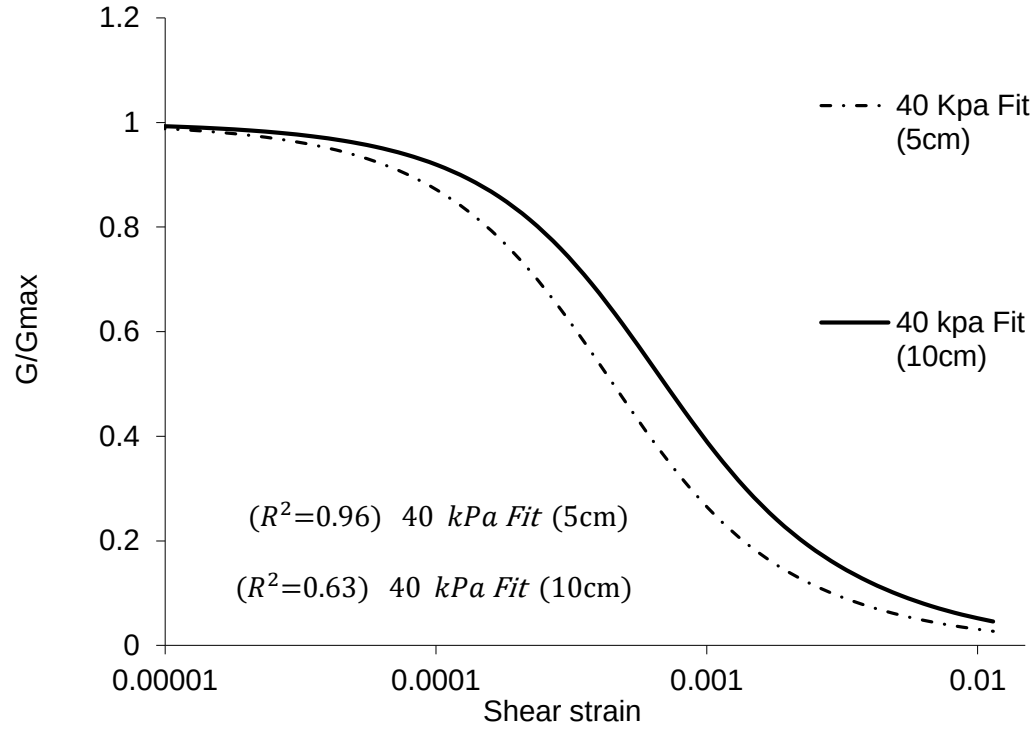

Figure 64: The effect of sample size on shear modulus variation with shear strain (Sample D, 40kPa)

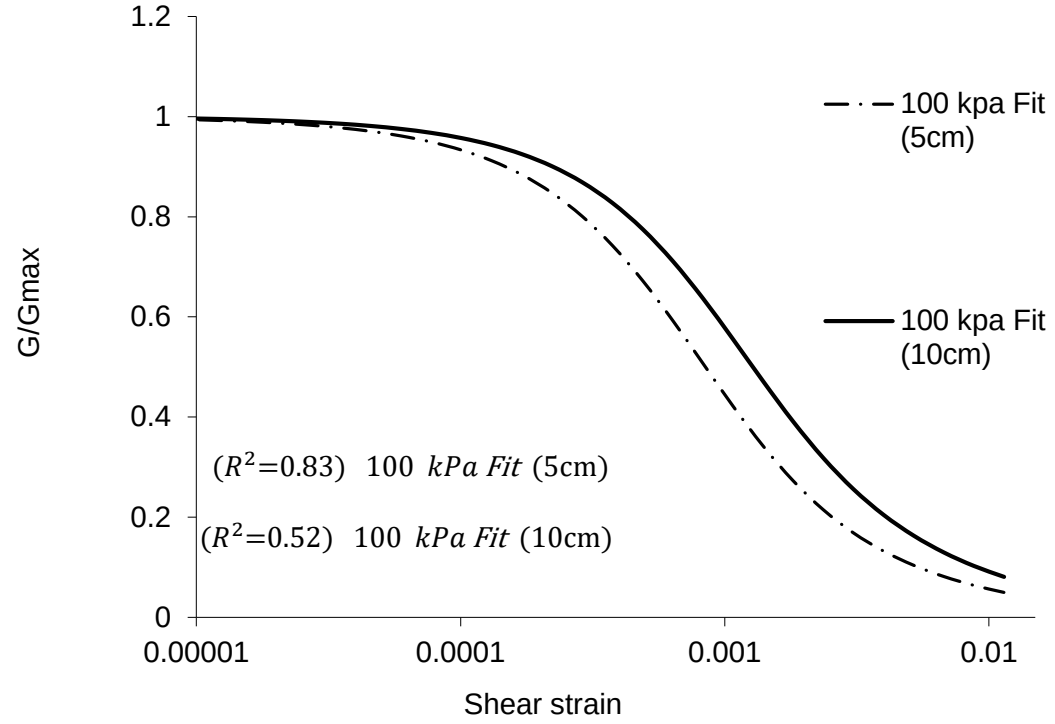

Figure 65: The effect of sample size on shear modulus variation with shear strain (Sample D, 100kPa)

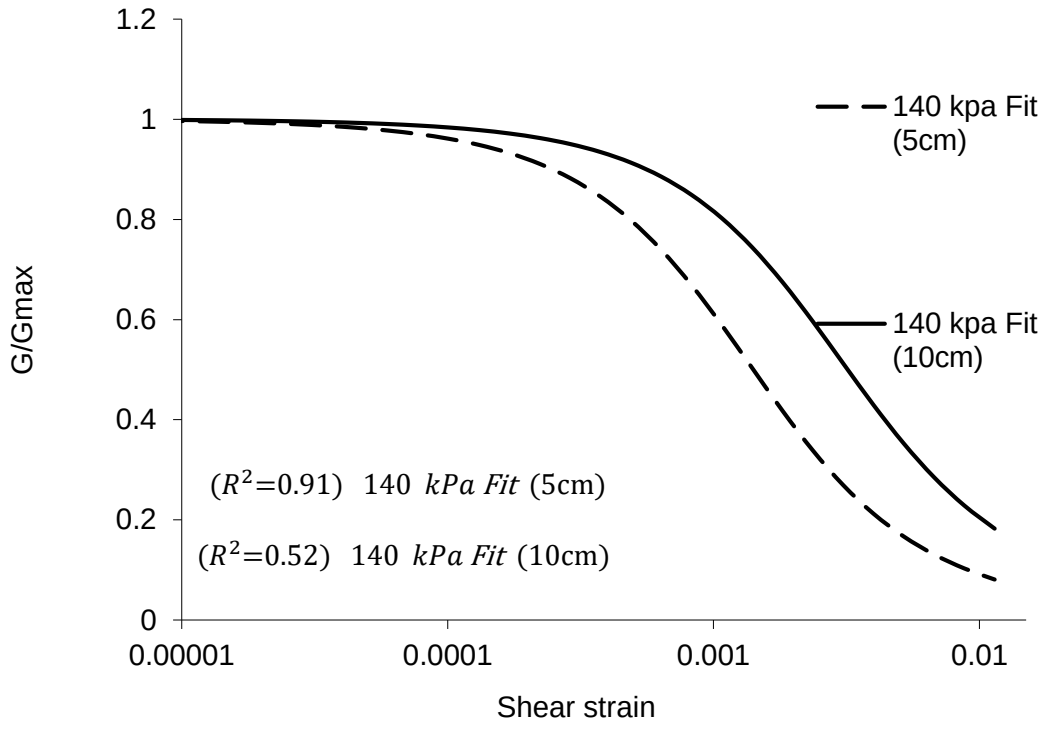

Figure 66: The effect of sample size on shear modulus variation with shear strain (Sample D, 140kPa)

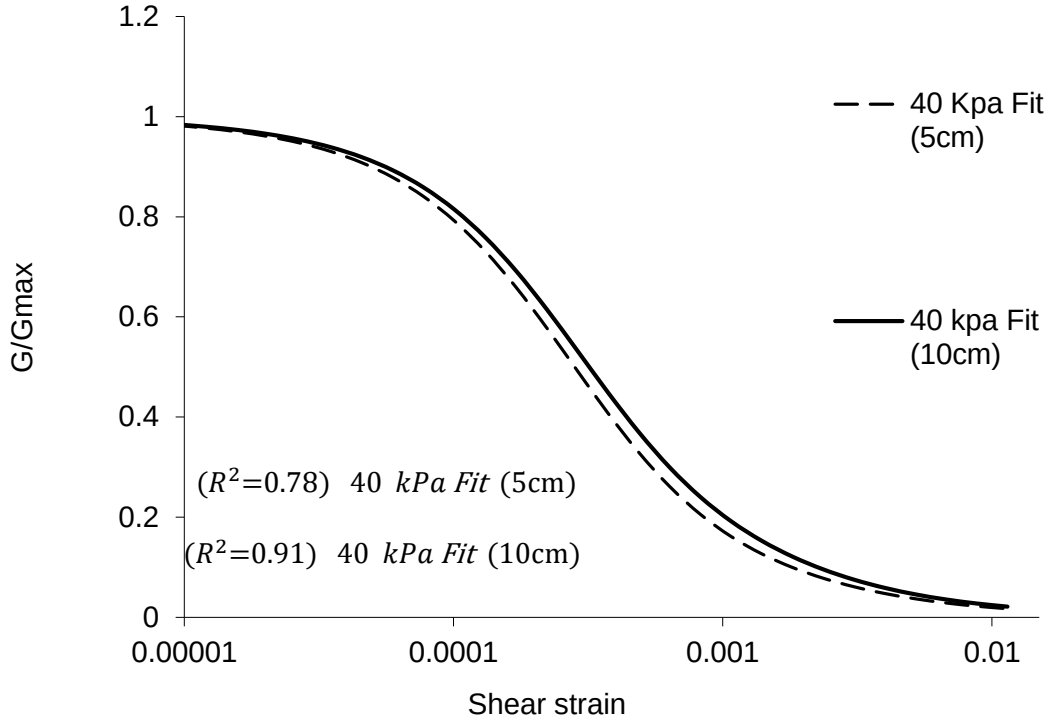

Figure 67: : The effect of sample size on shear modulus variation with shear strain (Sample E, 40kPa)

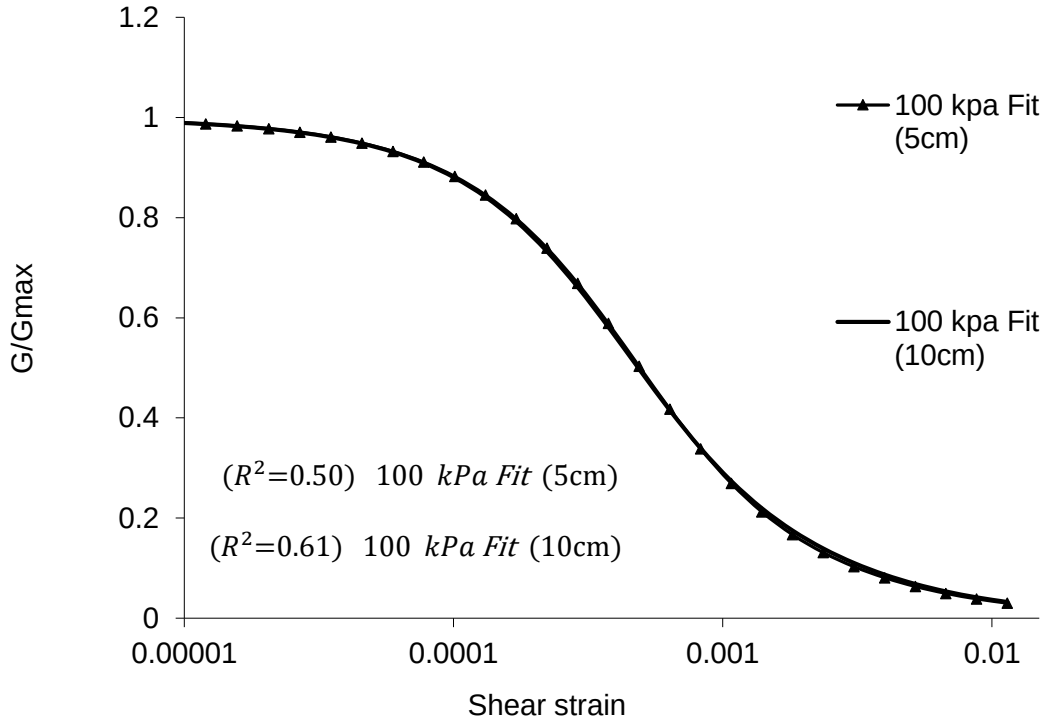

Figure 68: : The effect of sample size on shear modulus variation with shear strain (Sample E, 100kPa)

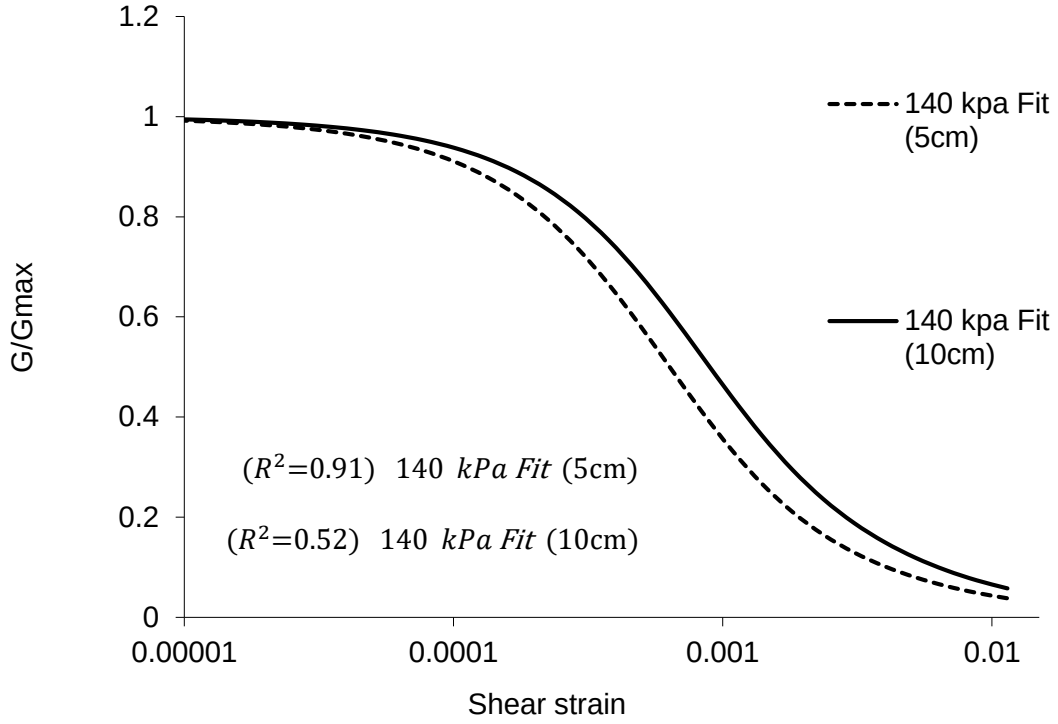

Figure 69: : The effect of sample size on shear modulus variation with shear strain (Sample E, 140kPa)

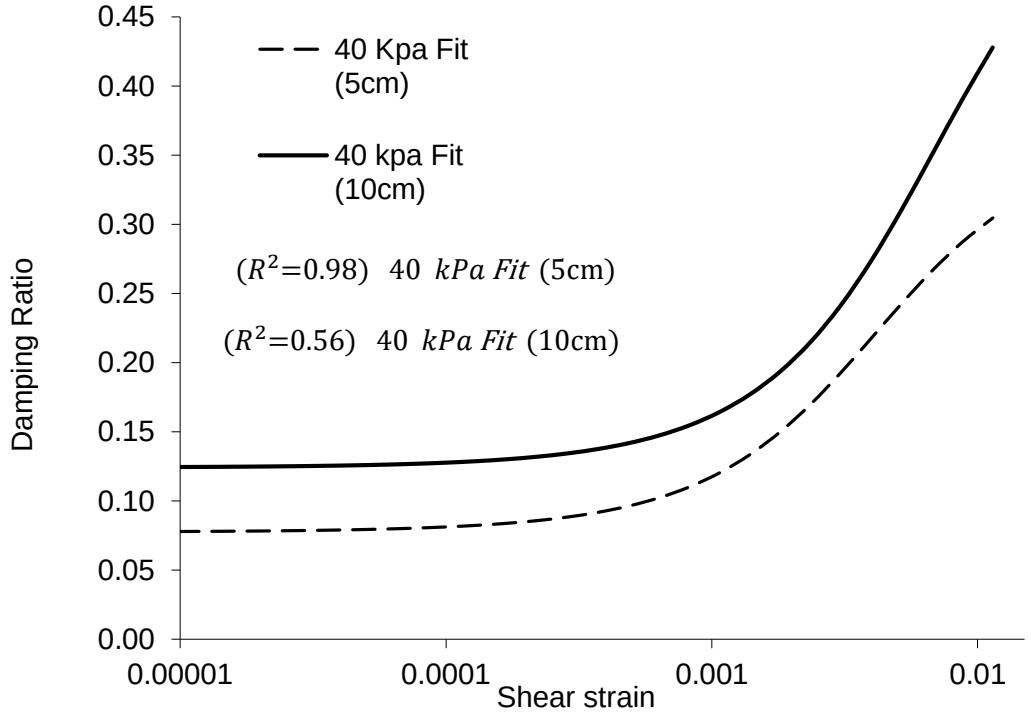

Figure 70: The effect of sample size on damping ratio variation with shear strain (Sample A, 40kPa)

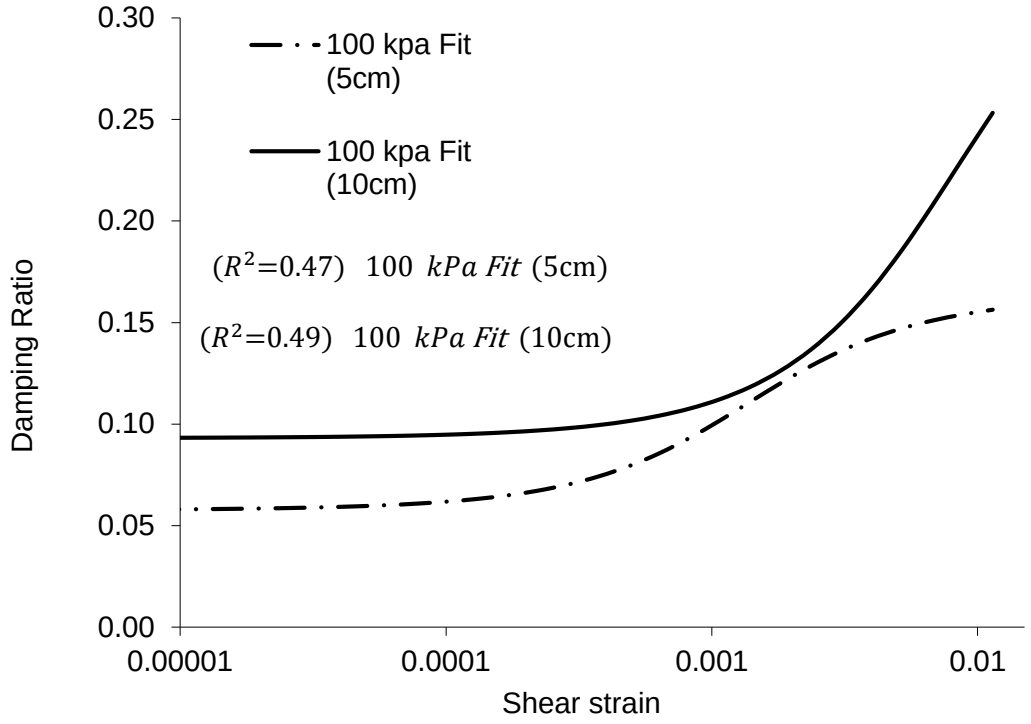

Figure 71: The effect of sample size on damping ratio variation with shear strain (Sample A, 100kPa)

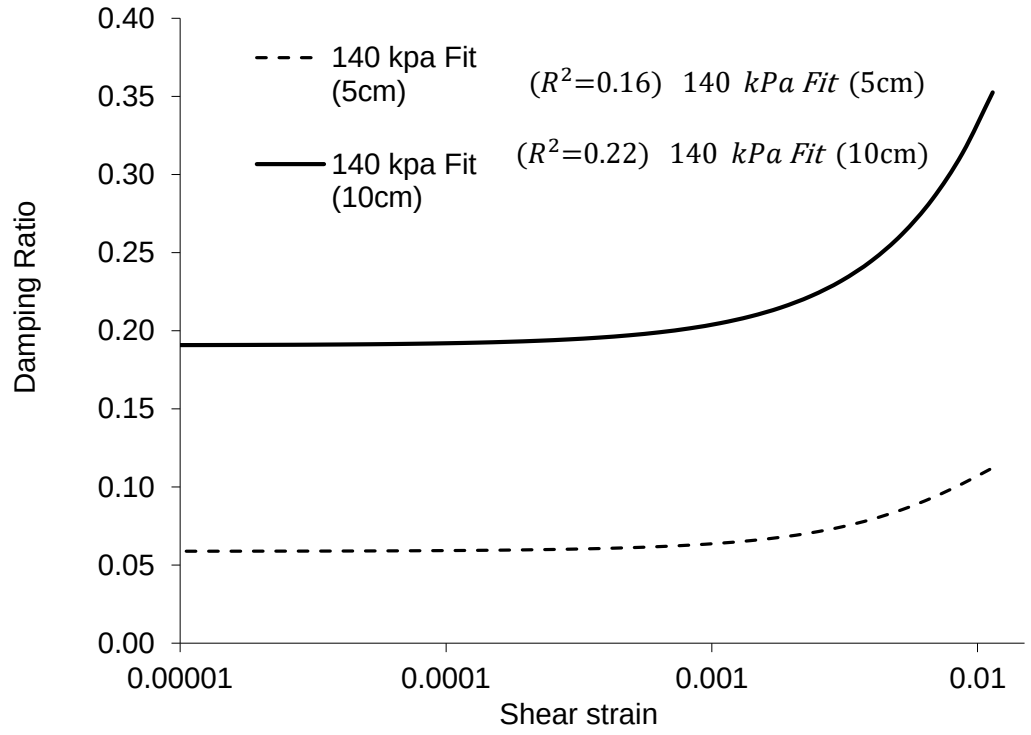

Figure 72: The effect of sample size on damping ratio variation with shear strain (Sample A, 140kPa)

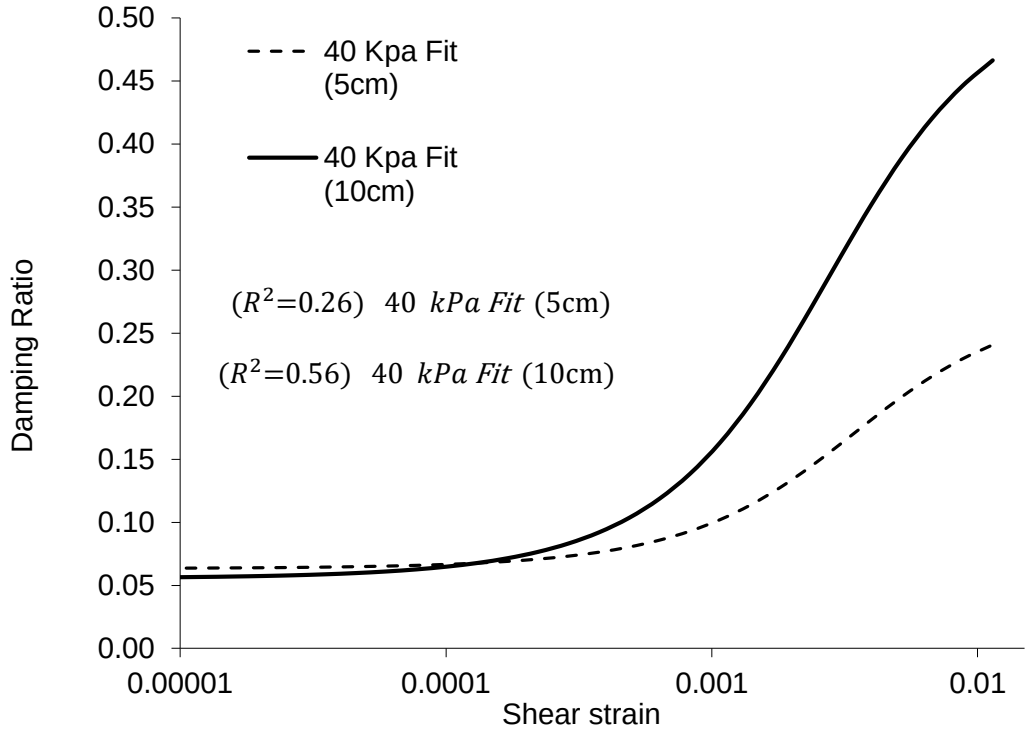

Figure 73: The effect of sample size on damping ratio variation with shear strain (Sample C, 40kPa)

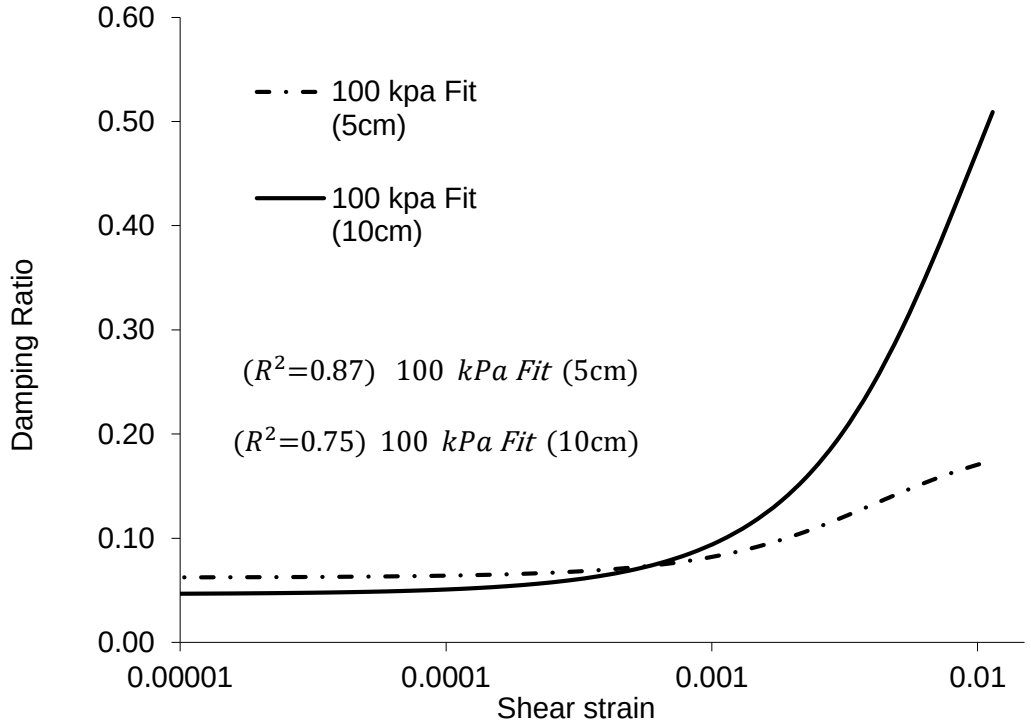

Figure 74: The effect of sample size on damping ratio variation with shear strain (Sample C, 100kPa)

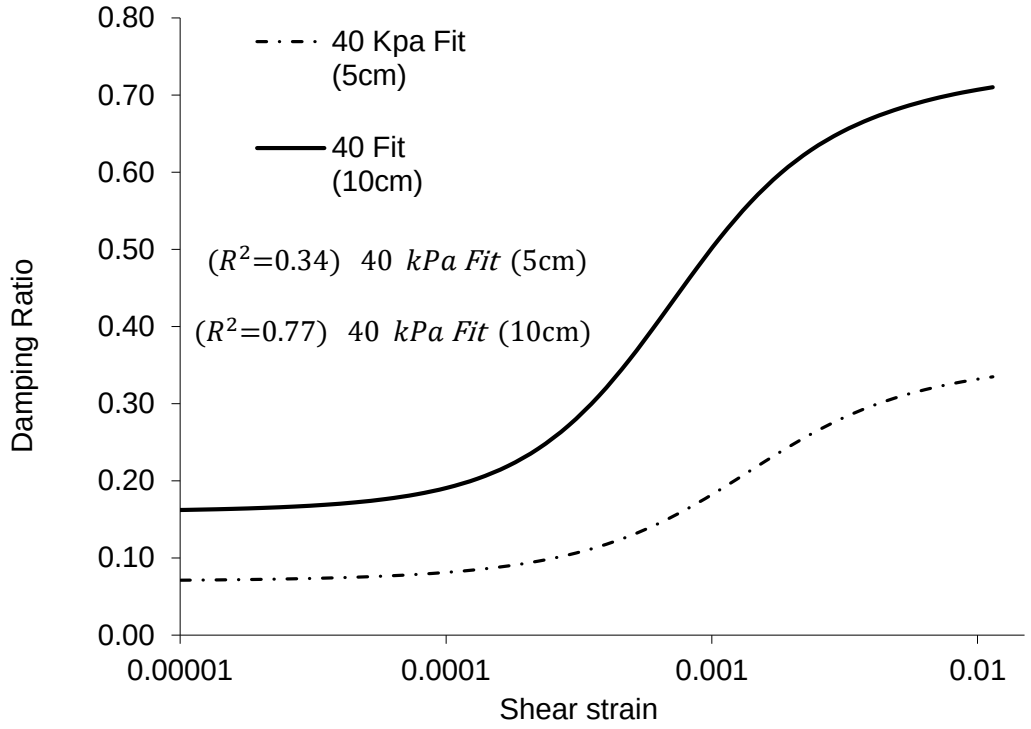

Figure 75: The effect of sample size on damping ratio variation with shear strain (Sample D, 40kPa)

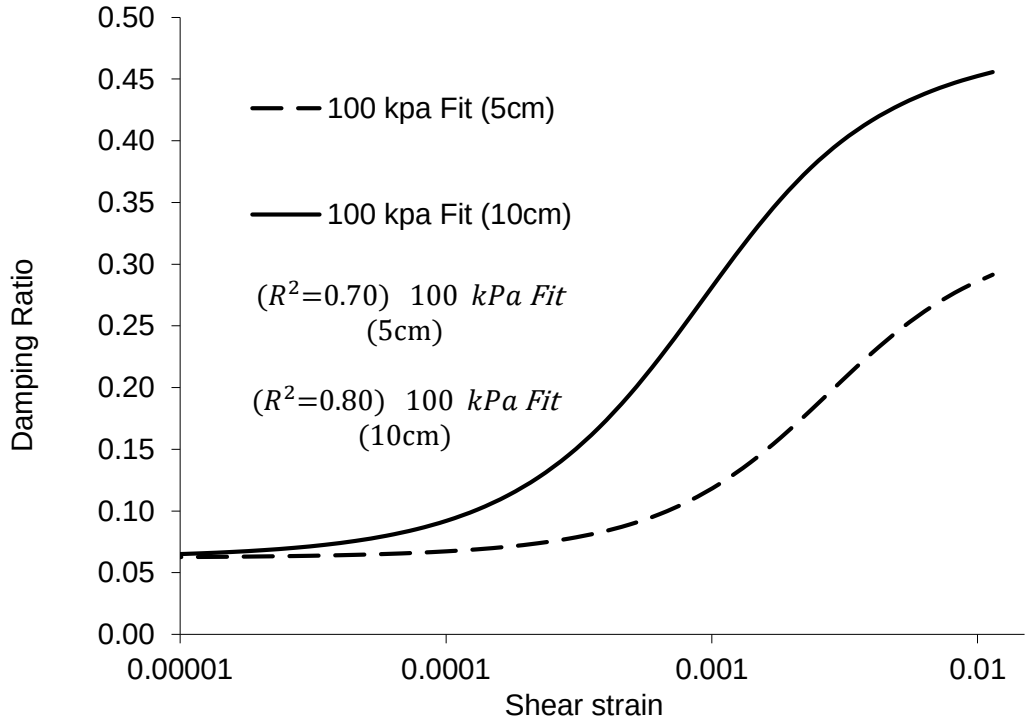

Figure 76: The effect of sample size on damping ratio variation with shear strain (Sample D, 100kPa)

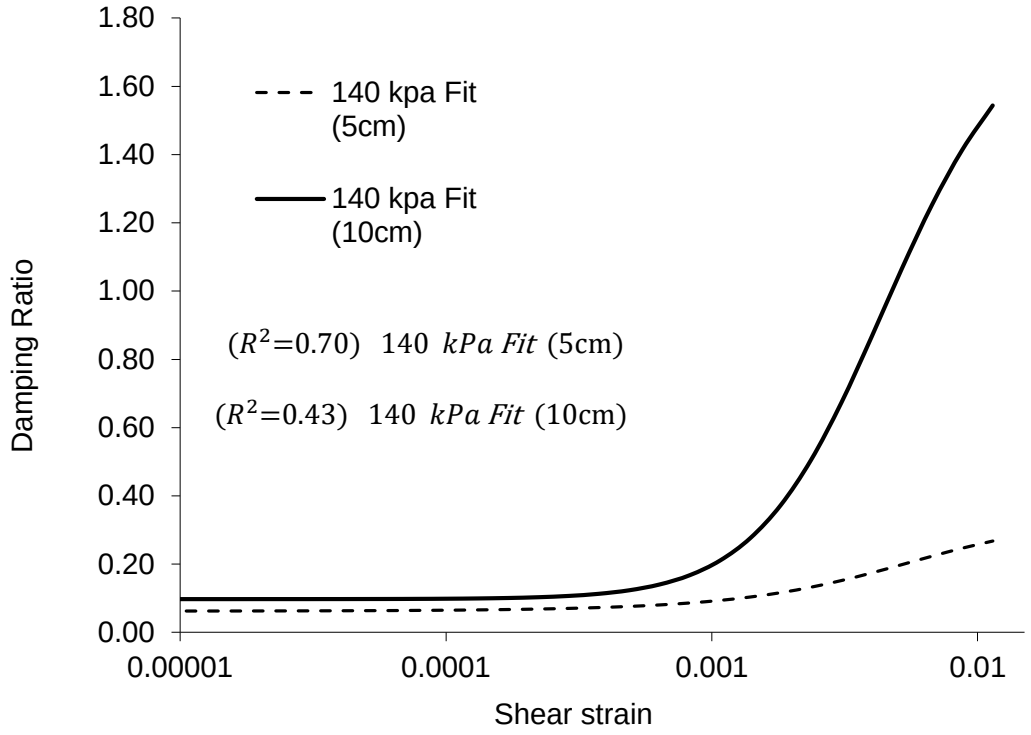

Figure 77: The effect of sample size on damping ratio variation with shear strain (Sample D, 140kPa)

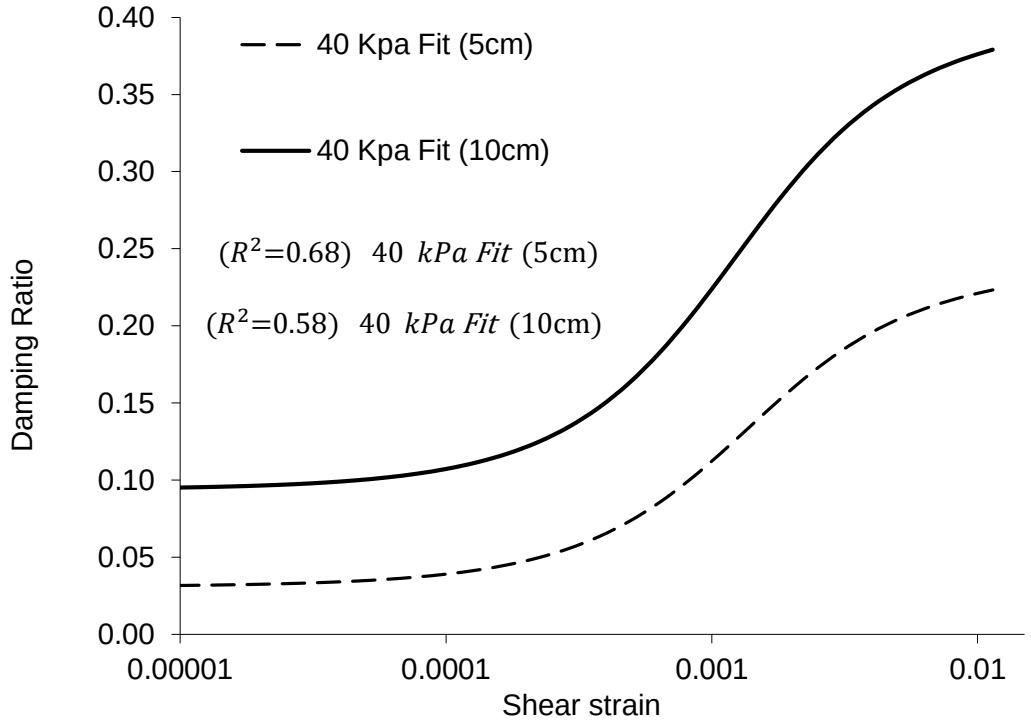

Figure 78: The effect of sample size on damping ratio variation with shear strain (Sample E , 40kPa)

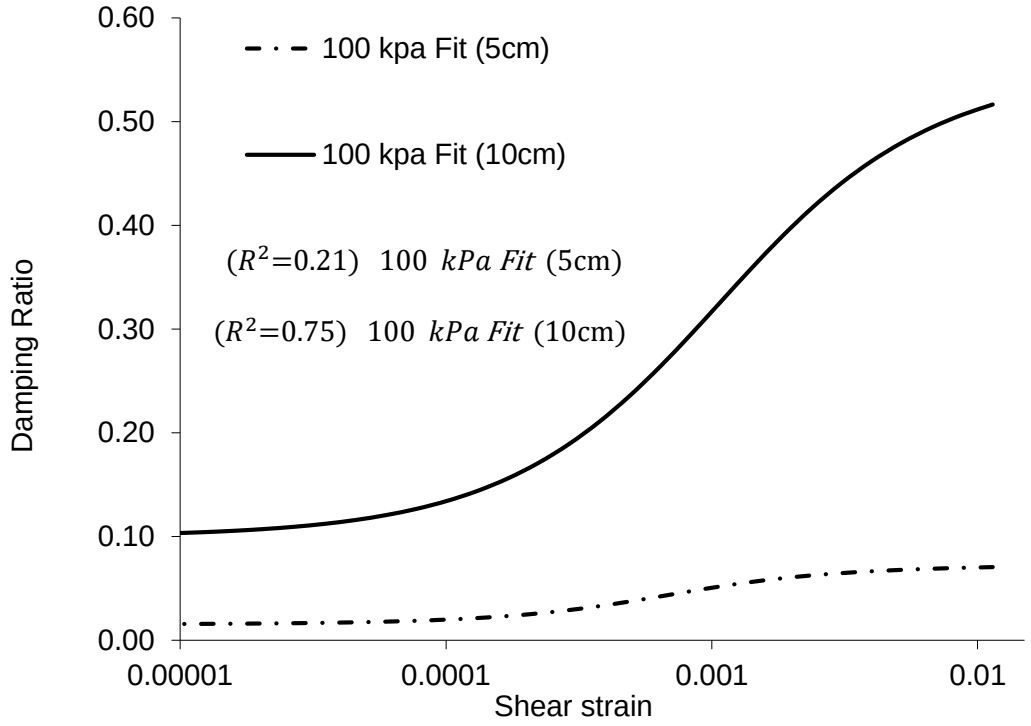

Figure 79: The effect of sample size on damping ratio variation with shear strain (Sample E, 100kPa)

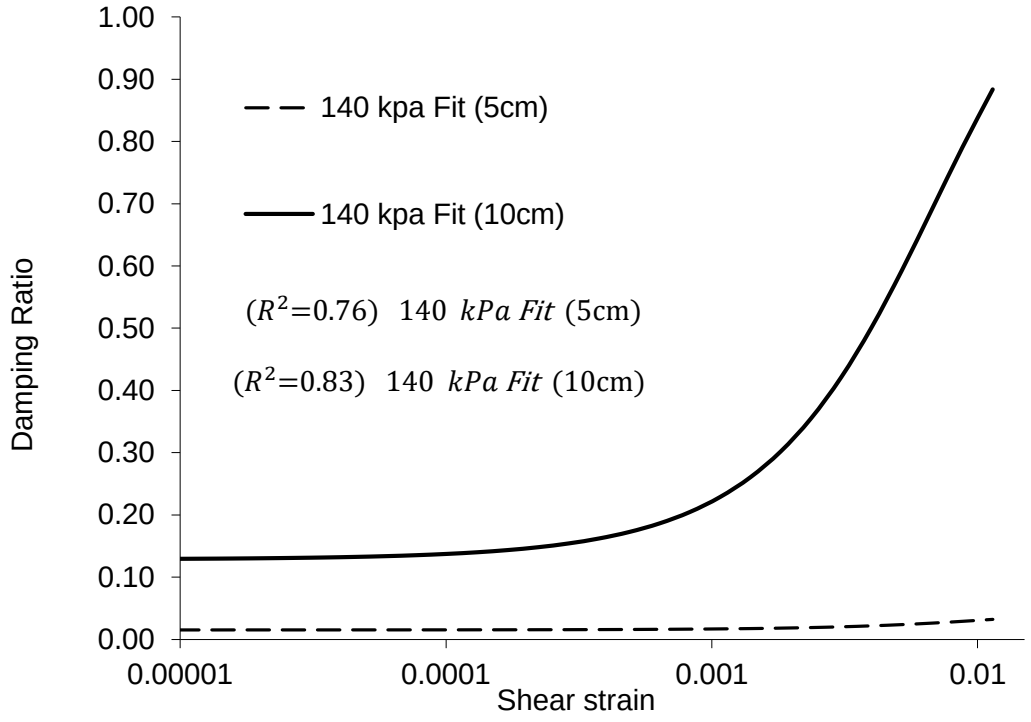

Figure 80: The effect of sample size on damping ratio variation with shear strain (Sample E, 140kPa)

4.6. Results of Quick Shear (QS) Test

The Quick Shear Test (QST) was performed using the triaxial machine. The purpose was to obtain shear strength properties of regional soils. During the QST, a couple of Linear Variable Differential Transformers (LVDT) were used to record the stain level against the cyclic stress. The stress-strain curve was developed by Excel after logging and analyzing the QST data. The obtained stress-strain curves are presented in Figures 81-83, show that the resistance of deformation of the soil is significantly influenced by the confining pressure, soil material and sample size.

The principal stresses ($\sigma 1$) and the confining pressure ($\sigma 3$) were varied in order to estimate the friction angle (ϕ) of the sandy specimens. Moreover, the sample size was gradually increased in order to observe the effect of sample size on the angle of friction. Table 19 presents the calculated friction angle of the tested samples with respect to sample size. The ϕ_{Avg} was the average friction angle between the two sample sizes. The ϕ_{Avg} was compared with ϕ mentioned in the soil investigation report. In Table 19, the difference between ϕ_{Avg} and the ϕ taken form the soil report is slightly small for samples C and E, however; the difference is relatively high for samples A, B and D. Mismatch of the angle of friction (ϕ) might be due to the measuring method. In the soil report the ϕ was measured from a field test however, the ϕ in the present study was obtained in the laboratory. Moreover, the elastic modulus (E) was evaluated for the tested soil. Table 20 presents the obtained E of the tested samples according to the sample geometry. Average modulus of elasticity (E_{Avg}) between the two sample sizes was obtained for each type of soil (Table 20).

4.6.1. The effect of confining pressure. The shearing data of samples A and B representing the effect of confining pressure on the stress-strain curves are presented in (Figures 81-82). All tested samples were prepared and tested under 3 confining pressures to observe the influence of confining pressure on the regional soils. The confining pressure was gradually increased from 50 to 150kPa in 50kPa increment. Figures 81-82 show that when the strain is constant and the confining pressure increases, the deviator stress increases. The resistance to deformation of soil was significantly affected by the confining pressure due to the increase in the friction between the soil particles, therefore elastic soil modulus (E) increased.

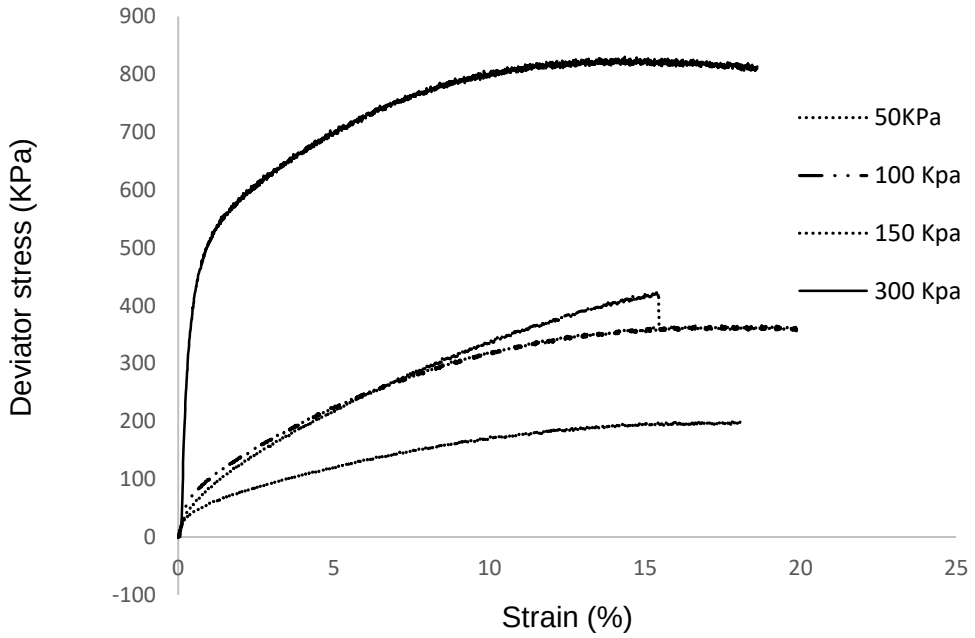

Figure 81: The effect of confining pressure on the Stress-Strain curve of Sample A (10cm Sample Diameter)

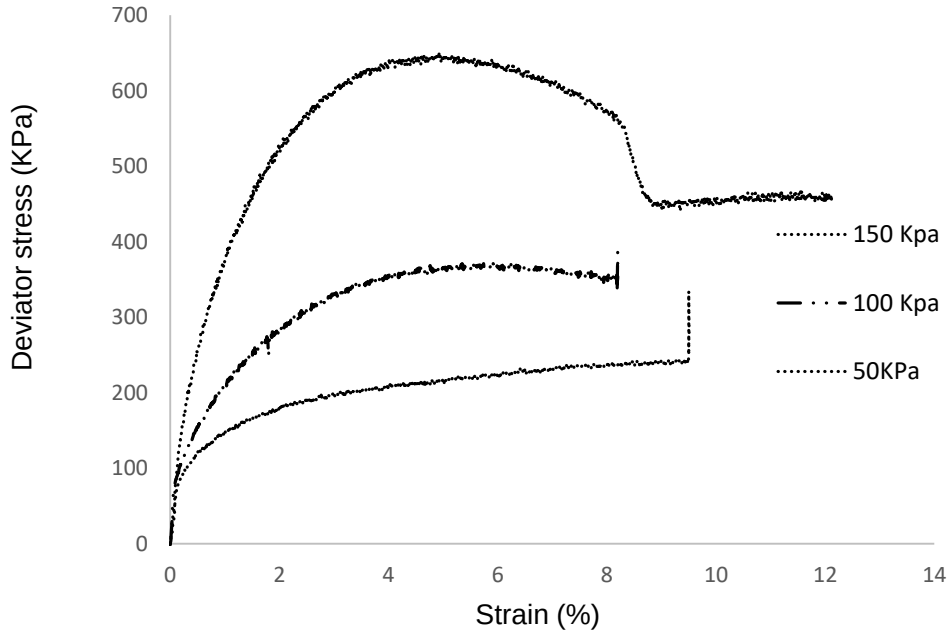

Figure 82: The effect of confining pressure on the stress-Strain curve of Sample B (10cm Sample Diameter).

Figure 82 shows the stress-strain curves of sample B at the three confining pressures (50, 100 and 150 kPa). The specimen prepared at confining pressure of 150 kPashowed a post-peak shear or residual strength, as shown in Figure 82. The residual or post rupture-strength refers to the strength that occurs after the first stage of strength reduction. This soil behavior is often identified as a post-peak plateau in the QST and

Triaxial test, and it also stands close to intrinsic critical state strength, as shown in Figure 82. The residual or the post rupture behavior is either resisted by the sustained bonds between the soil particles in the rupture plane or due to the rearrangement of the soil particles that creates new bonds between the soil particles. The behavior of post-rapture was unclear in the literature; therefore, the identified reasons are still under investigation.

4.6.2. The effect of soil material. The interpretation of the stress-strain diagrams of samples A and B indicates that the deviator stresses of sample B are significantly higher than the deviator stresses of sample A at any strain level. For example, the peak of deviator stress for sample B is about 650kPa at a confining pressure of 150kPa however, the peak is the only 420kPa for sample A at the same confining pressure. In fact, different deviator stresses are an indication of different samples' stiffness. The difference in the ultimate deviator stresses shows that sample B is significantly stiffer than sample A at the same confinement. Furthermore, the same is observed at the rest of the confining pressures, as demonstrated in Figures 81-82.

Table 19: The summary of evaluated principle stresses and angles of friction in the present study.

Sample	Size (Diameter x Height)	Confinement Stress σ3 (kPa)	Principle Stress σ1 (kPa)	Measured Angle of Friction ϕ (°)	Angle of Friction ϕ_{Avg} (°) (Average)	Angle of Friction ϕ (°) (soil report)
Sample A	5cm x 10cm	100	773.77	52.62	53.53	43
	7cm x 14cm	100	871.82	54.43		
Sample B	5cm x 10cm	100	798.40	53.10	47.65	36
	10cm x 20cm	100	409.21	42.20		
Sample C	5cm x 10cm	100	721.45	51.53	41.38	36
	10cm x 20cm	100	215.40	31.23		
Sample D	5cm x 10cm	100	611.63	48.90	47.67	34
	10cm x 20cm	100	526.49	46.44		
Sample E	5cm x 10cm	100	604.77	48.72	36.7	30
	10cm x 20cm	100	143.36	24.68		

Table 20: The summary of the measured elastic modulus in the present study.

Sample	Size (Diameter x Height)	Principle Stress σ1 (kPa)	Strain %	Measured Modulus of Elasticity E (kPa)	Modulus of Elasticity E (kPa) E_{Avg} (Average)
Sample A	5cm x 10cm	773.77	2.17	35657.60	27305.11
	7cm x 14cm	871.82	4.60	18952.61	
Sample B	5cm x 10cm	798.40	2.36	33830.51	21786.81
	10cm x 20cm	409.21	4.20	9743.10	
Sample C	5cm x 10cm	721.45	3.72	19393.82	14022.21
	10cm x 20cm	215.40	2.49	8650.60	
Sample D	5cm x 10cm	611.63	2.07	29547.34	25881.06
	10cm x 20cm	526.49	2.37	22214.77	
Sample E	5cm x 10cm	604.77	3.50	17279.14	11797.28
	10cm x 20cm	143.36	2.27	6315.42	

4.6.3. The effect of sample size. The static parameters of the cohesion-less soil depend on the soil particles interaction among the soil particles. The stress-strain relationship is fundamental to soil behavior and it is obtained from the quick shear test. The relationship shows the deformation resistance of the soil against the static loading. In QST, the stress-strain response depends on the displacement that is essentially unrelated to the sample size. However, the strain level is calculated based on the sample geometry, hence the sample size may affect the stress-strain behavior.

The main objective of the stress-strain relationship is to evaluate the static parameters of the soil. The stress-strain curve is usually used to evaluate the angle of friction of soil since the angle of friction is directly affected by the strain rate applied in the test. If the sample size impacts the stress-strain behavior as discussed in the previous paragraph, then the impact of sample size may be significant on the calculation of friction angle.

Figure 83 compares the deviator stress versus the axial strain behavior from the (QST) on different specimen sizes. The larger elastic modulus (stiffer specimen) exhibited in the smaller specimens (5cm sample diameter), as illustrated in Figure 83 In theory, the specimen stiffness depends on both the relative density and the void ratio

or one of them may have a valuable contribution. Figure 83 shows a slight influence of sample size on the stress-strain curve of samples A and D. In the stress-strain diagram, the 5cm specimens has slightly higher deviator stresses in

the 5cm specimens compared to 10cm samples; that could be due to the higher relative densities in the 5cm samples than the 10cm samples. In other words, the higher relative densities of 5cm samples could explain the rises in the deviator stresses in the 5cm specimens.

Figure 84 presents the influence of sample diameter on the friction angle (ϕ). The sample size effect was clearly observed in all of the sample sizes. Samples B, C and E showed significant decrease in the shear strength as the sample diameter increases, however; the trend differed for samples D and A. As shown in Figure 84, sample D shows a slight decrease in shear strength as the sample's diameter increases. In contrast, the shear strength of sample A is almost constant beyond the tested sample geometries (Figure 84). This trend was mentioned in the literature review section highlighting that no effect was seen when the sample size increased [24]. The extrapolation of sample A's trend (bigger sample's diameter) indicates that the trend diverges as the sample's diameter increases and ϕ slightly increases (Figure 85). Probably, the trend changed because sample A was a gypsiferous soil sample that contains a sufficient amount of gypsum (calcium and sulfate) and the gypsum has marked effects on the physical properties of soil. According to previous studies that tested gypsiferous soil samples, the gypsum was removed from the soil samples before obtaining the test by leaching the soil with distilled water or by extraction with a solution of ammonium oxalate [83]. More research is highly recommended on the Gypsiferous soil in order to clearly understand the effect of the gypsum material on the friction angle. The large sample size (Diameter more than 10cm) is not common in geotechnical laboratory testing, therefore; the influence of sample geometry could be disregarded in Gypsiferous soil and constant trend could be sufficient.

4.7. Correlation between static and dynamic properties

The relationship between the static and dynamic properties of soil has been frequently addressed in the literature. The standard penetration test (SPT-N-value) or the number of blows and the shear wave velocity (Vs) of the sand are among widely

used in geotechnical engineering projects. The SPT-N-value is commonly used to determine the in-site properties of soil and it is a good representation of the soil type. The SPT N-Values used in the present study are summarized in Table 5. Moreover, the SPT N-value has already been correlated with different soil parameters i.e., unit weight (γ), relative density (*Dr*), angle of internal friction (φ) and undrained compressive strength (*qu*) by different researchers [84]. Therefore, it is useful to use SPT N-vales to correlate different soil parameters.

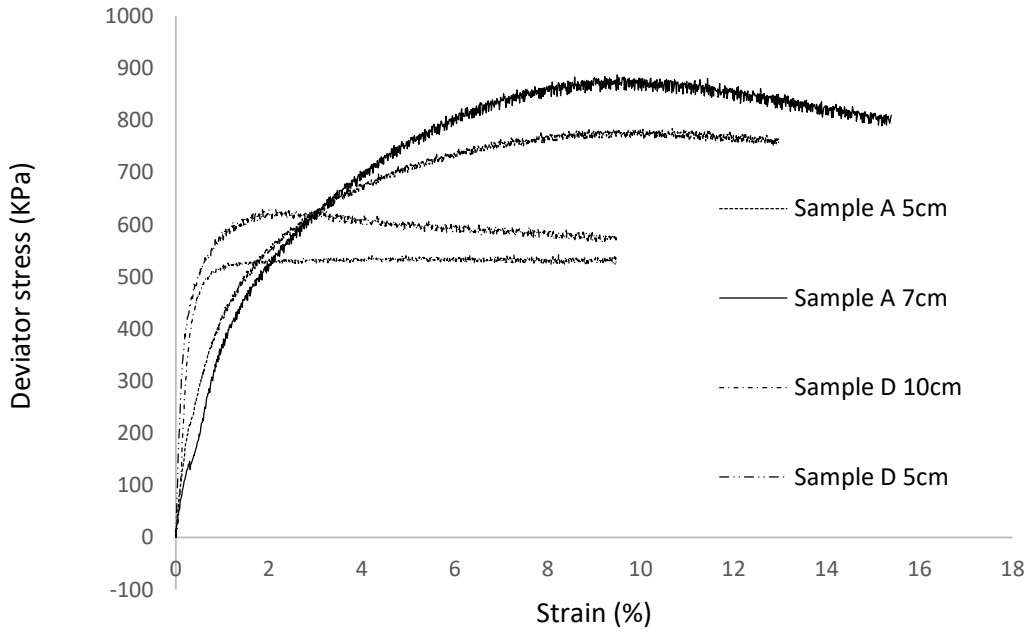

Figure 83: The effect of sample size on the stress-strain curves of samples A and D

Shear wave velocity (Vs) is an important dynamic property of soil. The Vs can be either measured from the in-situ field or laboratory tests. In the present study, the Vs is estimated from the laboratory testing of the Bender Element (BE) testing. The Vs can also be estimated based on empirical correlations with other soil parameters; therefore, it is valuable to have correlations that include the Vs.

In the present study, five undisturbed samples were tested. Also, each sample represents a different ground condition. Three samples were extracted from the same borehole, however; the other two samples were taken from different boreholes at different sites in the UAE region. According to the soil investigation reports, sample A was extracted from a depth of 11.5m under the ground level and classified as a mudstone specimen. The number of blows (N-value) was classified as more than 50 for

sample A's layer, conservatively, the N-Value was considered 50 for analysis. Secondly, samples B and C were taken from the same borehole but from shallower depths. The N-Values of the samples B and C were smaller comparing to Sample A as 48 and 21, respectively. Thirdly, samples D and E were silty sand specimens but from different boreholes and depths. Sample D and E were taken from shallow depths of 4.5 and 5.5m respectively from the ground level, respectively. According to the soil investigation reports, the N-Values of samples C and D were 21 and 17, respectively. Table 19 presents the findings of boreholes used in the present study.

4.7.1. Correlation between N-SPT Value and measured Vs. The relation between N-SPT and *Vs* is very useful in earthquake and geotechnical engineering. Several correlations have already been developed for regions like Japan, India, Turkey and United States. A summary of these correlations is provided in Table 3. The correlations developed for specific regions are not practical for use in other regions. Also, no systematic study has been conducted on the UAE's soil in order to develop such a relation for soil in the UAE using laboratory tests. One of the objectives in the present study is to develop a correlation between N-SPT and measured shear wave velocity (*Vs*). Since the tested samples were extracted from the UAE sites therefore the developed correlations are representative of the UAE's soil. In total, five samples were tested in this study, distributed throughout the capital city of the UAE, Abu Dhabi. Sand is the most common soil type in the UAE. The form of the Vs and N-SPT correlation is presenting in (8) where *A* and *B* are the regression coefficients. In literature, the two constants *A* and *B* are found to be inversely proportional to each other [33]- [43]. In the present study, the shear wave velocities were measured in the laboratory and plotted against the N-SPT value that were measured in the field, considering the sample size effect. The two tested sample geometries of 7cm and 10cm were used in the analysis. Figure 86 presents the developed correlation between shear wave velocity (Vs) and N-SPT value for sandy soil with repetitive data points. Each pair on the shear wave velocity (Vs) and the N-SPT value curve represents the measured Vs in the laboratory and the typical N-SPT value for the location of the sample. The confinement pressure is estimated for each sample to accommodate for the similar influence of confining pressure that applied in the ground. Hence, the shear wave velocities are obtained at confining pressure ranging between 30 to 50 kPa to simulate the ground condition at depths between 5 and 12 m using the CT set. Figure 86 also shows the correlations for

the two tested sizes. The correlations of both sample sizes are similar. The performance of any regression analysis is determined by the root-mean-square (*RMS*) value. The R^2 is evaluated based on the *RMS* and it is an indication of the goodness of the model's fit. The R^2 ranging between 0.7 to 0.99 is considered a good fit. The correlations for the 7cm and 10cm samples were presented in (15) - (16).

$$Vs = 92.642N^{0.197} \qquad (R^2 = 0.816) \tag{15}$$

$$Vs = 152.66N^{0.153} \qquad (R^2 = 0.774) \tag{16}$$

In order to simplify the obtained dataset, the developed correlations were combined and an average correlation was proposed. A graphical method was introduced by Dikmen [39] in order to validate the new relationships. This method obtains the comparison between measured and predicted datasets. The graphical method uses the normal consistency ratio (*Cd*) in order to compare the two datasets. The *Cd* is estimated using (17).

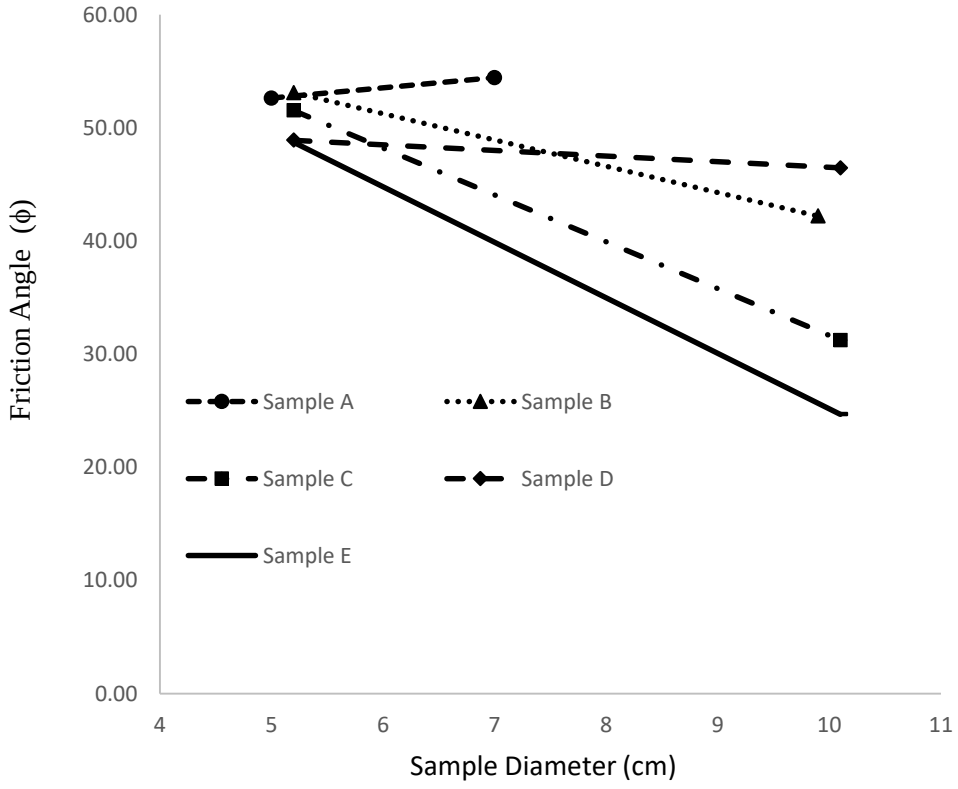

Figure 84: The effect of the sample's diameter on the shear strength of the tested specimens.

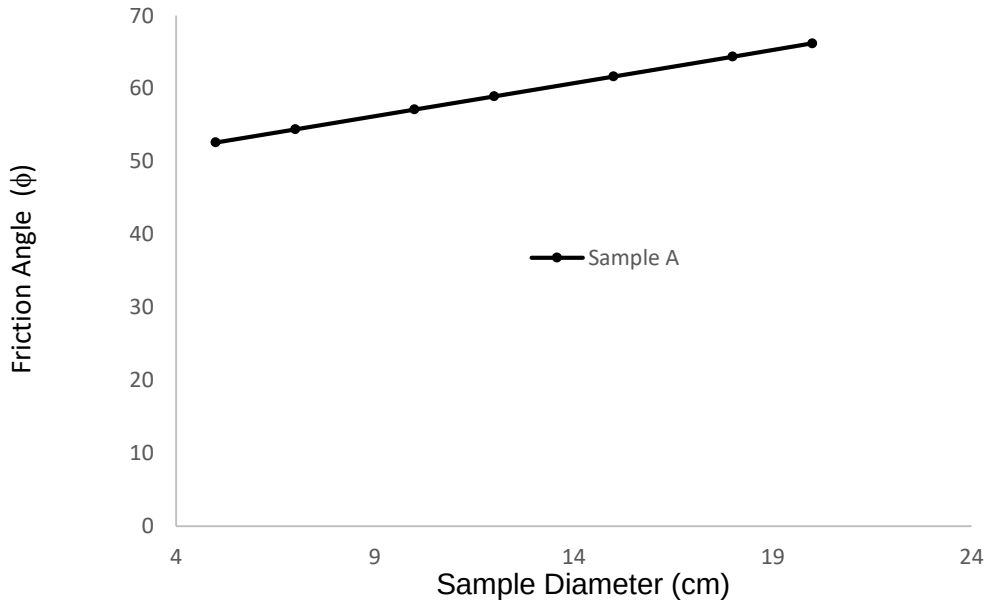

Figure 85: The influence of sample size for large sample's diameter of the gypsum sandy sample (Sample A).

$$C_d = (V_{SM} - V_{SC})/SPT - N \quad (17)$$

where V_{SM} is the *Vs* measured by the BE, V_{SC} is the *Vs* evaluated from the proposed equation (The average correlation) and the SPT-N is the corresponding measured N-value in the soil investigation report. Figure 87 shows the variation of the normalized consistency ratio (*Cd*) evaluated in (14) with the measured SPT-N. As presented in Figure 87, the average value of the *Cd* was closed to zero and indicates that, the predicted *Vs* are close to the measured *Vs* for the two sample sizes.

Figure 88, shows a comparison between the correlation developed in the present study and previously obtained relationships [36]- [44]. Most of these studies developed correlations based on in-site seismic surveys, however; the present study is based on BE laboratory testing. The evaluated shear wave velocities from BE testing were lower than the *S*-wave velocities obtained from the field seismic survey. Figure 88 highlights the drop in the *Vs-N* correlations in the laboratory testing (present study correlation). The main reason for the observed discrepancy could be in the change of the original soil volume that obtains strong bonds between the soil particles due to the cementation and fabric effects. Two sample sizes were tested in order to validate the cementation and fabric impact.

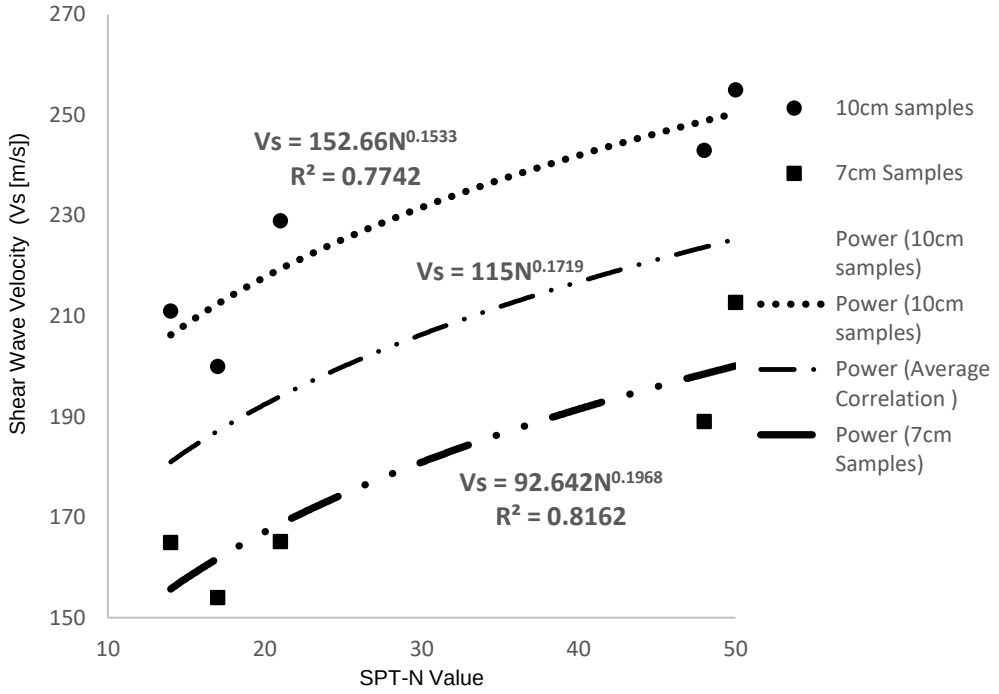

Figure 86:The developed correlation between *Vs* and SPT-N value.

The obtained correlation was comparable to other correlations developed for other regions and it overlaps the Dikmen's relationship [43] up to an N-SPT value of 20. However, this study represents correlations based on BE laboratory testing and it is relatively smaller than the field correlation obtained in the literature. The correlation discrepancy might be due to the soil variation in the region and the effect of cementation. Figure 88 demonstrates that the developed correlation is close to the correlations developed by anther researchers such as, Ohsaki and Iwasaki [38], Ohta and Goto [40], Imai and Tonouchi [37], Rollins et al [41] and Dikmen [43].

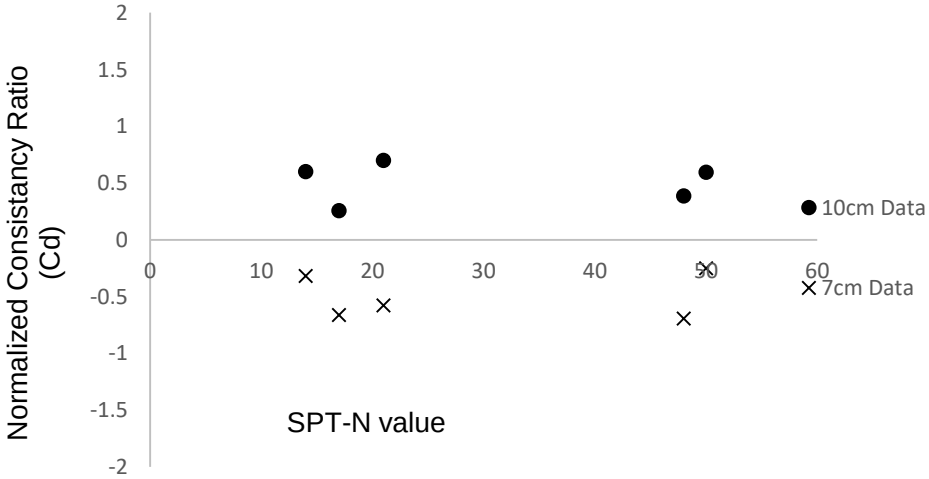

Figure 87: The validation plot of the proposed correlation for the present study

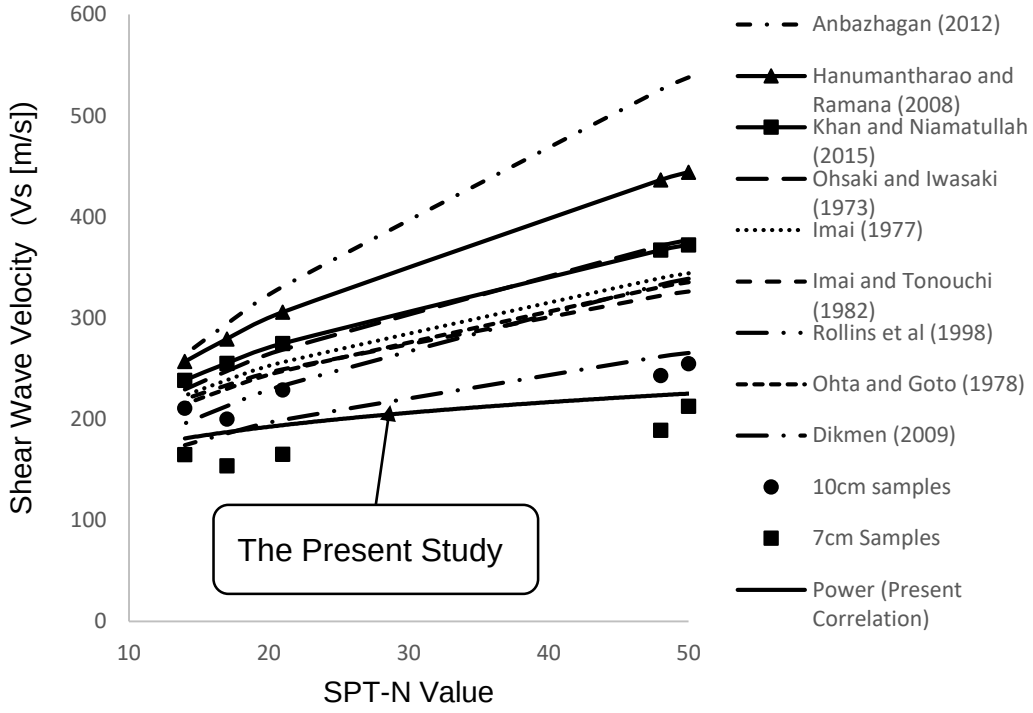

Figure 88: Comparison of proposed relation with other relations developed for other regions.

4.7.2. Correlation between φ and measured *Vs*. Data for which both *Vs* and φ were measured on the same soil material using two sample sizes of ratios H/D = 2 (height H = 10 cm, diameter D = 5 cm and height H = 20 cm, diameter D = 10 cm) is shown in form of *Vs* versus φ in Figure 89. In the present study, *Vs* is increased linearly as φ increases for both sample geometries. The linear function is fitted to the measured data of 5cm and 10cm sample's diameter and shows correlations of R^2= 0.53 and R^2= 0.49, respectively. Cha et.al [85] correlated Vs with φ indirectly through void ratio (e) and effective stresses (σ) that matched the developed correlations in the present study, as shown in Figure 89. In their study, Cha et.al [85] correlated Vs and φ based on a typical circular shear box with an inner diameter of 6cm. The correlation of Cha et.al [85] was located midway of the measured shear wave velocity for 10cm and 5cm sample diameter, as shown in Figure 89, which justifies the trend in the shear wave velocity. However, the shear strength of the small size samples (Diameter of 5cm) in the present study is not in agreement with the results of Cha et.al [85]. As shown in Figure 89, φ is significantly higher in 5cm samples than the 10cm sample diameter and that of Cha et.al [85]. The main reason for the observed divergence is believed to be the decrease in the void ratio (e) for the smaller samples and the presence of strong bonds

between the soil particles due to the cementation and fabric effects. This behavior was highlighted by Cha et.al [85], as the void ratio (e) increases the shear strength (φ) gradually decreases.

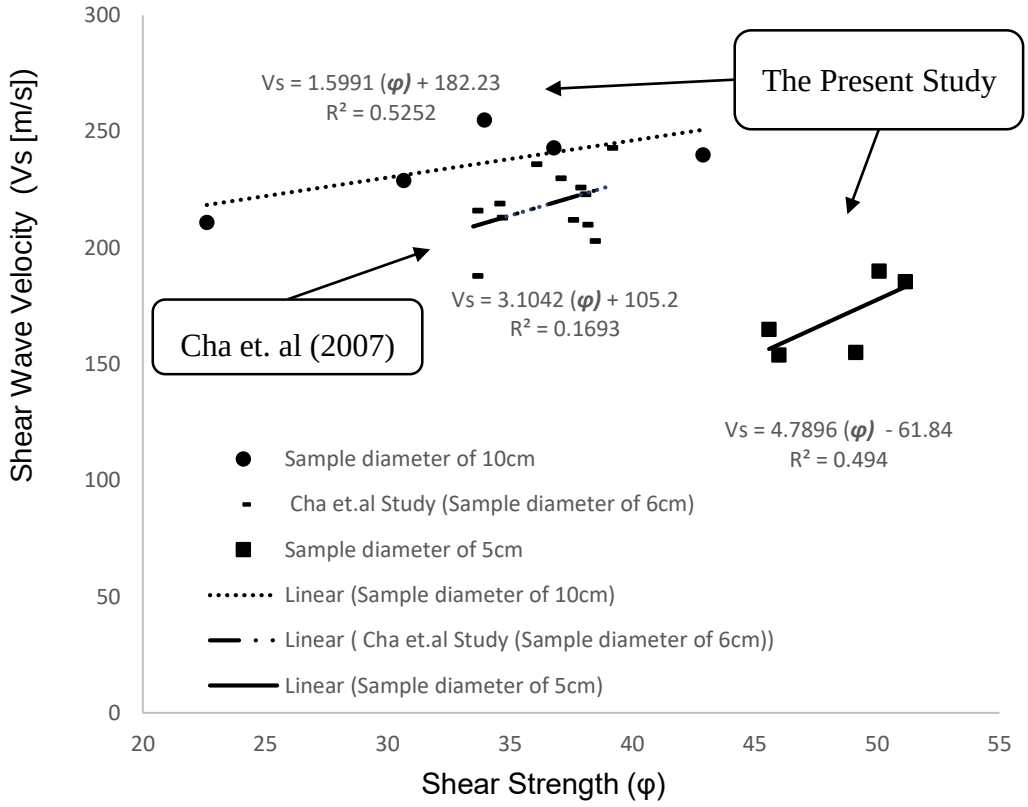

Figure 89: Comparison between the proposed relationships of shear strength (φ) and shear wave velocity (Vs) for 5cm and 10cm sample's diameter and the previous study conducted by Cha [85]et. al.

Chapter 5. Conclusion and Recommendation

United Arab Emirates (UAE) has seen a great economic growth in recent years. High-rise buildings are one of the factors that are contributing to the UAE's economy. According to the modern building code, the dynamic properties of the subsurface soil are needed in the seismic design of structures, since they provide the basis of the response due to ground shaking. Projects in the UAE compel designers to use values of dynamic properties that are either conservative or unreliable for region soils because they rely on correlations developed for other regions. Therefore, it is necessary to have a systematic study on the in-situ and laboratory evaluation of dynamic properties that are area-specific. Five undisturbed sandy soil samples representing the soils of UAE are taken from sites that cover the major developing areas of the capital city of the United Arab Emirates, Abu Dhabi. The samples with known SPT-N values were collected from different depths to represent different confining stresses. The dynamic Cyclic Triaxial (CT), Quick Shear (QS) and Bender Element (BE) tests were used to evaluate the dynamic and static properties of the representative soils of UAE as a function of confinement and shear strain level. Degradation models are used to fit the normalized shear modulus (G/Gmax) and material damping ratio (ξ) with the shear strain. Correlations between static and dynamic properties for typical soils of UAE were developed between SPT-N and shear wave velocity (Vs). The effect of sample size on the dynamic properties were also investigated. The main conclusions of the study are presented below:

- The larger sample size showed higher correlation coefficients whereas the smaller size samples showed smaller correlation coefficients. The effect of sample size on the dynamic properties was significant between the tested sizes.
- The evaluated G and ξ showed opposite trends as a function of the γ and σ. The variations are generally in agreement with the previous studies; however, the curvature coefficients of the hyperbolic models are not similar to previous studies indicating the importance of region-specific evaluation of the dynamic properties.
- The results of QS tests showed a slight decrease in ϕ as the sample's diameter increase, but this trend was not consistent in all tested samples. Gypsum-based sandy specimens showed an increase ϕ as the sample's geometry increased.

These results also indicate the effect of soil type on its properties which signifies the importance of non-generalization of its properties.

- Correlations between static properties and dynamic properties such as Vs-N value and Vs-ϕ were found to be in general agreement with some of the correlations from literature however, the agreement is considered as coincidental due to large variation among the correlations found in the literature.
- Vs correlated linearly with ϕ but Vs correlated with a power function with SPT N values. The correlations predicted higher values of Vs for larger specimens which were observed for both linear and power functions.

Recommendations:

- Soils in UAE are typically divided into either silicate rich or gypsum rich sands. The behavior of soil is found to be affected by the mineral content of the sands in this study. A detailed experimental program based on evaluating the effect of mineral type on the dynamic and static behavior of regional soils is strongly recommended.
- The degradation models are developed using cyclic triaxial and bender elements. It is recommended to use a resonant column (RC) for future studies to validate and compare the results of this study.

References

[1] D. J. Shirley. "Shear-wave measurements in laboratory sediments." *The Journal of the Acoustical Society of America*, vol. 33, no.3, pp. 607-613, 1987.

[2] R. Dyvik. (1987). "Lab measurements of Gmax using bender elements." *International Journal of Rock Mechanics and Mining Sciences & Geomechanics Abstracts*, vol.24, no.2, pp. 56, 1987.

[3] Z. Khan. "Novel evaluation of bender element transmitter response in transparent soil." *Géotechnique*, vol.70, no.3, pp. 1-33, 2020.

[4] J.S. Lee. "Bender Elements: Performance and Signal Interpretation," *Journal of Geotechnical and Geoenvironmental Engineering*, vol.131, no.9, pp. 1063-1070, 2005.

[5] WB. Gohl. "Use of Piezoceramic Bender Elements in Soil Dynamics Testing." *ASCE*, pp. 118-133, 1991.

[6] M. Arroyo."Source near-field effects and pulse tests in soil samples." *Géotechnique*, vol.53, no.3, pp. 337-345, 2003.

[7] G. Viggiani. "Interpretation of bender element tests." *Géotechnique*, vol. 45, no.1 pp. 149-154, 1995.

[8] H. Arai. "Vibration of dry sand layers." Proceeding, *Japan Earthquake Engineering Symposium*, Tokyo, P. 113, 1966.

[9] R. Arulnathan. "Analysis of Bender Element Tests," *Geotechnical Testing Journal*, vol.21, no.2, pp. 120-131, 1998.

[10] W. Sachse. "On the determination of phase and group velocities of dispersive waves in solids." *Journal of Applied Physics*, vol.49, no.8, pp. 4320-4327, 1978.

[11] J. Camacho-Tauta. "Experimental and Numerical Observations of the Frequency-Domain Method in Bender-Element Testing." *Journal of Geotechnical and Geoenvironmental Engineering*, vol.143, no.2, pp. 4016-096, 2017.

[12] L. D. Suits. "A Framework Interpreting Bender Element Tests, Combining Time-Domain and Frequency-Domain Methods," *Geotechnical Testing Journal*, vol.32, no.2, pp. 100-974, 2009.

[13] D. Brocanelli, V. Rinaldi. "Measurement of low-strain material damping and wave velocity with bender elements in the frequency domain," *Canadian Geotechnical Journal*, vol. 35, no. 6, pp. 1032-1040, 1998.

[14] Z. Khan. (2008)."Measurement of Frequency-Dependent Dynamic Properties of Soils Using the Resonant-Column Device," *Journal of Geotechnical and Geoenvironmental Engineering*, vol.134, no. 9, pp. 1319-1326, 2008.

[15] B. O. Hardin. "Shear Modulus and Damping In Soils: Design Equations and Curves," *Journal of Soil Mechanics & Foundations Div*, vol. 98, no. 7, pp. 92-667, 1972.

[16] HB. Seed, IM. Idrees."Moduli and damping factors for dynamic analyses of cohesionless soils." Journal of Geotechnical Engineering, vol.112, no. 11, pp.1016-1032, 1986.

[17] ML. Silver, HB Seed."The Behavior of Sands Under Seismic Loading Conditions." Univerisity of California, Berkeley, Engineering Research Center. No. EERC 69-16, 1969.

[18] Sadrekarimi. "Development of a new ring shear apparatus for investigating the critical state of sands," Ph.D. thesis, University of Illinois, Urbana Champaign, Urbana, Ill, 2009.

[19] Scott, "Failure." *Géotechnique*, vol. 37, no. 4, pp. 423-466, 2015.

[20] VK. Garga, H Zhang. "Volume changes in undrained triaxial tests on sands" *Canadian Geotechnical Journal*, vol. 34, no. 5, pp. 762–773, 1997.

[21] C. Ladd, "Preparing test specimens using undercompaction."*ASTM*, vol. 1, no. 1, pp. 16-23, 1978.

[22] W. Hu, C. Dano. "Effect of sample size on the behavior of granular materials." *ASTM*, vol. 34, no. 3, pp. 1-12, 2011.

[23] V. K. Garga, "Effect of sample size on shear strength of basaltic residual soils." *Canadian Geotechnical Journal*, vol. 25, no. 3, pp. 478-487, 1988.

[24] J. Wan, M. Gray. "Influence of Soil Structure on the Stress-Strain Behavior of Sand-Bentonite Mixtures," *Geotechnical Testing Journal* , vol. 13, no. 3, pp. 179-187, 1990.

[25] A. Cerato, A. Lutenegger. "Specimen Size and Scale Effects of Direct Shear Box Tests of Sands." *Geotechnical Testing Journal,* vol. 29, no. 6, pp. 507-516, 2006.

[26] PK. Wu, F. Tatsuoka. "Effects of Specimen Size and Some Other Factors on the Strength and Deformation of Granular Soil in Direct Shear Tests." *Geotechnical Testing Journal* , vol. 31, no. 1, pp. 45-64, 2008.

[27] R. Jardine. "Characterization of soils for engineering purposes" *Soils and Foundations*, vol. 1, no. 3, pp. 255-360, 2003.

[28] W. Kovacs, E.Leo, "Cyclic Simple Shear of Large Scale Sand Samples: Effects of Diameter to Height Ratio." *International Conference on Recent Advances in Geotechnical Earthquake Engineering & Soil Dynamic*s, Missouri, 1981.

[29] DM. Lee. "Angles of friction of granular fills, Cambridge. " PhD Dissertation, University of Cambridge, United Kingdom, 1992.

[30] M. Vucetic, S. Lacasse. "Specimen Size Effect in Simple Shear Test." *Journal of the Geotechnical Engineering Division*, vol. 108, no. 12, pp. 1567-1585, 1982.

[31] K. Chan. "Effect of bender element installation in clay samples." *Géotechnique*, vol. 60, no. 4, pp. 287-291, 2010.

[32] M. Fener. "The Effect of Rock Sample Dimension on the P-Wave Velocity." *Journal of Nondestructive Evaluation*, vol. 30, no. 2, pp. 99-105, 2011.

[33] S. Yamashita. "Interpretation of International Parallel Test on the Measurement of Gmax Using Bender Elements," *Soils and Foundations*, vol. 49, no. 4, pp. 631-650, 2009.

[34] ASTM Standard D1586, 2011e1, "Standard Test Method For Standard Penetration Test (SPT) and Split-Barrel Sampling Of Soils." *ASTM*, West Conshohocken, PA, 2011, www.astm.org.

[35] G. Meyerhof. "Penetration Tests and Bearing Capacity of Cohesionless Soils" *Journal of the soil mechanics and foundations division*, vol. 82, no. 1, pp. 1-19, 1956.

[36] C. Hanumantharao. "Dynamic soil properties for microzonation of Delhi, India." *Journal of Earth System Science*, vol. 117, no. 2, pp. 719-730, 2008.

[37] T. Imai. "Correlation of N value with S-wave velocity and shear modulus." *Exact Sciences and Technology*, pp. 67-72, 1982.

[38] Y. Ohsaki, "On dynamic shear moduli and poisson's ratios of soil deposits." *Soils and Foundations*, vol. 13, no. 4, pp. 61-73, 1973.

[39] T. Kamei. "Comparison of elastic wave velocities using downhole and suspension technioues." *Journal of the Geotechnical Engineering Division*, vol. 103, no. 2, pp. 257-260, 1977.

[40] Y. Ohta, "Empirical shear wave velocity equations in terms of characteristic soil indexes." *Earthquake Engineering & Structural Dynamics*, vol. 6, no. 2, pp. 167-187, 1978.

[41] K. M. Rollins, "Shear Modulus and Damping Relationships for Gravels," *Journal of Geotechnical and Geoenvironmental Engineering*, vol. 124, no. 5, pp. 396-405, 1998.

[42] P. Anbazhagan, " Seismic Site Classification and Correlation between Standard Penetration Test N Value and Shear Wave Velocity for Lucknow City in Indo-Gangetic Basin," *Pure and Applied Geophysics*, vol. 170, no. 3, pp. 299-318, 2012.

[43] Ü. Dikmen, "Statistical correlations of shear wave velocity and penetration resistance for soils," *Journal of Geophysics and Engineering*, vol. 6, no. 1, pp. 61-72, 2009.

[44] Z. Khan, A. Ahmed and H. Bismillah, "Variation of shear wave velocity with SPT-N values for Sharjah, UAE," *International Journal of Geotechnical Engineering*, vol. 1, no. 10, pp. 46-51, 2016.

[45] SHH. Lee, "Regression models of shear wave velocities in Taipei basin." *Journal of the Chinese Institute of Engineers*, no. 13, pp. 519-532, 1990.

[46] R. Woods. "Borehole Methods in Shallow Seismic Exploration." Geophysical Characterization of Sites, ISSMFE, Technical Committee 10 for XIII ICSMFE, New York, vol. 134, no.10, pp. 91-100, 1994.

[47] RJ. Whiteley. "Seismic refraction testing a tutorial." In Geophysical Characterization of Sites, vol. 10, pp. 45-47, 1994.

[48] N. Kobayashi, "A method of determining the underground structure by means of SH waves." in *Proceedings Zisin*, Tokyo, Japan, vol.12, no.1, pp. 19-24, 1959.

[49] "ASTM Standard Guide for Using the Seismic Refraction Method for Subsurface Investigation" ASTM, West Conshohocken, 2000, www.astm.org. [Sep 22, 2020].

[50] D. Motazedian. "Development of a Vs (30) (NEHRP) map for the city of Ottawa, Ontario, Canada" *Canadian Geotechnical Journal*, vol. 48(3), pp. 458-472, 2011.

[51] S. L. Kramer. "Geotechnical earthquake engineering" *Pearson Education India*, 1996.

[52] L. Rayleigh. "Waves propagated along the plane surface of an elastic solid," *in Proceedings of London Mathematical Society*, vol. 17, pp. 4-11, 1885.

[53] D. Palmer. "The generalized reciprocal method of seismic refraction interpretation" in *Proceedings Society of Exploration Geophysicists*, Tulsa, Oklahoma, 1980.

[54] V. Pereyra. "Ray tracing methods for inverse problems" *Inverse Problems*, vol. 16, no.6, 2000.

[55] NK. Yacoub. "Computer ray tracing through complex geological models for ground motion studies" *Geophysics*, vol. 35, no. 4, pp. 586-602, 1970.

[56] JH. Scott. "Seismic refraction modeling by computer." *Geophysics*, vol. 38, no. 2, pp. 271-284, 1973.

[57] W. Menke. "Geophysical data analysis: Discrete inverse theory."*International Geophysics Series*, vol. 45, p. 289, 1989.

[58] J. Rickett, J. Claerbout. "Passive seismic imaging applied to synthetic data." *Stanford Exploration Project*, vol. 92, pp. 83-90, 1996.

[59] M. Shahrukh, P Soupios. "Geophysical investigations at the intron archaeological site, eastern Crete, Greece using seismic refraction and electrical

resistivity tomography" *Journal of Geophysics and Engineering*, vol. 9, no.6, pp. 749-760, 2012.

[60] A. Turesson. "A comparison of methods for the analysis of compressional, shear, and surface wave seismic data, and determination of the shear modulus" *Journal of Applied Geophysics*, vol. 61, no. 2, pp. 83-91, 2007.

[61] J.R. Sheehan, WE Doll. "An evaluation of methods and available software for seismic refraction tomography analysis" *Journal of Environmental & Engineering Geophysics*, vol. 10, no. 1, pp. 21-34, 2005.

[62] AV. Da Fonseca, J. Carvalho. "Characterization of a profile of residual soil from granite combining geological, geophysical and mechanical testing techniques" *Geotechnical and Geological Engineering*, vol. 24, no. 5, pp. 1307-1348, 2006.

[63] M.K. Kockar, H. Akgun. "Evaluation of site conditions for the Ankara basin of Turkey based on seismic site characterization of near surface geologic materials" *Soil Dynamics and Earthquake Engineering*, vol. 30, no. 1-2, pp. 8-20, 2010.

[64] H. Crow, M. Pyne. "Shear wave measurements for earthquake response evaluation in orleans, Ontario." *Proceedings of the 60th Canadian Geotechnical Conference*, Ottawa, Cannada, 2007, pp. 871-879.

[65] J. Luetgert, "MacRay: Interactive two-dimensional seismic raytracing for the Macintosh" *US Geological Survay* , vol. 93, pp. 43, 1992.

[66] E. Cardarelli, M. Cercato. "Electrical resistivity and seismic refraction tomography to detect buried cavities" *70th European Association of Geoscientists and Engineers Conference and Exhibition*, Rome, 2008, pp. 1103-1107.

[67] I. Koulakov. "LOTOS code for local earthquake tomographic inversion: Benchmarks for testing tomographic algorithms" *Bulletin of the Seismological Society of America*, vol. 99, no. 1, pp. 194-214, 2009.

[68] R.A. Williams, WJ. Stephenson. "Comparison of P-and S-wave velocity profiles obtained from surface seismic refraction/reflection and downhole data" *Tectonophysics*, vol. 368, no. 1, pp. 71-88, 2003.

[69] W. Wightman, F. Jalinoos."Application of Geophysical Methods to Highway-Related Problems" *Publication No. FHWA-IF-04-021*, Department of Transportation, Central Federal Lands Highway Division, FHWA,US., 2004.

[70] B. Redpath, "Seismic Refraction Exploration for Engineering Site Investigations." *Publication No. EERL-TR-E-73-4.* Army Engineer Waterways Experiment Station, Livermore, California, USA. Explosive Excavation Research Lab. , 1973.

[71] DI. Doser, RP Langford. "Seasonal variations in geophysical surveys of alluvial sediments near the Rio Grande, west Texas" *Environmental & Engineering Geoscience*, vol. 9, no. 3, pp. 253-266, 2003.

[72] G. Bonnet, M. Meyer. "Seismic refraction tests above water table." *Journal of Geotechnical Engineering*, vol. 114, no. 10, pp. 1183-1189, 1988.

[73] D. Raptakis. "Pre-loading effect on dynamic soil properties: Seismic methods and their efficiency in geotechnical aspects," *Soil Dynamics and Earthquake Engineering*, vol. 34, no. 1, pp. 69-77, 2012.

[74] T. Kokusho. "Cyclic triaxial test of dynamic soil properties for wide strain range. Soil Found." *Soils and Foundations*, vol. 20, pp. 45-60, 1980.

[75] KM. Rollins, MD. Evans. "Shear modulus and damping ratio for gravels" *Journal of Geotechnical and Geoenvironmental Engineering*, vol. 124, no.5, pp. 396-405, 1998.

[76] G. Lanzo, M. Vucetic. "Reduction of shear modulus at small strains in simple shear." *Journal of Geotechnical and Geoenvironmental Engineering*, vol. 123, no. 11, pp. 1035–42, 1997.

[77] SS. Kumar, AM. Krishna, A. Dey. "High Strain Dynamic Properties of Perfectly Dry and Saturated Cohesionless Soil," *Indian Geotechnical Journa*l, vol. 43, no. 3, 2018.

[78] K. H. Stokoe MB. Darendeli. "Dynamic soil properties: laboratory, field and correction studies," *Earthquake Geotechnical Engineering*, vol. 3, pp. 811-845, 1999.

[79] J. Camacho-Tauta, Evaluation of the small-strain stiffness of soil by non-conventional dynamic testing methods" PhD Thesis, Technical University of Lisbon, Lisbon, 2011.

[80] "ASTM D3999. Standard test methods for the determination of the modulus and damping properties of soils using the cyclic triaxial apparatus" ASTM, West Conshohocken, PA, 2011, www.astm.org. [Oct 13, 2020].

[81] M. B. Darendeli, "Development of a new family of normalized modulus reduction and material damping curves" PhD Thesis, University of Taxas at Austin, US, Taxas, 2001.

[82] Z. Khan and S. Moayerian, "Evaluation of strain level and frequency effects on the dynamic properties of sand." *in Pan-Am CGS Geotechnical Conference*, Toronto, Canada, 2011.

[83] Coutinet S. "Analyses methods used for saltye, calcarous and gypsum soils." *Tropical Agronomy*, vol. 12, pp. 1242-1253, 1965.

[84] K. Terzaghi, RB Peak, G Mesri. Soil Mechanics in Engineering Practice. New York: John Wiley and Sons , 1967.

[85] M. Cha, GC Cho. "Shear Strength Estimation of Sandy Soils Using Shear Wave Velocity," *Geotechnical Testing Journal*, vol. 30, no. 6, pp. 484-495, 2007.

Appendix A

[This appendix includes grain size distribution curves of the tested samples].

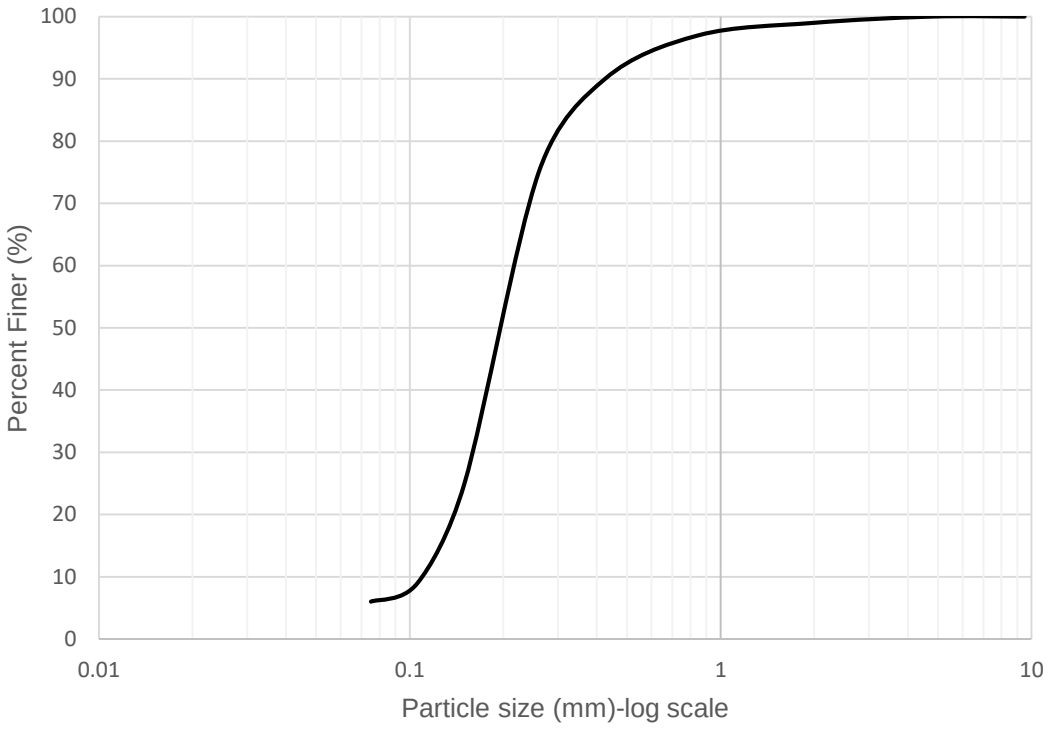

Figure 90: Grain size distribution of the tested soil (Sample A).

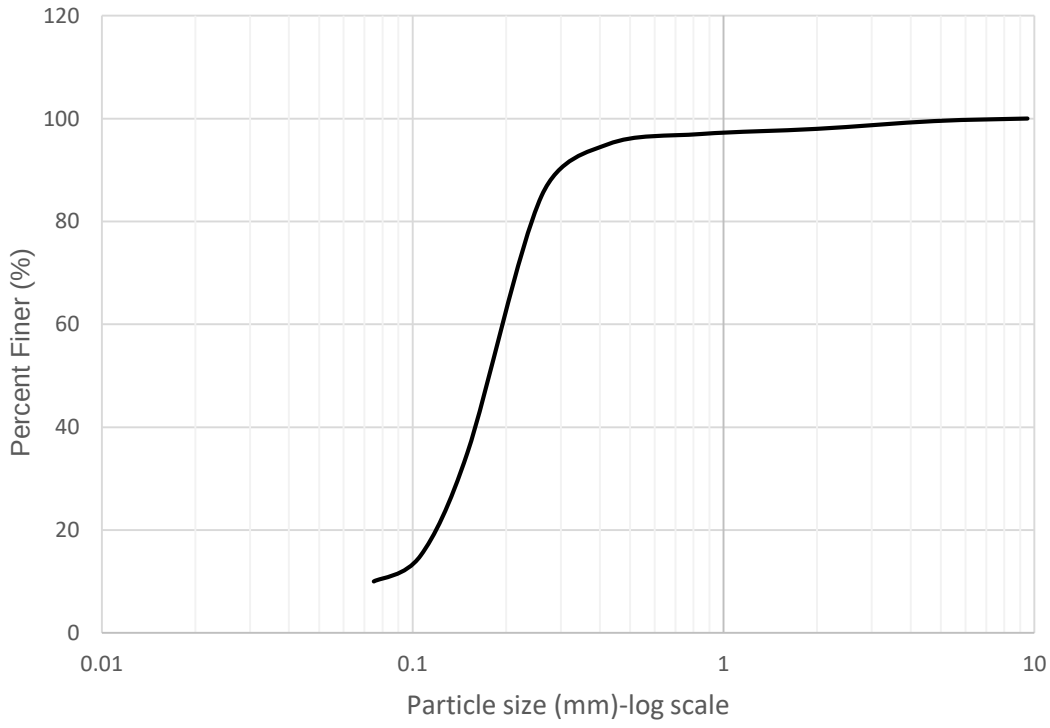

Figure 91: Grain size distribution of the tested soil (Sample B).

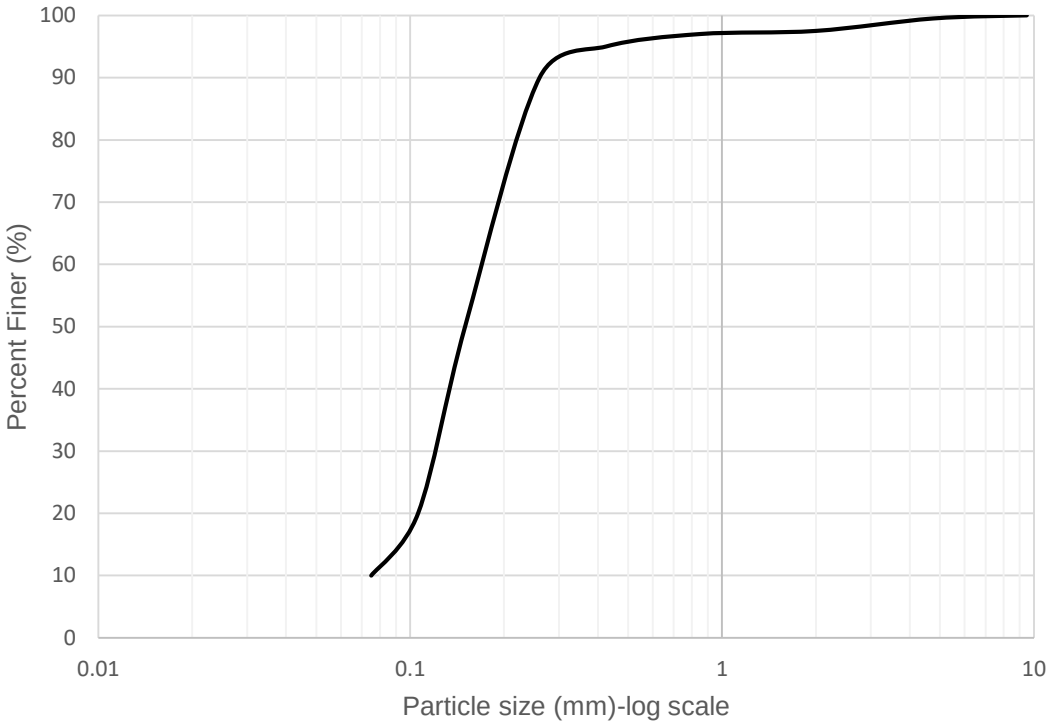

Figure 92: Grain size distribution of the tested soil (Sample C).

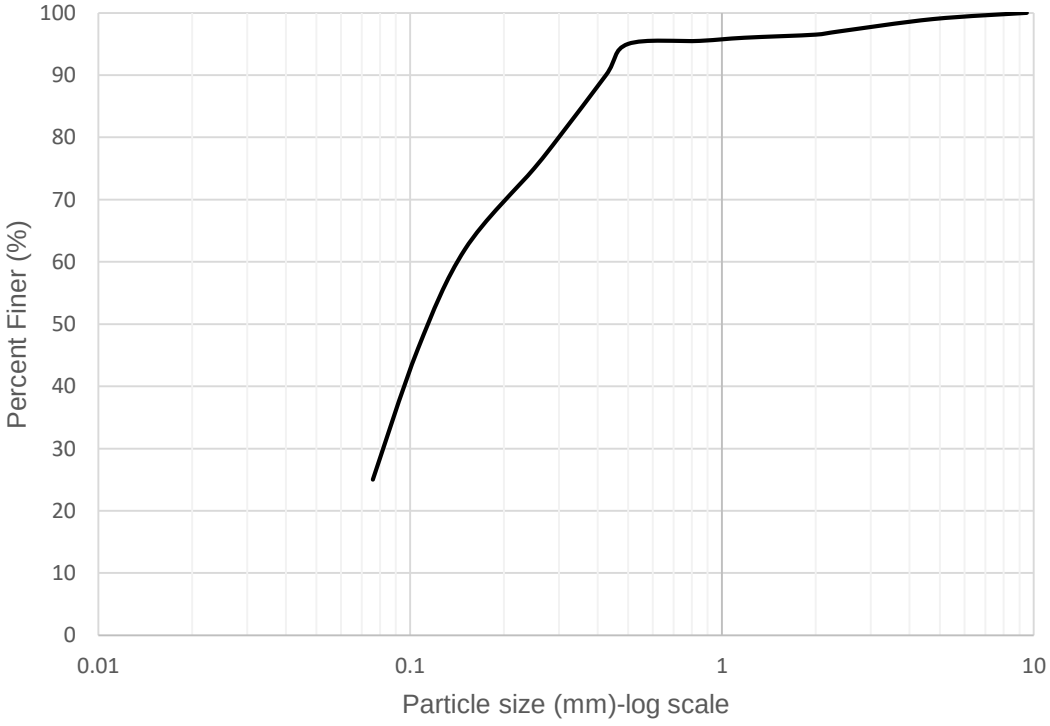

Figure 93: Grain size distribution of the tested soil (Sample D).

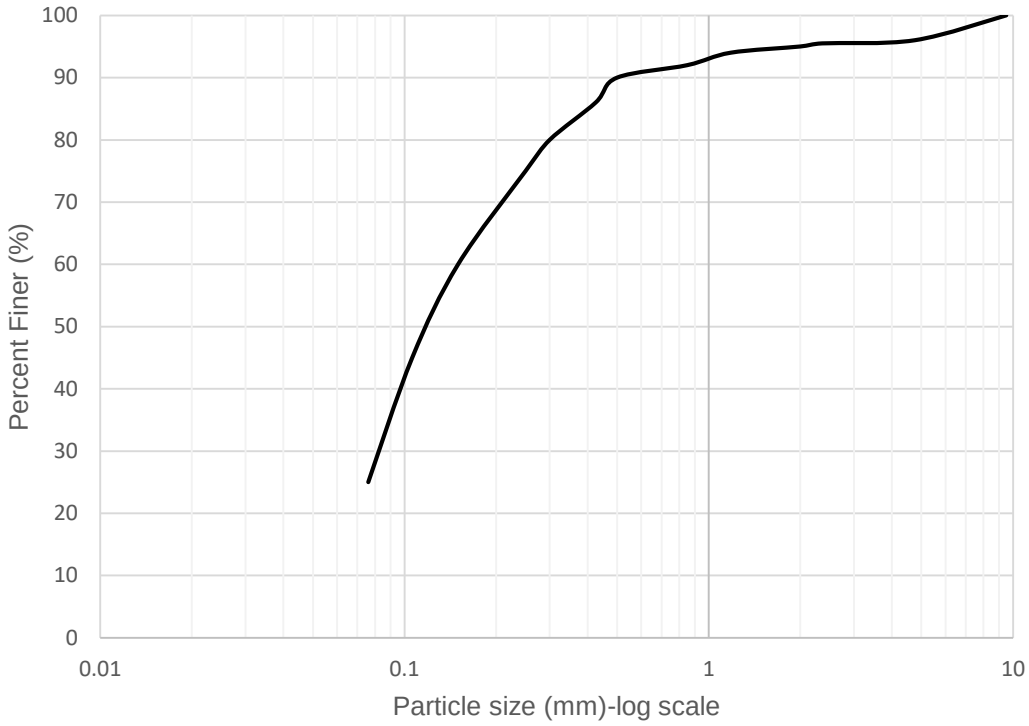

Figure 94: Grain size distribution of the tested soil (Sample E).

Vita

Ahmed Mohsen Khalil was born in 1997, in the City of Zagazig, Egypt. He received his primary and secondary education in Abu Dhabi, UAE. He received his B.Sc. degree in Civil Engineering from Abu Dhabi University in 2018. From 2014 to 2018, he worked as an Intern Site Engineer in Ali&Sons Contractor Company.

In September 2018, he joined the Civil Engineering master's program at the American University of Sharjah as a graduate teaching/and research assistant. During his master's study, he co-authored three papers that were presented at international conferences. His research interests are in Geo-Structural Engineering, Soil Dynamic Earthquake Engineering, and Structural Engineering.